Cholesterol homeostasis in Development: Molecular cloning and functional characterisation of the *Xenopus* 7-dehydrocholesterol reductase (Xdhcr7)

Dissertation
zur Erlangung des Doktorgrades
der Mathematisch-Naturwissenschaftlichen Fakultäten
der Georg-August-Universität zu Göttingen

Vorgelegt von
Emmanuel Tadjuidje
aus Baham, Kamerun

Göttingen 2004

D7
Referent: Prof. Dr. Tomas Pieler
Korreferent: Prof. Dr. Ernst A. Wimmer
Tag der Mündlichen Prüfung: 26.01.2005

Herewith I certify, that I prepared the Ph.D Thesis on " **Cholesterol homeostasis in Development: Molecular cloning and functional characterisation of the *Xenopus* 7-dehydrocholesterol reductase (Xdhcr7)"** on my own and with no other sources and aids than quoted.

Göttingen,13. 12. 2004

Emmanuel Tadjuidje

To my mother, Elisabeth Meghi

and my grand-mother, Tapia Tago

TABLE OF CONTENTS

LIST OF FIGURES

LIST OF ABBREVIATIONS

°C	degree Celsius
μ	micro
APB	alkaline phosphtase buffer
APS	ammonium peroxodisulfate
BCIP	5-bromo-4chloro-3.indolyl-phosphate
BMB	Boehringer blocking buffer
bp	base pairs
BSA	bovine serum albumin
cDNA	complementary DNA
CHAPS	3-((3-chlolamidopropyl)dimethylammonio)1-propansulfate
CTP	cytosinetriphosphate
DAB	4-Dimethylaminoazobenzene
DAPI	4',6-Diamidino-2-phenylindole
dATP	deoxyriboadenosintriphosphate
dCTP	deoxyribocytosintriphosphate
DEPC	diethylpyrocarbonate
dGTP	deoxyriboguanosintriphosphate
dH_2O	distilled H_2O
DIG-	digoxigenin-11-2´-deoxuridin-5´-triphosphate
DMSO	dimethylsulfoxide
DNA	deoxyribonucleic acid
DNase	deoxyribonuclease
dNTP	deoxyribonucleotidtriphosphate (dATP, dCTP, dGTP, dTTP)
DTT	dithiotreitol
dTTP	deoxyribotymidintriphosphate
EDTA	ethylendiamintetraacetic acid
EGTA	ethylenglycol-bis(2-aminoethylether)-N,N´-tetraacetic acid
F	forward (primer)
GTP	guanosintriphosphate
h	hour
HCG	human chorionic gonadotropin
HEPES	N-(hydroxymethyl)piperazin, N´-3-propansulfoneacid
HS	Horse serum
IPTG	isopropyl-β-D-thiogalactopyranoside
Kb	kilobase
Kda	kilodalton
LB	Luria-Bertani medium
LiOAc	lithium acetate
M	Molar
m	milli
MAB	maleic acid buffer
MBT	mitblastula transition
MEM	MOPS-EGTA-$MgSO_4$ buffer
MEMFA	MEM-formaldehyde buffer
min	minute
Mo	morpholino oligo

MOPS	3-(N-morpholino)propanesulfonic acid
mRNA	messenger-RNA
NBT	nitro-blue-tetrazolium
NTP	ribonucleotidetriphosphate
PBS	phosphate buffer saline
PBSS	PBS - Sorbitol
PBT	PBS – Triton-X-100
PCR	polymerase chain reaction
PEG	polyethylene glycol
pH	hydrogen potential
PTw	PBS - Tween
PVP	polyvinyl pyrrolidon
R	riverse (primer)
RNA	ribonucleic acid
rpm	revolution per minute
RT	room temperature
RT-PCR	reverse transcriptase PCR
SDS	sodiumdodecylsulfate
SSC	standard saline citrate buffer
Taq	Thermus aquaticus
TBE	tris-borate-EDTA buffer
TBS	tris buffer saline
TdT	terminal deoxynucleotidyl transferase
TE	tris-EDTA buffer
TEMED	N,N,N´,N´-tetramethyl-ethylenediamine
Tris	trihydroxymethylaminomethane
TTP	tymidinetriphosphate
U	unit
X-gal	5-bromo-4-chloro-3-indolyl-β-D-galatoside

I. INTRODUCTION

Looking at a single zygotic cell that develops to a complex adult organism has always been fascinating. This becomes more than a fascination, when one takes into consideration the molecular complexity of a cell. From a mother cell to two identical daughter cells, the mean by which the cellular materials are equally shared is already not understandable at the first glance. As to understand how a single cell gives rise to a complex organism, with complex organs (which means multiple type of cells differing in their organisation, structures and functions), this may sound as a mystery. Solving this puzzle is the daily combat of those working in the field of Developmental Biology. Developmental biology is a multidisciplinary field of scientific investigations with the common goal of understanding the molecular and / or cellular processes that govern the formation of a complex adult organism from a single zygotic cell, as well as the renewal of adult tissues. The main questions of developmental biologists are not only to understand the functions of different molecules, but also to find out what directs the differential expression and / or function of genes in particular tissues and / or developmental time points. One (and the main) purpose of developmental biologists´ investigations is to elucidate the molecular basis of human genetic diseases, from the genetic defects to their morphological and / or physiological manifestations. Use of animal models is of great help in this field, as it allows researchers to design a handful of experimental protocols without facing ethical barriers. *Xenopus leavis*, the african claw-toad frog, is one of the most popular systems used in the field of developmental biology. Its advantages come from the easy accessibility and large size (1 mm in diameter) of the egg, which can be easily fertilized *in vitro*. Moreover, the embryos can be obtained in high number (up to 1,500 per female), develop rapidly (see fig. 1 for life cycle), are easy to handle in culture, and survive well to microsurgical manipulations (microinjections and transplantations). The (round-shaped) egg has an initial radial (animal-vegetal) axis of asymmetry. Sperm entry induces the microtubule-driven rotation of the egg cortex by 30° relative to the inner cytoplasm (Gerhart et al., 1989).

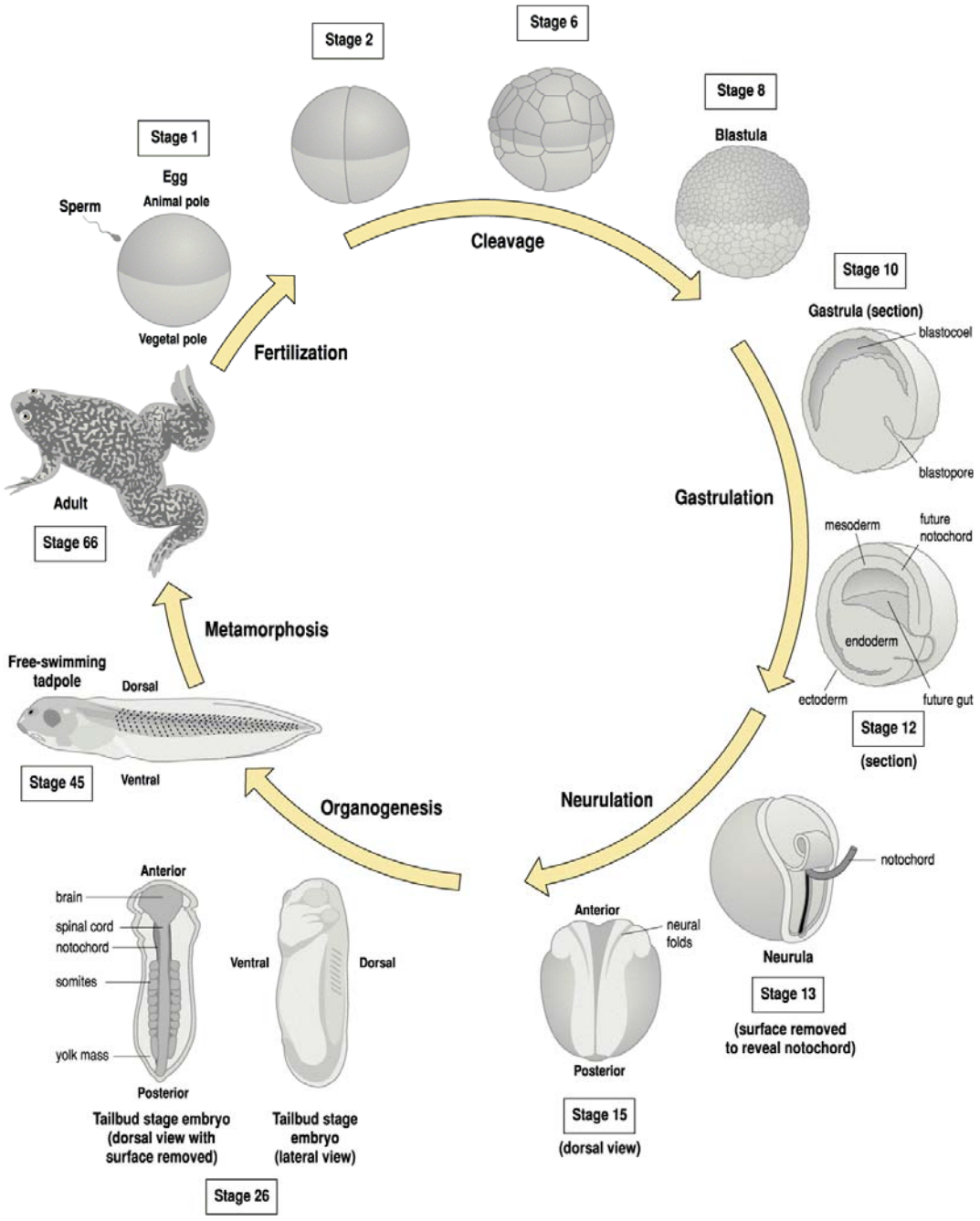

Figure 1: Basic stages of *Xenopus laevis* development (Wolpert, 1998)
At 25° C, the gastrulation process occurs within the next 10 to 15 hours after fertilization while neurulation is completed after about 20 hours. The tailbud embryo is obtained after one day and the free-swimming tadpole after 4 days. Depending on the type of food, an adult can be raised after one year or more.

As a result, maternal determinants are displaced to the equatorial region opposite the sperm entry point; this defines the future dorso-ventral axis of the embryo (Harland and Gerhart, 1997; De Robertis et al. 2000). Under the control of maternal regulators (cyclins and cyclin-dependent kinases), the fertilized egg undergoes synchronised divisions, which lead successively to the morula (mass of cell without an internal cavity), and the blastula,

which has an internal cavity (blastocoel). The morphology and radial symmetry of the embryo are maintained until late blastula stage. Following the onset of zygotic transcription at midblastula, a signalling center (the Spemann organizer) becomes established in the future dorsal side of the embryo. In a process known as gastrulation, cell migrate and extend from this so-called blastopore lip, to form the three germ layers of the gastrula embryo. The ectoderm is at the outside of the embryo, the endoderm is at the inside and the mesoderm is in between the two. Cells of different germ layers interact with each other to initiate differentiation; these interactions are known as primary inductions. At the completion of gastrulation (early neurulation), a second signalling centre called notochord is form by a rod of mesodermal cells in the most dorsal portion of the embryo (Scott, 2003; Johnson and Raven, 2002). Organogenesis starts when the notochord signals to the dorsal ectoderm and induces it to form the neural tube (neurula stage). Once the neural tube has formed, it induces changes in the neighbouring cells. During organogenesis, already differentiated cells (or tissues) interact with each other, in processes known as secondary inductions. At the end of organogenesis, the neurons have made connections between themselves, and with muscles. The larva (tadpole) is then ready to hatch (Scott, 2003; Johnson and Raven, 2002).

I.1. Eye development in vertebrates

I.1.1. A shortened story of vertebrates' eye development.

The first morphological sign of vertebrate eye development (Fig. 2) is the bilateral evagination of the diencephalon in the early neurula stage (Chow and Lang, 2001). However, the very history of *Xenopus* eye starts as earlier as the midgastrula stage, when the presumptive retinal tissues and the presumptive lens ectoderm are already specified in the anterior ectoderm and the head ectoderm respectively (Scott, 2003). As neurulation proceeds, the retinal primordia are positioned in two distinct regions on either side of the midline of the anterior neural plate. By late neurula stage, when the brain has already formed, a bilateral evagination of the diencephalon (optic vesicle) brings the retina primordia into contact with the lens ectoderm, which is induced to form the lens placode (by thickening). Then follows the invagination of both the optic vesicle, which forms the optic cup and the lens placode which forms the lens cup, and subsequently the lens vesicle. At this step, the overall structure of the eye is established (Chow and Lang, 2001). Signals from the forming lens induce the bilayered optic cup to differentiate into

pigmented epithelium (outer layer), comprising melanin secreting cells, and the neural retina (inner layer), comprising glia cells, ganglion cells, interneurons and photoreceptor neurons.

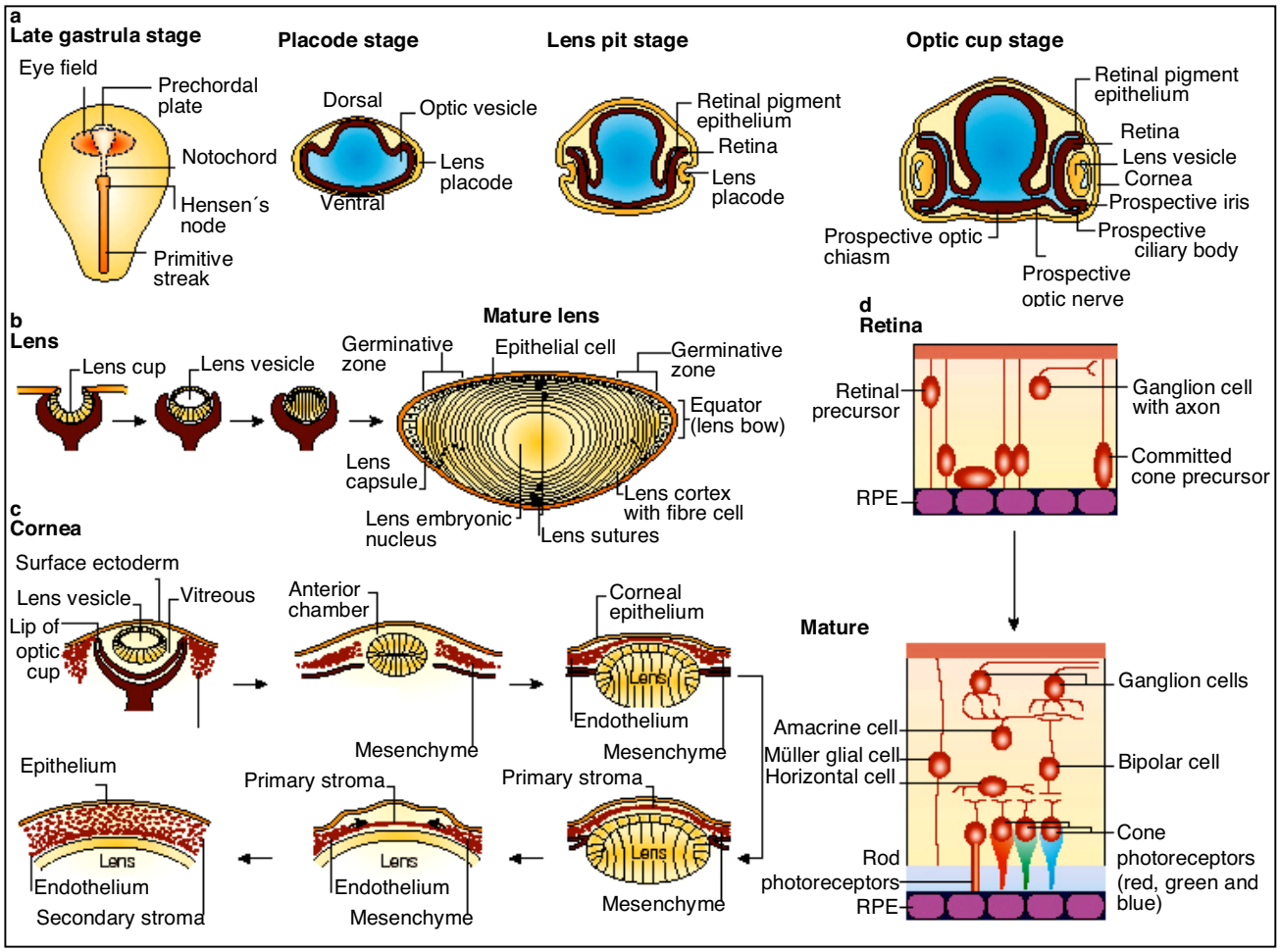

Figure 2. Schematic view of a developing vertebrate eye. (Graw, 2003)
a) The most important stages — from the late gastrula to the optic cup stage — are shown. The first main step occurs when the single central eye field splits into two lateral parts to form the optic vesicle and the lens placode at embryonic day (E) 9.5 in the mouse and 28 days of gestation in the human (placode stage). The invagination of the lens placode occurs at E10.5 in the mouse (lens pit stage). By the optic cup stage, at E11.5 in the mouse and 31–35 days of gestation in the human, the lens pit closes to form the lens vesicle, the future cornea becomes visible and the retina begins to differentiate. b) Once the lens vesicle has formed, the primary lens fibres elongate from the posterior epithelium of the lens vesicle and fill its entire lumen. The secondary fibre cells start to elongate at the lens bow region; the fibres from opposite sides meet at the anterior and posterior pole, and give rise to the lens sutures. The final step in lens differentiation is the degradation of the cell nuclei and mitochondria, which takes place around the time of birth in the mouse. c) The cornea begins to develop when the surface ectoderm closes after the formation of the lens vesicle and its detachment from the surface ectoderm. Two waves of mesenchymal cells (neural crest cells) invade the cornea and form the corneal stroma after condensation. d) The outer layer of the optic cup gives rise to the retinal pigmented epithelium (RPE), whereas the inner layer differentiates into the neural retina (beginning at E10.5 in the mouse and 4–5 weeks after gestation in the human; pigmented epithelium is visible in 6-week-old human embryos). The first rods and cones appear in human embryos at 10–15 weeks, and the horizontal, bipolar and ganglion cell layers appear in the middle of embryonic development. The retina is fully developed in the mouse a few days after birth and several months after birth in humans.

The forming eye is connected to the brain by the optic stalk, the future optic nerve. Meanwhile, the lens induces the overlying corneal ectoderm cells to become columnar and secrete multiple layers of collagen. Mesenchymal cells from the neural crest use this matrix to enter the area and secrete a set of proteins that further differentiate the cornea. The cornea is further made transparent by dehydratation through the influence of the hormone thyroxin. The full differentiation of the lens involves changing in cell structure and shape (conversion of epithelial cells into lens fibres) as well as the synthesis of lens-specific proteins called crystallins. This is achieved under the influence of the neural retina (Scott, 2003).

II.1.2. Molecular control of vertebrate eye development.

Different crucial developmental events have to take place to perform the how beautiful art of forming the highly specialized and complex vertebrate eye. 1) The eye field has to be specified in the anterior neural plate, and (2) be bisected into two distinct bilateral fields; 3) the evagination of the optic vesicle should follow, followed itself by (4) the invagination of the optic cup which later (5) differentiates into different retinal structures. Meanwhile, i) the lens competence has to be specified (within the eye field) in the head ectoderm, followed by ii) the thickening of the lens placode, iii) the invagination of the lens vesicle and iv) the maturation of the lens by the formation of primary and secondary fibres.

The paired box gene 6 (PAX6) is the model for a master control gene in eye development (Graw, 2003). However, the vertebrate eye anlage (eye field) is specified at the neural plate stage when a group of eye field transcription factors, EFTFs are expressed in the anterior neural plate (Zuber et al., 2003; Chuand and Raymond, 2002). These factors include ET, Rx1, Pax6, Six3, Lhx2, tll and Optx2 (also know as Six6). The *Xenopus* EFTFs are expressed prior to stage 15. Experimental data suggest that they are not only necessary, but also sufficient, as they can induce ectopic eyes in areas outside of the nervous system, when overexpressed as a cocktail. In a model suggested by Zuber et al. (2003), the neural plate arise through the action of neuralizing factors like noggin; anterior identity is specified by the expression of Otx2 (which demarcates the fore / midbrain), and EFTFs are induced in an area comprised within the Otx2 expression domain. In zebrafish, the forebrain territory (which comprises the eye field) is specified by the opposing ventralizing influences of Bmp2b and Bmp7 and the posteriorizing influences of Wnt8,

secreted by the ventral and lateral ectoderm, and the marginal mesoderm respectively (Chuang and Raymond, 2002).

The bilateral segregation of the eye field into two distinct optic anlagen is achieved under the influence of signals from the prechordal mesoderm underlying the anterior mesoderm. In zebrafish, a secreted Nodal-related member of the TGF-β superfamily encoded by *cyc* (*cylclops*), coming from the prechordal mesoderm, may induce hedgehog (hh) expression in the overlying neural midline. Hedgehog in turn locally inhibits genes such as Pax6 that direct dorso-distal eye development (Chow and Lang, 2001). This prevents eye formation in the midline, splitting the single eye field into two distinct bilateral eye primordia.

The evagination of the optic vesicle is the first morphogenetic movement that occurs during vertebrate eye development. As suggested by Kennedy et al. (2004) and Loosli et al. (2003), in zebrafish, the homeobox transcription factor RX3 plays a crucial role in this process. The further proximo-ventral / dorso-distal patterning of the optic vesicle involves SHH which triggers the expression of proximo-ventral markers like Pax2, Vax1 and Tll at the expense of dorso-distal markers like Pax6 and Rx1 (Hallonet et al., 1999). A reciprocal transcriptional repression between Pax6 and Pax2 may establish the boundary between the presumptive optic stalk and neural retina (Chow and Lang, 2001).

The transition from optic vesicle to optic cup involves the activity of the LIM homeodomain transcription factor LHX2 (Porter et al.1997), which along with Chx10, is induced in the presumptive neural retina by extrinsic signals from the overlying lens ectoderm, probably members of the fibroblast growth factors (FGF) family, which specify retinal fate (Nguyen and Arnheiter, 2000). Chx10 is essential for normal eye development, and functions by promoting the proliferation of retinal progenitor cells. The retinal-pigmented epithelium (RPE) is specified by secreted signal from the extraocular mesenchyme, probably activin A (Chow and Lang, 2001). The dorso-ventral patterning of the optic primordium is achieved through antagonistic activities of ventrally derived Shh and dorsally derived BMP4. In addition, Shh is involved in multiple other processes comprising retinal cell proliferation, retinal neurogenesis, differentiation of various cell types, optic nerve growth and guidance, as well as proliferation of astrocytes in the optic nerve (Russell, 2003). Pax6 defines the eye field in both neurectoderm (retina primordium) and surface ectoderm of the head (lens primordium), and is necessary to specify lens competence in the surface ectoderm. Its expression is restricted and maintained in the lens placode by a reciprocal regulation by

Sox2/3, which are expressed in the ventral surface ectoderm bordering the presumptive lens region, prior to lens placode formation. The production of the optic vesicle derived lens-forming signal involves Six3, which is expressed in the optic vesicle. The subsequent differentiation of the lens involves multiple factors, including Pitx3 and Eya1. Signalling molecules like BMP7, BMP4 and retinoic acid also contribute to lens development. The terminal differentiation of lens fibres is under the control of the bZIP transcription factor Maf, which is expressed in the lens vesicle after invagination, and regulates crystalline gene expression (Baker and Bronner-Fraser, 2001; Chow and Lang, 2001).

I.2. Cholesterol homeostasis and development.

I.2.1. A shortened recall of Cholesterol´s history.

Cholesterol (Cholest-5-en-3 -ol) is the most abundant sterol in vertebrates. First isolated from bile stones by Poulletier de La Salle in the years 1770, cholesterol was later isolated from unsaponifiable fraction of animal fats by ME Chevreul (1815), who named it Cholesterine (Greek *Khole*, bile and *stereos*, solid). The exact formula of cholesterol ($C_{27}H_{46}O$) was proposed by Reinitzer by 1880, and the right structure and exact steric representation were elucidated between 1900 and 1932, mainly by works from HO Wieland and AOR Windaus. Meanwhile, Schmidt E (1914) measured for the first time high serum cholesterol levels in patients with xanthomatosis, thus recognised it as essential hypercholesterolemia. By the early 1950s, F Lynen demonstrated that the acetylation of coenzyme A is the key first step in a chain of reactions that result in the formation of cholesterol and fatty acids. Together with K Bloch, Lynen successively received the Nobel price for medicine (1954) and Nobel price for physiology and medicine (1964) for their discoveries concerning the mechanism and regulation of cholesterol and fatty acids metabolism (pathway from “activated acetic acid” to terpenes and fatty acids). Meanwhile, Tavormina et al. (1956) discovered that mevalonic acid is quantitatively incorporated in cholesterol in cell-free systems with loss of carbon dioxide (Weiss et al., 1961). The biological function of cholesterol gained insights from work by Fisher (1976) who, by freeze-fracture and biochemical analysis in human erythrocytes, demonstrated that cholesterol is asymmetrically distributed across the plane of the membrane, being more present on the exterior side than on the interior side. Works to elucidate the very nature and metabolism of cholesterol were just starting that it was already pointed for its involvement in artheriosclerogenesis. The first hint came from work by Windaus who

reported that atherosclerotic plaques from aortas of human subjects contained 20- to 26-fold higher concentrations of cholesterol than did normal aortas. This observation opened nearly a century of research, which leaded to the recognition of the cholesterol carrying low density lipoprotein (LDL) particles as the primary cause of atherosclerosis (Rader et al., 2003). With the discovery of the mevalonic aciduria as first inborn error of cholesterol biosynthesis (Hoffman et al., 1986; Berger et a., 1985), a new era of cholesterol history started, era in which cholesterol was no longer considered just as heart breaking molecule, but also as a key player in developmental processes.

I.2.2. Cholesterol functions in vertebrates.

The cholesterol molecule (Fig. 3) consists of three main parts: a rigid lipophilic steroid core, which can trigger anchoring to lipids bilayer, a non-polar hydrocarbon tail that can undergo oxidation, and a polar hydroxyl head, which can take part in several esterification reactions. As can be predicted from its molecular structure, the biochemistry of cholesterol covers a wide spectrum of biological processes, of which a lot is still to be understood. More than 80 % of the cellular pool of cholesterol is located in the plasma membrane (Hoekstra and van Ijzendoorn, 2000), in which it accounts for 20 to 25 % of the lipid molecules (Dietschy and Turley, 2004). The plasma membrane (PM) cholesterol functions not only as a structural entity, but influences many properties of the PM. In addition to generally affecting membrane fluidity and permeabilitly (Khan et al., 2003), as well as integral protein function, cholesterol-induced membrane packing in lateral microdomains (rafts) can provide a scaffold for variety of membrane-associated signalling proteins (Tabas, 2002a). Rafts are small platforms, composed of sphingolipids and cholesterol in the outer exoplasmic leaflet, and connected to phospholipids and cholesterol in the inner cytoplasmic leaflet of the lipid bilayer. These assemblies are fluid but more ordered and tightly packed than the surrounding bilayer.

The presence of this liquid-ordered microdomains in cells transforms the classical membrane fluid mosaic model of into a more complex system, where proteins and lipid rafts diffuse laterally within a two-dimensional liquid. Membrane proteins are assigned to three categories: those that are mainly found in the rafts, those that are present in the liquid-disordered phase (phospholipids bilayer), and those that represent an intermediate state, moving in and out of rafts.

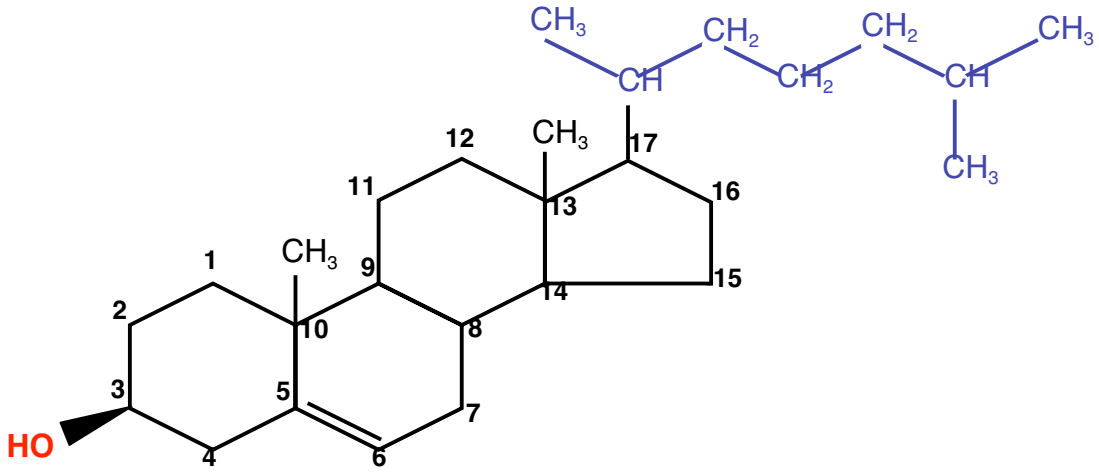

Figure 3: Structure of the cholesterol molecule
The cholesterol molecule consists of an aliphatic tail (blue), a rigid steroid core (black) and a polar hydroxyl head (red). This structure summarizes the main functions of cholesterol: the oxidation of the aliphatic side chain leads to important metabolites including bile acids; the rigid steroid core the anchoring of cholesterol and cholesterol modified proteins to membranes; and the hydroxyl head can participate in esterification reaction with different compounds, including proteins. Numbers indicate the carbon atoms of the steroid core.

Constitutive raft residents include glycophosphatidylinositol-anchored (GPI-anchored) proteins; doubly acylated protein, such as tyrosine kinase, Gα subunit of heterotrimeric G proteins, the cholesterol-linked and palmitate-anchored protein Hedgehog (Simons and Ehehalt, 2002) among others. In rafts, cholesterol is thought to serve as a spacer between the hydrocarbon chains of the sphingolipids and to function as dynamic glue that keeps the raft assembly together (Simons and Ehehalt, 2002; van Meer, 2001). Cholesterol depletion has been reported to block redistribution of lipid raft component and insulin-mimetic signalling in rat adipocytes (Müller et al., 2002), moreover, the specificity of cholesterol in raft formation has been proven by the modification of raft protein profile upon replacement on cholesterol by its direct precursor 7-dehydrocholesterol in raft structures (Keller et al., 2003). Lipid rafts function in different cellular processes including biosynthetic delivery of proteins to the cell surface (Bagnat et al., 2000), endocytosis (Nabi and Le, 2003) and signalling. In the later case, rafts can be viewed as signalling platforms that serve to colocalize the required components, facilitating their interaction and supporting signalling. In this scenario, receptors, coupling factors, effectors, enzymes and substrates would be colocalized in the same raft. In this way, signal transduction would occur rapidly because

of the spatial proximity of the interacting components. A more complex model would suppose complementary components of a signalling pathway to be segregated into different lipid rafts under basal conditions; stimulation of the cell upon ligand binding would lead to a transient fusion of lipid rafts. In this way, rafts provide a physical separation of proteins that would otherwise interact, leading to unregulated activation of a pathway (Pike, 2003). Apart from its function as component of the PM, free cholesterol is the precursor in the biosynthesis of physiologically important substances like bile acids and steroid hormones, linking this fascinating molecule to vital functions like nutrition and reproduction.

I.2.3. Cholesterol in the hedgehog signalling pathway.

One of the most surprising and important discoveries in the biology of cholesterol was the finding that the Hedgehog signal is formed through an unusual autocatalytic process that involves cleavage of a precursor protein into two parts and the attachment of a cholesterol molecule to the signalling (N-terminal) portion of the molecule (Porter et al., 1996). Sonic hedgehog (Shh) carries out diverse functions during vertebrate development. Humans or mice lacking Shh develop holoprosencephaly and cyclopia due to a failure of the forebrain to split into two lobes. In the developing vertebrate central nervous system, graded Shh signal is believed to dose-dependently establish different cell types along the dorso-ventral axis of the neural tube (Ho and Scott, 2002; Wijgerde et al., 2002; Briscoe and Ericson, 1999). The spectrum of Shh in development covers multiple organs, comprising the brain and eye (Schell-Apacik et al., 2003; Ishibashi and McMahon, 2002; Zhang and Yang, 2001; Liem et al., 2000; Odent et al., 1999; Macdonald et al., 1995), the lung (Yu et al., 2004), the early pancreas (Dilorio et al., 2002), the limb (Lewis et al., 2001) among others. In the Hedgehog signalling cascade (Fig. 4), the Hedgehog protein is synthesised in sending cells as an inactive precursor which is subsequently autocatalytically cleaved at a cystein site into a cholesterol linked N-terminal signalling fragment (HhN), and a C-terminal processing fragment. The N-terminal signalling fragment is subsequently palmitoylated at the its N-terminal end and is probably recruited to the PM, in rafts structures (Mann and Beachy, 2004; Ingham, 2000; Incardona and Eaton, 2000). The export of the signal from producing cell involves the sterol-sensing domain (SSD) containing membrane-bound protein Dispatched which displaced the HhN from rafts by binding to its SSD (Burke et al., 1999).

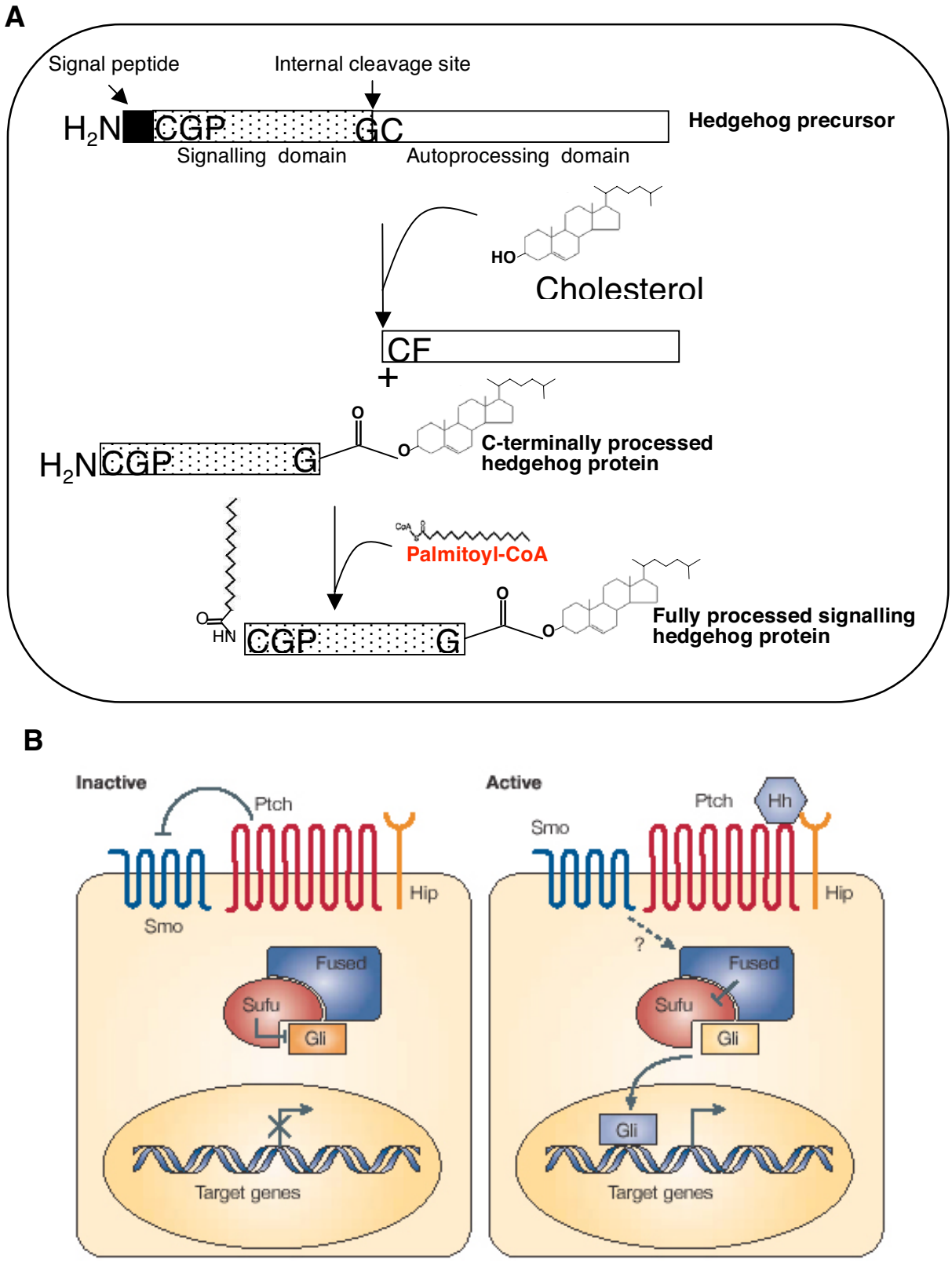

Figure 4: Hedgehog processing and signalling cascade (adapted from Mann and Beachy, 2004; and Pasca di Magliano and Hebrok, 2003)
A) In sending cells, the Hedgehog protein is synthesised as an inactive precursor, which is subsequently autocatalytically cleaved at a conserved cystein site, into a N-terminal signalling domain, and a C-terminal processing domain. Concomitantly, a cholesterol molecule is covalently added to the C-terminus of the

signalling domain. This signalling domain is subsequently palmitoylated at its N-terminus, thus leading to the fully processed signalling hedgehog protein, which is ready for export.
B) In receiving cells, in the absence of ligand, the Hh signalling pathway is inactive (left panel). In this case, the transmembrane protein receptor Patched (Ptch) inhibits the activity of Smoothened (Smo), a seven transmembrane protein. The transcription factor Gli, a downstream component of Hh signalling, is prevented from entering the nucleus through interactions with cytoplasmic proteins, including Fused and Suppressor of fused (Sufu). As a consequence, transcriptional activation of Hh target genes is repressed. Ligand binding (right panel) results in de-repression of Smo, thereby activating a cascade that leads to the translocation of the active form of the transcription factor Gli to the nucleus. Nuclear Gli activates target gene expression, including *Ptch* and *Gli* itself, as well as *Hip*, the Hh interacting protein that attenuates ligand diffusion. Other target genes that are important for the oncogenic function of the Hh pathway are genes that are involved in controlling cell proliferation (cyclin D, cyclin E, *Myc* and components of the epidermal-growth-factor pathway) and in angiogenesis (components of the platelet-derivedgrowth-factor and vascular-epithelial-growth-factor pathway).

In receiving cell, HhN is bound by it receptor Patched, which is also a membrane bound SSD-containing protein. Upon binding, Hh abolishes the inhibitory effect of Patched on Smoothened, which can then transduce the signal to downstream targets (Taipale et al., 2002; Strutt et al., 2001). In this process, cholesterol is important in more than one way. (1) No other molecule has yet been suggested to be likely to replace cholesterol in the hedgehog processing reaction, meaning that this is a cholesterol specific activity. (2) Both Dispatched and Patched contain a SSD, and megalin, which functions as an endocytic sonic hedgehog receptor, belongs to the low density lipoprotein receptor family; this suggests that the cholesterol moiety may serve as sensor, both for the sending, the transcytosis and the receiving of the Hh signal (McCarthy and Argaves, 2003; McCarthy et al., 2002; Kuwabara and Labouesse, 2002). (3) Fully processed Hh protein is recruited in rafts, which are cholesterol-rich microdomains. Cholesterol might then play a quasi central role in pattern formation through its involvement in signal transduction (Ingham, 2000; Incardona and Eaton, 2000).

The developing central nervous need considerable amount of cholesterol for myelin build up and for synaptogenesis. Although the brain represents only 2.1 % of the total body weight, it contains almost a quarter of the total body cholesterol (Dietschy and Turley, 2004). The brain cholesterol serves not only as constituent, but is involved in normal brain function. Dementia, aggressivity auto-mutilation and suicidal behaviours have been reported for patients with low circulating cholesterol (Dietschy and Turley, 2004). Moreover, during development, synapses connection and neuronal growth are highly dependent on cholesterol metabolism.

I.2.4. Cholesterol homeostasis and the *DHCR7* gene.

Homeostasis defines the ability or tendency of an organism or cell to maintain internal equilibrium by adjusting its physiological processes. With regard to a single compound, homeostasis will then define all the metabolic and regulatory processes undertaken by the cell or the organism to maintain its pool at optimal value. Depending on their type, vertebrates' cells produce their own cholesterol and/or receive cholesterol by uptake from lipoproteins. Cells also continuously lose cholesterol or cholesterol metabolites to the outside circulation. In a given cell, the cholesterol input consists of uptake of cholesterol-rich lipoprotein from the extracellular circulation, and endogenous *de novo* biosynthesis; depending on the type of the cell, the two processes may coexist or not. Cholesterol output can be achieved through esterification, transformation to other products (like steroid hormones or bile acid), and efflux to extracellular acceptors. In normal situation, regulation of synthesis, influx and efflux keeps cellular cholesterol levels precisely controlled. During development, the de novo cholesterol biosynthesis is of great importance, especially for organs like the brain, which are unable to use extracellularly uptaken cholesterol. The cholesterol biosynthesis pathway (Fig. 5) consists of a series of approximately 30 enzymatic reactions, with all the carbon atoms originally derived from acetate (Herman, 2003). The rate-limiting step of this pathway is the conversion of Hydroxymethylglutaryl Coenzyme A to mevalonate. The catalysing enzyme, Hydroxymethylglutaryl Coenzyme A reductase (HMGR) is under the transcriptional control of sterol regulatory element binding proteins (SREBPs). The subsequent steps consist on the formation of 5 carbon atoms units isoprenes, and the formation of squalene is the first enzymatic reaction which is unique to cholesterol biosynthesis. The postsqualene steps constitute the very phase of sterol synthesis, since lanosterol, which arises from the cyclization of squalene through the action of squalene epoxidase and oxidosqualene cyclase, is the first sterol intermediate of the pathway. Lanosterol is converted to cholesterol by a series of oxidations, demethylations and reductions (Liscum, 2002). Apart from the production of cholesterol with the already discussed multiple functions, the cholesterol biosynthesis pathway interacts with diverse cellular process in the way that both isoprenoids and postsqualene sterol intermediates serve as precursor for the biosynthesis of multiple biologic end products (Fig. 5). Heme A and ubiquinone are necessary for mitochondrial electron transport in the respiratory chain; isopentenyl-tRNA is involved in protein translation;

protein prenylation by farnesyl and geranylgeranyl groups is important in cell signalling and differentiation; dolichol is essential for N-linked protein glycosylation; and 7-dehydrocholesterol is the precursor for vitamin D synthesis (Santos and Lehmann, 2004; Nwokoro et al., 2001; Tabas, 2002a; Edwards and Ericsson, 1999).

With regard to the large spectrum of functions fulfilled by cholesterol and its biosynthesis intermediates and metabolites, it is predictable that a disregulation of cholesterol balance may end up in severe biological perturbation. Cellular accumulation of free cholesterol may affect rafts structures by rendering them too rigid; may lead to the formation of needle-shaped cholesterol crystals; or trigger apoptotic pathway. Cells that rely totally or mostly on endogenous cholesterol synthesis cannot accumulate excess endogenous cholesterol because of homeostatic regulation at multiple steps in the cholesterol biosynthetic pathway (Tabas, 2002b). Cell that internalise exogenous cholesterol also repress endogenous cholesterol synthesis and LDL receptor expression in response to cholesterol loading. Moreover, cholesterol esterification by the microsomal enzyme acyl-coenzyme A:cholesterol acyl transferase (ACAT), as well as endosomal / lysosomal cholesterol trafficking by the Niemann-Pick Type C1 disease protein (NPC1) contribute to the regulation of free cholesterol content in the cell (Garver and Heindenreich, 2002; Tabas, 2002a; Tabas, 2002b; Kuwabara and Labouesse, 2002; Schmitz and Orsó, 2001; Hoekstra and Ijzendoorn, 2000; Simons and Ikonen, 2000).

Since the discovery of mevalonic acidura (caused by the deficiency of the mevalonate Kinase) as the first disorders of cholesterol biosynthesis (leading to low cholesterol content), several inborn errors of cholesterol biosynthesis have been reported, all characterised by dysmorphogenesis of multiple organs (Kelley and Herman, 2001; Nwokoro et al., 2001). The Smith-Lemli-Opitz syndrome (SLOS), was the first described disorder of post-squalene cholesterol biosynthsis, and is by far the most common (Herman, 2003). First identified in 1964 as a recessive multiple malformation syndrome; its biochemical characterization came in 1993, when SLOS patients were reported to have high serum 7-dehydrocholesterol; a deficiency in the 7-dehydrocholesterol reductases (DHCR7; EC: 1.3.1.21) activity was reported in SLOS patients in 1995. Finally in 1998, data from three different teams brought the final evidence that mutations of the DHCR7 gene were responsible for the SLOS condition.

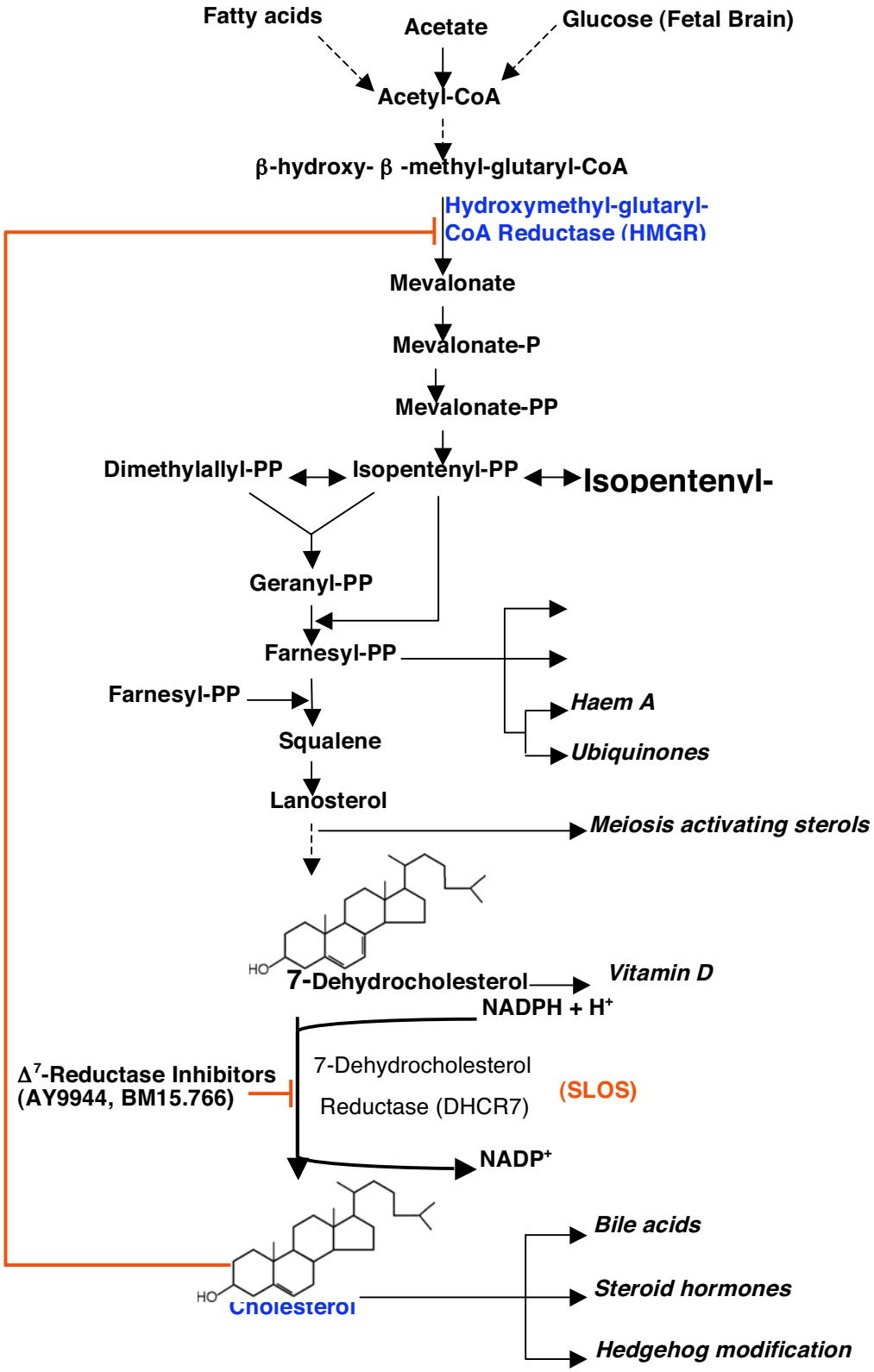

Figure 5: Cholesterol biosynthesis pathway, and its biologically important derivatives (adapted from Kelley and Herman, 2001)

The biosynthesis of cholesterol can start from the two carbon unit acetyl coenzyme A (acetyl-CoA). The phase starting from acetyl-CoA to β-hydroxy- β -methyl-glutaryl-CoA is common to sterols, isoprenoids and keton bodies synthesis. The conversion of β-hydroxy- β -methyl-glutaryl-CoA to mevalonate is the first and rate-limiting step of sterols and isoprenoids synthesis. This enzyme is under the feedback control by

cholesterol (Red bar). The very first sterol specific step is the oxidative cyclization of squalene to lanosterol. The very cholesterol specific step is catalysed by the enzyme 7-dehydrocholesterol reductases (DHCR7), which is deficient in SLOS patients. Derivatives of isoprenoids and sterols are indicated in italic. –P, phosphate; -PP, pyrophosphate; SLOS, Smith-Lemli-Opitz syndrome.

The human *DHCR7* gene is located on chromosome 11q13, and spans approximately 14 kb. The gene contains 9 exons and 8 introns, with the translation initiation codon located in exon 3. The predicted molecular mass of the DHCR7 protein is 55 Kda and it is structurally related to many other plant and vertebrates sterol reductases. It is localised to the endoplasmic reticulum and has 9 putative transmembrane domains. The large fourth cytoplasmic loop likely contains the active site of the enzyme and site for NADPH. The C-terminus is predicted to be within the endoplasmic reticulum. To date, nearly a hundred of *DHCR7* mutations have been reported, with most of them located in the highly conserved fourth cytoplasmic loop.

The spectrum of SLOS symptoms includes global developmental delay, microcephaly, cleft palate, cataract, syndactily of toes 2/3, polydactily, visceral malformations, variable anomalies of the heart and kidneys, and ambiguous genitalia in males (Witsch-Baumgartner et al., 2001; Nwokoro et al., 2001; Nowaczyk et al., 2001; Kelley and Herman, 2001). Mental retardation is a common feature of SLOS patients, who display a characteristic spectrum of behavioural phenotype, comprising hyperactivity, self-injury, abnormal sleep pattern, tactile hypersensivity of hands and feet, hypersensivity to certain types of sound and visual stimuli, and food aversion (Nowaczyk et al., 2001). Since the identification of DHCR7 mutations as cause of the SLOS, the DHCR7 gene has been characterised in several species. Animal models have also been developed, in order to better understand the molecular background of the SLOS physiopathology. Evidence has been shown that cholesterol deficit but not accumulation of aberrant sterols is the major cause of teratogenic activity in animal models for SLOS (Gaoua et al., 2000). A first clue pointing to and alteration of the Shh signalling came from the observation that a significant number of SLOS patient also display holoprosencephaly. Holoprosencephaly (HPE) is a condition in which the cerebral hemispheres of the brain fail to separate into distinct left and right hemispheres. Due to the improper specification and formation of the forebrain during early development, this malformation has also been reported in mutations affecting the SHH protein or its endocytic receptor Megalin (Wallis and Muenke, 2000; Gaoua et al., 2000). Recent data from Cooper et al. (2003) reported a defective response to Hedgehog

signalling as a possible molecular explanation of the disorder of cholesterol synthesis syndrome. However, very role of cholesterol in both development and hedgehog signalling is still a real matter of investigation.

I.3. Gaols and experimental approach

In the present project, our main gaol was to investigate the interaction between cholesterol homeostasis and the development of *Xenopus*, using the eye as model organ. Our main interest in the DHCR7 gene was motivated by the reported multiple development defects caused its mutations, of which a lot was still to be understood. In our experimental approach, we took advantage of the sequence homology of previously characterised vertebrate dhcr7 cDNAs, and the existence of a *Xenopus* expressed sequence tag (EST) database. A database search allowed us to identify some EST clones, which we used to design RT-PCR primer for the isolation of the full-length Xdhcr7 ORF. In the description of the expression pattern of *Xdhcr7*, we made use of both RT-PCR and whole mount in situ hybridization, since the two methods are complementary. In the gain-of-function analysis, we performed overexpression by synthetic cap-mRNA injection, and analysed embryos both for eye phenotypes and by means of eye and neural markers. Loss-of-function study was performed both by means of morpholino oligos knock-down (which inhibited the translation of the mRNA) and by direct chemical inhibition of the enzymatic activity. Since we isolated three alternatively spliced isoforms of Xdhcr7 cDNA, we were also interested in analysing the enzymatic activity, by heterologous expression in yeast. Our data suggest that *Xdhcr7* consist of three alternatively spliced isoforms with differential activities upon overexpression. Data from functional analysis, a tight regulation of cholesterol metabolism is necessary for normal neural and eye development.

II. RESULTS

II.1. Molecular cloning of *Xenopus* 7-dehydrocholesterol reductase (Xdhcr7).

The DHCR7s of different species share a relatively high degree of sequence similarity in their open reading frames (ORF) (Bae et al., 1999). Based on the assumption that the *Xenopus* DHCR7 gene could also share this sequence similarity, a database search in *Xenopus* EST was performed, using the human dhcr7 sequence (Moebius et al., 1998). This database search revealed three *Xenopus* ESTs (accession numbers AW765630, AW766251 and AI031454) with high homology to the human dhcr7 cDNA. Sequence analysis revealed that AW765630 and AI031454 had the same open reading frame, encoding a peptide homologous to the N-terminus of human DHCR7, whereas AW766251 showed homology to the 3´end of the cDNA.

II.1.1. Nucleotide sequence of the Xdhcr7 cDNA

In an attempt to isolate the full-length Xdhcr7 cDNA, forward and reverse primers were designed to flank the entire putative open reading frame as predicted from ESTs sequence analysis. RT-PCR, performed using a whole eye cDNA, generated three products of 1.5, 1.3 and 0.6 kb respectively. The RT-PCR products were cloned into pGEM-T vector and sequenced from both ends, using Sp6 and T7 primers. A BLAST search using the sequence information, confirmed the identity of these products as delta-7-sterol reductases. Sequence analysis (Fig. 6) revealed that they all contained a start and a stop codon, and shared the same sequence and ORF, encoding 478 AA (54 Kda), 433 AA (49 Kda) and 189 AA (21Kda) respectively. Although the short form showed a frame shift at the 3´-end (black filled end in fig. 6B), these cDNAs represent alternatively spliced isoforms of the *Xenopus* dhcr7 gene. These isoforms were termed Xdhcr7-L (large form: 1.5 kb), Xdhcr7-M (medium form: 1.3 kb) and Xdhcr7-S (short form: 0.6 kb) according to their size.

A

```
           1                                                                  80
Xdhcr7-L   ATGGGAGAGCGGAGAAGAGCGAATGCATCCAGGGGGGGACAAGAAAGTGGCCAATGGAGAAAAGCAACATGTGGGCCAGTG
Xdhcr7-M   ATGGGAGAGCGGAGAAGAGCGAATGCATCCAGGGGGGGACAAGAAAGTGGCCAATGGAGAAAAGCAACATGTGGGCCAGTG
Xdhcr7-S   ATGGGAGAGCGGAGAAGAGCGAATGCGTCCAGGGGGGGACAAGAAAGTGGCCGATGGAGAAAAGCAACATGTGGGCCAGTG
                                                                             160
Xdhcr7-L   GGGCAGAGCTTGGGAAGTCGATTACTTCTCATTGGCCTCAGTCATATTCCTGTTGGCGTTTGCTCCGCTGATAGTCTACT
Xdhcr7-M   GGGCAGAGCTTGGGAAGTCGATTACTTCTCATTGGCCTCAGTCATATTCCTGTAGGCGTTTGCTCCGCTGATAGTCTACT
Xdhcr7-S   GGGCAGAGCCTGGGAAGTCGATTACTTCTCATTGGCCTCAGTCATATTCCTGTTGGCGTTTGCTCCGCTGATAGTCTACT
                                                                             240
Xdhcr7-L   ACTTTGTCATGTCGTGTGATCAGTACCAGTGCGCCCTCACCGCCCCAGTCCTGGACCTATACTCTGGCAAAGCGCGGCTG
Xdhcr7-M   ACTTTGTCATGTCGTGTGATCAGTACCAGTGCGCCCTCACCGCCCCAGTCCTGGACCTATACTCTGGCAAAGCGCGGCTG
Xdhcr7-S   ACTTTGTCATGTCATGTGATCAGTACCAGTGCGCCCTCACCGCCCCAGTCCTGGACCTATACTCTGGCAAAGCGCAGCTG
                                                                             320
Xdhcr7-L   TCCGACATCTGGGACAAGACTCCCGCACTCACCTGGACTGCCGTCAAGATCTACCTAGCGTGGGTCTCTTTCCAGGTGTT
Xdhcr7-M   TCCGACATCTGGGACAAGACTCCCGCACTCACCTGGACTGCCGTCAAGATCTACCTAGCGTGGGTCTCTTTCCAGGTGTT
Xdhcr7-S   TCCGACATCTGGGACAAGACTCCCGCACTCACCTGGACTGCCGTCAAGATCTACCTAGCGTGGGTCTCTTTCCAGGTGTT
                                                                             400
Xdhcr7-L   CCTGTATATGTTCCTTCCTGATATCTTACATAAATTTGTGCCTGGTTACGAGGGAGGAGTGCAAGAAGGAGCAAGGACTC
Xdhcr7-M   CCTGTATATGTTCCTTCCTGATATCTTACATAAATTTGTGCCTGGTTACGAGGGAGGAGTGCAAGAAGGAGCAAGGACTC
Xdhcr7-S   CCTGTATATGTTCCTTCCTGATATCTTACATAAATTTGTGCCTGGTTACGAGGGAGGAGTGCAAGAAGGAGCGAGGACCC
                                                                             480
Xdhcr7-L   CTGCTGGCTTGATAAACAAGTACCAAGTCAACGGACTGCAGGCCTGGACTATTACCCACCTCCTGTGGTTTGCCAATGCT
Xdhcr7-M   CTGCTGGCTTGATAAACAAGTACCAAGTCAACGGACTGCAGGCCTGGACTATTACCCACCTCCTGTGGTTTGCCAATGCT
Xdhcr7-S   CTGCTGGCTTGATAAACAAGTACCAAGTCAACGGACTGCAGGCCTGGACTATTACCCACCTCCTGTGGTTTGCCAATGCT
                                                                             560
Xdhcr7-L   TACCATTTCCACTGGTTCTCCCCAACCATTGTCATTGACAACTGGATCCCGCTGCTGTGGTGCGCCAATCTCCTGGGCTA
Xdhcr7-M   TACCATTTCCACTGGTTCTCCCCAACCATTGTCATTGACAACTGGATCCCGCTGCTGTGGTGCGCCAATCTCCTGGGCTA
Xdhcr7-S   TACCATTTCCACTGGTTCTCCCCAACCATTGTCATTGACAACTGGATCCCGCTGC--------------------------
                                                                             640
Xdhcr7-L   TTCTGCTGCCACCTTCGCTTTGGTGAAAGCCAACTTCTTCCCCCACTAATGCCAACGACTGCAAATTCACAGGCAATTTCT
Xdhcr7-M   TTCTGTTGCCACCTTCGCTTTGGTGAAAGCCAACTTCTTCCCCCACTAATGCCAACGACTGCAAATTCACAGGCAATTTCT
Xdhcr7-S   --------------------------------------------------------------------------------
                                                                             720
Xdhcr7-L   TCTACGACTACATGATGGGCATTGAGTTCAACCCCCGCATTGGAAAGTGGTTTGACTTCAAACTGTTCTTTAATGGGCGA
Xdhcr7-M   TCTACGACTACATGATGGGCATTGAGTTCAACCCCCGCATTGGAAAGTGGTTTGACTTCAAACTGTTCTTTAATGGGCGA
Xdhcr7-S   --------------------------------------------------------------------------------
                                                                             800
Xdhcr7-L   CCCGGGATCGTCGCCTGGACCTTAATTAACTTGTCGTATGCTGCCAAACAGCAAGAGCTCTACGGGCAGGTCACCAACTC
Xdhcr7-M   CCCGGGATCGTCGCCTGGACCTTAATTAACTTGTCGTATGCTGCCAAACAGCAAGAGCTCTACGGGCAGGTCACCAACTC
Xdhcr7-S   --------------------------------------------------------------------------------
                                                                             880
Xdhcr7-L   CATGATTCTGGTCAATGTTCTTCAGGCAATCTATGTAGTGGACTTTTTCTGGAACGAATCCTGGTACCTGAAGACTATTG
Xdhcr7-M   CATGATTCTGGTCAATGTTCTTCAGG----------------------------------------------------
Xdhcr7-S   --------------------------------------------------------------------------------
                                                                             960
Xdhcr7-L   ACATTTGCCATGACCACTTTGGCTGGTATCTGGGATGGGGAGATTGTGTCTGGTTGCCCTACCTCTATACCCTACAGGGT
Xdhcr7-M   ----------------------------------------------------------------------------GT
Xdhcr7-S   --------------------------------------------------------------------------------
                                                                            1040
Xdhcr7-L   TTATATCTGGTGTACAACCCAGTTGAGCTCTCTACCACTGCTGCCGTTGCAGTCCTCCTGCTCGGTTTGATTGGCTATTA
Xdhcr7-M   TTATATCTGGTGTACAACCCAGTTGAGCTCTCTACCACTGCTGCCGTTGCAGTCCTCCTGCTCGGTTTGATTGGCTATTA
Xdhcr7-S   --------------------------------------------------------------------------------
                                                                            1120
Xdhcr7-L   CATCTTCAGAATGACCAATCACCAGAAAGACCTCTTCCGACGCACTAACGACAACTGCAAGATCTGGGGGAAGAAGCCTA
Xdhcr7-M   CATCTTCAGAATGACCAATCACCAGAAAGACCTCTTCCGACGCACTAACGGCAACTGCAAGATCTGGGGGAAGAAGCCTA
Xdhcr7-S   --------------------------------------------------------------------------------
                                                                            1200
Xdhcr7-L   AATCCATCGAATGTTTTTACGTGTCAGCGGACGGCAAGCGACACTACAGCAAGTTGATGATTTCAGGGTTTTGGGGGGTG
Xdhcr7-M   AATCCATCGAATGTTTTTACGTGTCAGCGGACGGCAAGCGACACTACAGCAAGTTGATGATTTCAGGGTTTTGGGGGGTG
Xdhcr7-S   --------------------------------------------------------------------------------
                                                                            1280
Xdhcr7-L   GCGAGGCATTTAAACTACACAGGAGATTTAATGGGGTCCCTGGCGTACTGCCTGGCCTGTGGCTTTGACCACCTCCTGCC
Xdhcr7-M   GCGAGGCACTTAAACTACACAGGAGATTTAATGGGGTCCCTGGCGTACTGCCTGGCCTGTGGCTTTGACCACCTCCTGCC
Xdhcr7-S   --------------------------------------------------------------------------------
                                                                            1360
Xdhcr7-L   TTACTTCTACTTCATCTACATGACCATCTTGCTGGTGCACCGCTGCATAAGGGACGAACACCGCTGCTCGAGTAAATACG
Xdhcr7-M   TTACTTCTACTTCATCTACATGACCATCTTGCTGGTGCACCGCTGCATAAGGGACGAACACCGCTGCTCGAGTAAATACG
Xdhcr7-S   ----------------------------------------------ATAAGGGACGAACACCGCTGCTCGAGTAAATAcg
                                                                            1440
Xdhcr7-L   GGAAGGACTGGAAGCTTTACACCAGCGCCGTGCCCTATAGGTTACTCCCCGGACTATTCTAAtctagacgggaatcccgc
Xdhcr7-M   GGAAGGACTGGAAGCTTTACACCAGCGCCGTGCCCTATAGGTTACTCCCCGGACTATTCTAAtctaga------------
Xdhcr7-S   ggaaggactggaagctttacaccagcgccgtgccctataggttactccccggactattctaatctaga------------
                          1459
Xdhcr7-L   ggccaggcggccgggagca
Xdhcr7-M   --------------------
Xdhcr7-S   --------------------
```

B

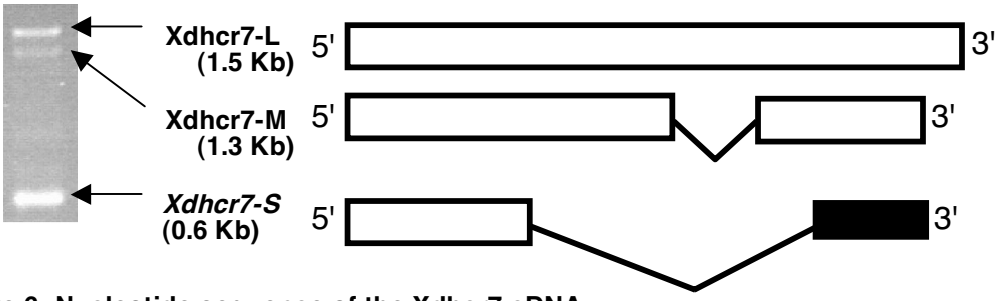

Figure 6: Nucleotide sequence of the Xdhcr7 cDNA.
A) Alignment of the three isoforms cDNA sequences. The start and stop codons are marked in bold.
B) A schematic representation of the 3 isoforms. The black filled 3´-end of the short version indicated a frame-shift, leading to a different N-terminus sequence as compared to the M and L versions.

II.1.2. Structural features of the XDHCR7 protein

The *Xenopus* dhcr7 cDNAs encode for predicted proteins of 478 AA (54 Kda), 433 AA (49 Kda) and 189 AA (21 Kda) for the large, medium and the short isoforms respectively. At the sequence level (Fig. 7A), the M isoform is truncated between amino acids 278 and 324 (red arrows), with the rest of the sequence being identical to that of the L version. Unlike the M version, the S version is truncated at amino acid 180 (green arrow), with a C-terminal tail (red asterisk: HKGRTPLLE) different from the L version. Amino acid residues corresponding to the transmembrane domains (TMD) were derived by comparison to the rat DHCR7 (Bae et al., 1999). The XDHCR7-L contains in total, 9 putative transmembrane domains, distributed between amino acids 39 and 437. The M version lacks the 6^{th} and 7^{th} domains, and the S version contains only the three first ones. The looping feature of the XDHCR7 protein (Fig. 7B) was predicted by analogy to the proposed topology of the human (Fitzky et al. 1998) and rat (Bae et al., 1999) DHCR7 proteins. The N-terminus faces the cytoplasm, whereas the C-terminus faces the ER lumen. The large fourth cytoplasmic loop is likely to contain the active site of the enzyme and the binding site for NADPH, as suggested by Nowaczyk and Waye (2001) for the human DHCR7. Alignment of XDHCR7-L with Δ^7-sterol reductases from other species (Fig. 8A and 8B) reveals a high homology with other vertebrate DHCR7 proteins; a strong identity is shared with mouse (76 %), rat (76 %) and human (75.1 %) DHCR7. The sequence homology is highest in the transmembrane domains (*bold* residues), as only a few amino acids substitutions (residues marked in *red*) can be detected. With plant Δ^7-sterol reductases, represented here by the nasturtium (32.2 %) and the thale cress (31,9 %), the sequence homology is lower. The XDHCR7-L also contains a total of 21 serine (4.4 %) and 22 threonine (4.6 %) residues distributed throughout the backbone. Three putative N-linked glycosilation sites (black *asterisks*) are present at positions 8 – 11 (NASR); 253 – 256 (NLSY) and 410 – 413 (NYTG); as well as a highly conserved N-myristilation site (*boxed* residues) at position 127 – 132 (GVQEGA) (Fig. 8A). The XDHCR7 also contains a potential sterol-sensing domain (SSD) comprising TMD4, TMD5, TMD6, TMD7 and TMD8 (amino acids 174 – 352), which is highly homologous in all vertebrate DHCR7 proteins compared (marked as grey highlight in fig. 8A). This corresponds to the sterols (comprising the substrate) binding domain (Fitzky et al., 2001).

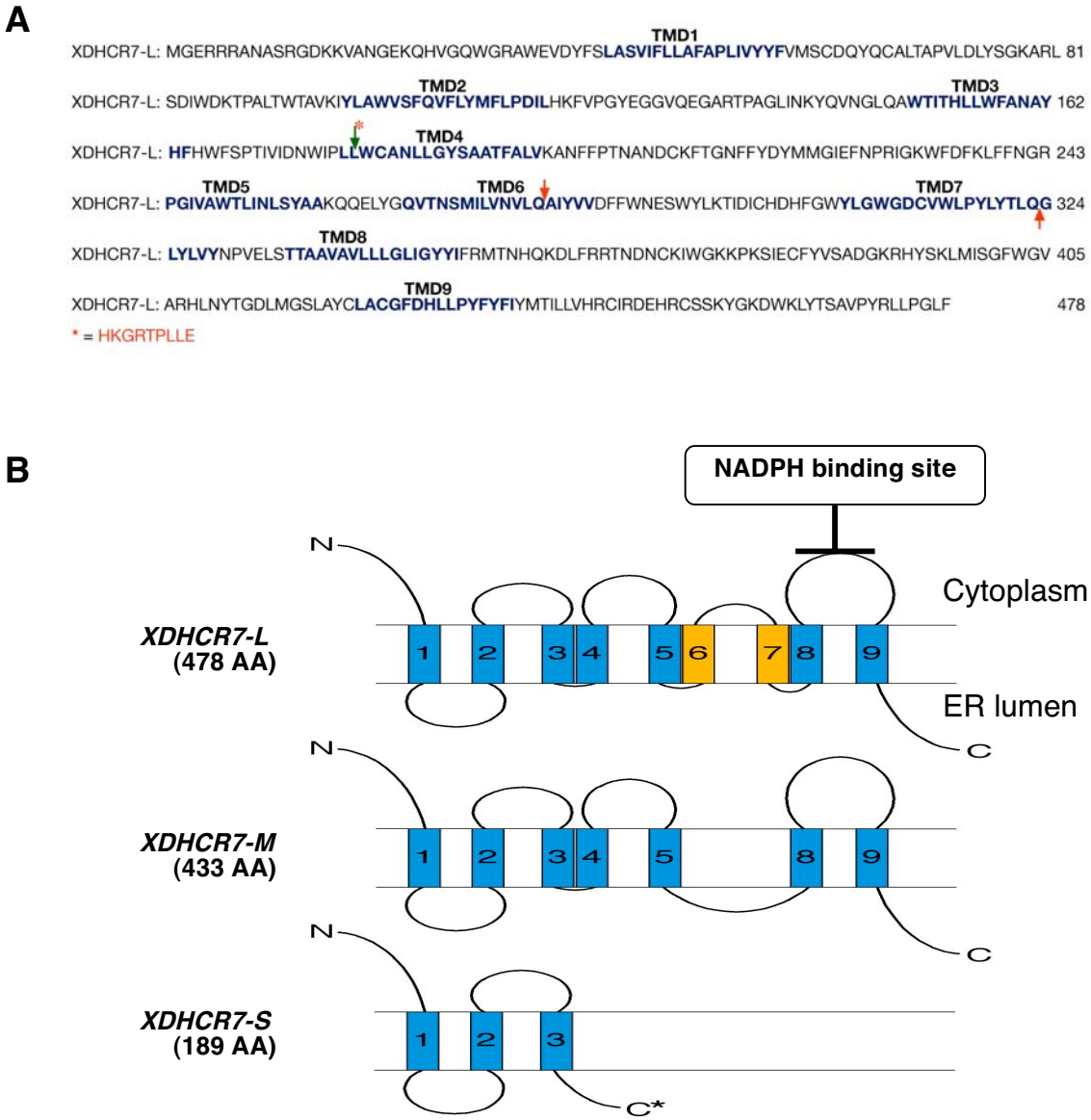

Figure 7: Predicted amino acid sequence and topology of the XDHCR7 proteins.

A) Predicted amino acid sequence of XDHCR7-L. Arrows indicate the truncated portions missing in the medium (red arrows) and the short (green arrow) isoforms. The red asterisk indicates the frame shifted N-terminal sequence of the short isoform. Residues (bold) corresponding to the transmembrane domains (TMD) were derived by comparison to the rat DHCR7 (Bae et al., 1999).
B) A proposed topology of the 3 isoforms of XDHCR7 is shown. The full length (L version) is a membrane protein with 9 putative transmembrane domains. The M isoform lacks the 6th and 7th domains, whereas the S comprises only the three first domains. The putative NADPH binding domain is indicated.

A

```
                1                 ****                                                  81
XDHCR7-L        MGERRR---------ANASRGDKK--VANGEKQHVGQWGRAWEVDYFSLASVIFLLAF-APLIVY-YFVMSCDQ--YQCAL
MDHCR7          MASKSQ---------HNAPKVKSPNG----KAGSQGQWGRAWEVDWFSLASIIFLLLF-APFIVY-YFIMACDQ--YSCSL
RDHCR7          MASKSQ---------HNASKAKNHNV----KAESQGQWGRAWEVDWFSLVSVIFLLLF-APFIVY-YFIMACDQ--YSCSL
HDHCR7          MAAKLQ---------PNIPKAKSLDGVTNDRTASQGQWGRAWEVDWFSLASVIFLLLF-APFIVY-YFIMACDQ--YSCAL
ADHCR7          MA-------------E---TVHSPIVT--------------------YASMLSLLAFCPPFVILLWYTMVHQD--GSVTQ
TDSR7           MA-------------AEAKTVHSAVVT--------------------YASMLSLLSLCPPFVILLWYTMVHAD--GSIGQ
Ce-SR           MKELNRIRRSSLGGSTSSLTRRSSISQKDIQALQETLQKQQKV---SAQMVLALLIIVPPATFFLFYSISIHTGLFVPTI
                                                                                          162
XDHCR7-L        TAPVLDLYSGKARLSDIWDKTPALTWTAVKIYLAWVSFQVFLYMFLPDILHKFVPGYEGGVQEGARTPAGLINKYQVNGL
MDHCR7          TAPALDIATGHASLADIWAKTPPVTAKAAQLYALWVSFQVLLYSWLPDFCHRFLPGYVGGVQEGAITPAGVVNKYEVNGL
RDHCR7          TAPILDVATGRASLADIWAKTPPVTAKAAQLYALWVSFQVLLYSWLPDFCHRFLPGYVGGVQEGAITPAGIVNKYEVNGL
HDHCR7          TGPVVDIVTGHARLSDIWAKTPPITRKAAQLYTLWVTFQVLLYTSLPDFCHKFLPGYVGGIQEGAVTPAGVVNKYQINGL
ADHCR7          TFGFF-WENGVQGLINIWPRPTLIAWKIIFCYG---AFEAILQLLLP-----------GKRVEGPISPAGNRPVYKANGL
TDSR7           TWDYL-RQNGLQGFIDIWPRPTVIAWKIIFCYG---AFEAALQLLLP-----------GKRVEGPISPAGNRPIYKANGL
Ce-SR           TALFLRFPLVLQCVPPVWDT---VAWKFSAVH---CAIQLIFYWVLPH-------------DQALVMSSAGDQMREVNSF
                                                                                          243
XDHCR7-L        QAWTITHLLWFANAYHFHW----FSPTIVIDNWIPLLWCANLLGYSAATFA-LVKANFFPTNAND--CKFTGNFFYDYMM
MDHCR7          QAWLITHILWFVNAYLLSW----FSPTIIFDNWIPLLWCANILGYAVSTFA-MIKGYLFPTSAED--CKFTGNFFYNYMM
RDHCR7          QAWLITHFLWFVNAYLLSW----FSPTIIFDNWIPLLWCANILGYAVSTFA-MIKGYLFPTSAED--CKFTGNFFYNYMM
HDHCR7          QAWLLTHLLWFANAHLLSW----FSPTIIFDNWIPLLWCANILGYAVSTFA-MVKGYFFPTSARD--CKFTGNFFYNYMM
ADHCR7          AAYFVTLA-----TYLGLWWFGIFNPAIVYDHLGEIFSALIFGSFIFCVLL-YIKGHVAPSSSDSGSC---GNLIIDFYW
TDSR7           AAFAVTLI-----TYLGLWWYGIFNPTIVYDHLGEIFSALIFGSFIFCIFL-YLKGHLAPSSSDSGSC---GNLIIDFYW
Ce-SR           FSCILTCLL-----YVLGASAGVYRGDLVYLHFNSII--LIFAIFAVLIWAALIATYHFGTGNSVTT-------ISEFWF
                                          ****                                  ****      324
XDHCR7-L        GIEFNPRIGKWFDFKLFFNGRPGIVAWTLINLSYAAKQQELYGQVTNSMILVNVLQAIYVVDFFWNESWYLKTIDICHDH
MDHCR7          GIEFNPRIGKWFDFKLFFNGRPGIVAWTLINLSFAAKQQELYGHVTNSMILVNVLQAIYVLDFFWNETWYLKTIDICHDH
RDHCR7          GIEFNPRIGKWFDFKLFFNGRPGIVAWTLINLSFAAKQQELYGHVTNSMILVNVLQAIYVLDFFWNETWYLKTIDICHDH
HDHCR7          GIEFNPRIGKWFDFKLFFNGRPGIVAWTLINLSFAAKQRELHSHVTNAMVLVNVLQAIYVIDFFWNETWYLKTIDICHDH
ADHCR7          GMELYPRIGKSFDIKVFTNCRFGMMSWAVLAVTYCIKQYEINGKVSDSMLVNTILMLVYVTKFFWWEAGYWNTMDIAHDR
TDSR7           GMELYPRIGKNFDIKVFTNCRFGMMSWAVLAVTYCIKQYELNGRVADSMLVSTILMLVYVTKFFWWEAGYWNTMDIAHDR
Ce-SR           GIENHPKILD-IDLKSFIRTRFTFVIWPLFVISAMYFHKITYGQISTSLVCLSSVQLLYIFQFHWNEDLFLNSLDSKRCD
                                                                                          405
XDHCR7-L        FGWYLGWGDC-VWLPYLYTLQGLYLVYNPVELSTTAAVAVLLLGLIGYYIFRMTNHQKDLFRRTNDNCKIWGKKPKSIEC
MDHCR7          FGWYLGWGDC-VWLPYLYTLQGLYLVYHPVQLSTPNALGILLLGLVGYYIFRMTNHQKDLFRRTDGRCLIWGKKPKAIEC
RDHCR7          FGWYLGWGDC-VWLPYLYTLQGLYLVYHPVQLSTPNALGVLLLGLVGYYIFRMTNHQKDLFRRTDGHCLIWGKKPKAIEC
HDHCR7          FGWYLGWGDC-VWLPYLYTLQGLYLVYHPVQLSTPHAVGVLLLGLVGYYIFRVANHQKDLFRRTDGRCLIWGRKPKVIEC
ADHCR7          AGFYICWG-CLVWVPSVYTSPGMYLVNHPVELGTQLAIYILVAGILCIYINYDCDRQRQEFRRTNGKCLVWGRAPSKIVA
TDSR7           AGFYICWG-CLVWVPSIYTSPGMYLVNHPVDLGTQLAIYILVAGILCIYINYDCDRQRQEFRRTNGKCTVWGKSPSKILA
Ce-SR           FGFYRIWAD-FVLGPIIYTSPVTILVATNRSVGVISNCLFCAVAIGSMVFTAKCDRQKYEFRKSKGTLKVGGVDAFFISA
                                          ****                                          484
XDHCR7-L        FYVSADGKRHYSKLMISGFWGVARHLNYTGDLMGSLAYCLACGFDHLLPYFYFIYMTILLVHRCIRDEHRCSSKYGKDWK
MDHCR7          SYTSADGLKHHSKLLVSGFWGVARHFNYTGDLMGSLAYCLACGGGHLLPYFYIIYMTILLTHRCLRDEHRCANKYGRDWE
RDHCR7          SYTSADGLKHRSKLLVSGFWGVARHFNYTGDLMGSLAYCLACGGGHLLPYFYIIYMTILLTHRCLRDEHRCANKYGRDWE
HDHCR7          SYTSADGQRHHSKLLVSGFWGVARHFNYVGDLMGSLAYCLACGGGHLLPYFYIIYMAILLTHRCLRDEHRCASKYGRDWE
ADHCR7          SYTTTSGETKTSLLLTSGWWGLARHFHYVPEILSAFFWTVPALFDNFLAYFYVIFLTLLLFDRAKRDDDRCRSKYGKYWK
TDSR7           SYTTTSGETKSSLLLTSGWWGLARHFHYVPEILSAFFWTVPALFNHVLPYFYVVFLTILLFDRAKRDDDRCRSKYGKYWK
Ce-SR           KYRTDSGDANTNLLLGSGHWGVCRHPNYASEAITFAAFSAFQGFPSTIAHIPSLFVILFLVARAFTDENRCLIKYGQYWA
                                  495
XDHCR7-L        LYTSAVPYRLLPGLF
MDHCR7          RYTAAVPYRLLPGIF
RDHCR7          RYVAAVPYRLLPGIF
HDHCR7          RYTAAVPYRLLPGIF
ADHCR7          LYCEKVKYRIIPGIY
TDSR7           LYCQRVPYKIIPGIY
Ce-SR           QYCSKVKYRFLPGVF
```

B

Percent Similarity

	1	2	3	4	5	6	7		
1		76.0	76.0	75.1	31.9	32.2	20.6	1	XDHCR7-L
2	23.7		96.4	87.9	32.6	33.3	20.8	2	MDHCR7
3	23.5	3.6		86.6	32.2	32.9	20.4	3	RDHCR7
4	24.5	11.5	13.0		32.2	32.0	21.4	4	HDHCR7
5	62.5	61.5	62.0	61.9		88.0	25.7	5	ADHCR7
6	62.0	60.1	60.6	61.5	11.8		24.4	6	TDSR7
7	74.7	75.5	75.1	76.4	70.2	72.3		7	Ce-SR
	1	2	3	4	5	6	7		

Percent Divergence

Figure 8: Alignment of XDHCR7 with Δ^7-sterol reductases from other species.

A) An alignment of XDHCR7 protein with Δ^7-sterol reductases from mouse (MDHCR7), rat (RDHCR7), human (HDHCR7), thale cress (ADHCR7, from Arabidopsis thaliana), nasturtium (TDSR7, from Tropaeolum majus), and worm (Ce-SR) is shown. The overall sequence appears to be highly conserved between *Xenopus*, human, rat and mouse (vertebrates), and much less between plant (thale cress and naturtium) and vertebrates. Black asterisks indicate potential N-linked glycosilation sites, transmembrane domains are marked as bold residues. The grey highlight indicates the putative sterol-sensing domain (SSD). Boxed are residues corresponding to a putative N-myristilation site.

B) The *Xenopus* DHCR7 protein shares strong identity with mouse (76 %), rat (76 %) and human (75.1 %) homologues. The sequence homology is lower with plant Δ^7-sterol reductases, represented here by the nasturtium (32.2 %) and the thale cress (31,9 %).

II.2. Temporal and spatial expression of the *Xenopus* dhcr7.

In order to analyse the expression pattern of Xdhcr7, a pGEM-T construct of Xdhcr7-S was linearized and used as template to synthesize a digoxiginine-labelled antisense RNA, which was further used as probe in whole mount in situ hybridization (WMISH) analysis. Embryos were staged according to Nieuwkoop´s table of *Xenopus* development (Nieuwkoop and Faber, 1975). In parallel, total RNA was extracted from consecutive embryonic stages, and from different adults frog tissues. cDNA was synthesised using random hexamer, and further PCR analysis was carried out using primers specific to Xdhcr7, *Xenopus* sonic hedgehog (Xshh) and *Xenopus* histone 4 (H4) genes. The amount of cDNA per PCR reaction was an equivalent of 25 ng of total RNA, and one half of each reaction was analysed on a 2 % agarose gel.

By RT-PCR, the Xdhcr7 transcripts can already be detected in the unfertilised egg (Fig. 9A). This maternal level of Xdhcr7 mRNA is maintained until the start of gastrulation (stage 10), and shows a strong activation that decreases by stage 28. Interestingly, the increase of Xdhcr7 expression coincides with the start of Xshh expression. In adult tissues (Fig. 9B), Xdhcr7 is highly expressed in ectoderm-derived tissues (brain, eye, spinal chord and skin), and less constantly in mesodermal and endodermal derivatives. Xshh also shares this tissue distribution.

By WMISH (Fig. 10 and Fig 11), the expression of Xdhcr7 is first visible at the onset of gastrulation (stage 10.5), in the dorsal blastopore lip (Fig. 10a). As gastrulation proceeds (stages 11 – 13), the expression of Xdhcr7 is activated from posterior to anterior in the forming dorsal midline (Fig. 10b – e), and is revealed in the floor of the neural groove by neurula stages (Fig. 10f – h). On transversal sections of stage 14 and stage 20 embryos (Fig. 11a1 and 11b1) the Xdhcr7 transcripts can be revealed exclusively in the notochord.

As organogenesis proceeds, by tailbud stages (23 – 30), Xdhcr7 gains additional expression territories (Fig. 10i – k´´), and can then be revealed in the brain, the spinal cord, the olfactory placode, the epibranchial placodes, the optic nerve, the otic vesicle, the optic vesicle and at the boarder of the cement gland. A close look at the expression at stage 23 and stage 30 reveals an interestingly dynamic expression in the midline. On transversal sections of stage 23 (Fig. 11c), from anterior to posterior, Xdhcr7 transcripts are revealed in the notochord, subnotochordal rod (hypochord) and interneurons (Fig. 11c1 – 11c1´), the interneurons and notochord (Fig. 11c2 – 11c2´), and notochord only

(Fig. 11c5 – 11c5´). By stage 30 (Fig. 11e), where staining can also be seen in the lateral placode (lp, fig. 11e1) and otic vesicle (ot, fig. 11e2), the same dynamic expression pattern is maintained. Interestingly, the expression in the neural tube seems to be gradually lost posteriorly.

At late tailbud stage (st. 36), the expression of Xdhcr7 is restricted to the head, mostly to neural structures and neural derivatives (fig. 10l – l´´). On transversal sections (Fig. 11f1 – f4), expression is revealed in the dorsal neural tube (nt), the eye (ey), the branchial arches (ba) and the otic vesicle (ot). A horizontal section through the brain (Fig. 11g1) shows a continuous expression in the forebrain (fb), midbrain (mb) and hindbrain (hb). Interestingly, no expression is revealed in the notochord at this stage.

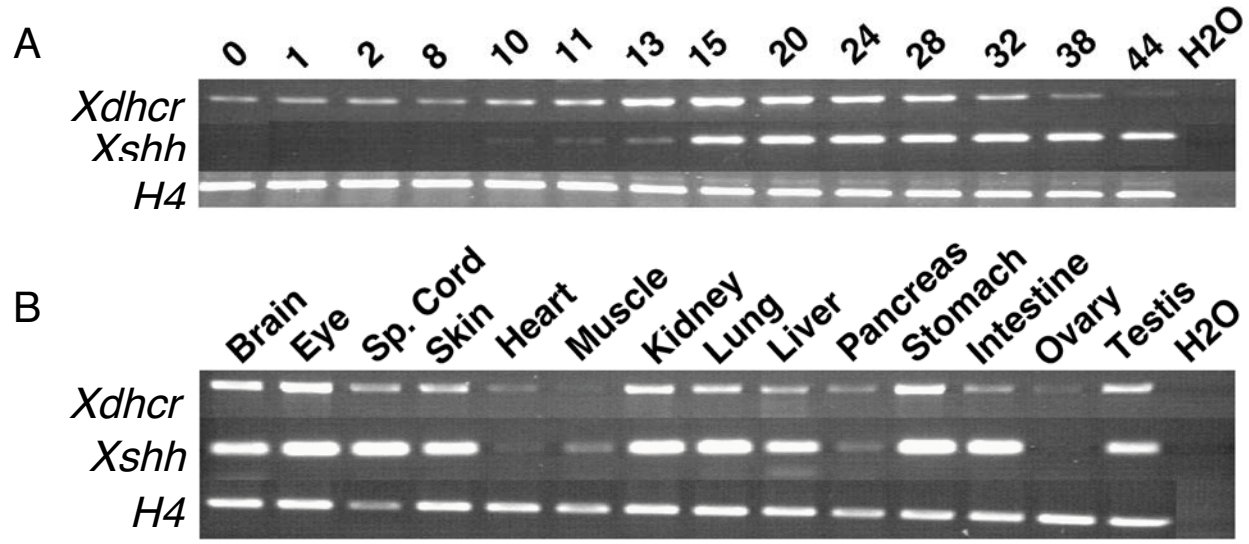

Figure 9: RT-PCR analysis of *Xdhcr7* expression in comparison to *Xshh*
A) The *Xdhcr7* mRNA is already detectable in the unfertilized egg (stage O); its expression shows an activation by the end of gastrulation (stage 11), and this activation is maintained during the neurulation processes and the beginning of organogenesis (stage 28). This activation of the *Xdhcr7* expression matches with the onset of *Xshh* expression, as can be shown by the expression of *Xshh,* which is visible by stage 10.
B) In the adult frog, the *Xdhcr7* is expressed mostly in ectoderm-derived tissues like brain, eye, spinal cord and skin, and is more or least present in the rest. Like the developmental expression (A), this spatial distribution in the adult frog also matches the expression of *Xshh.*
The H4 primers were used as RNA loading control.

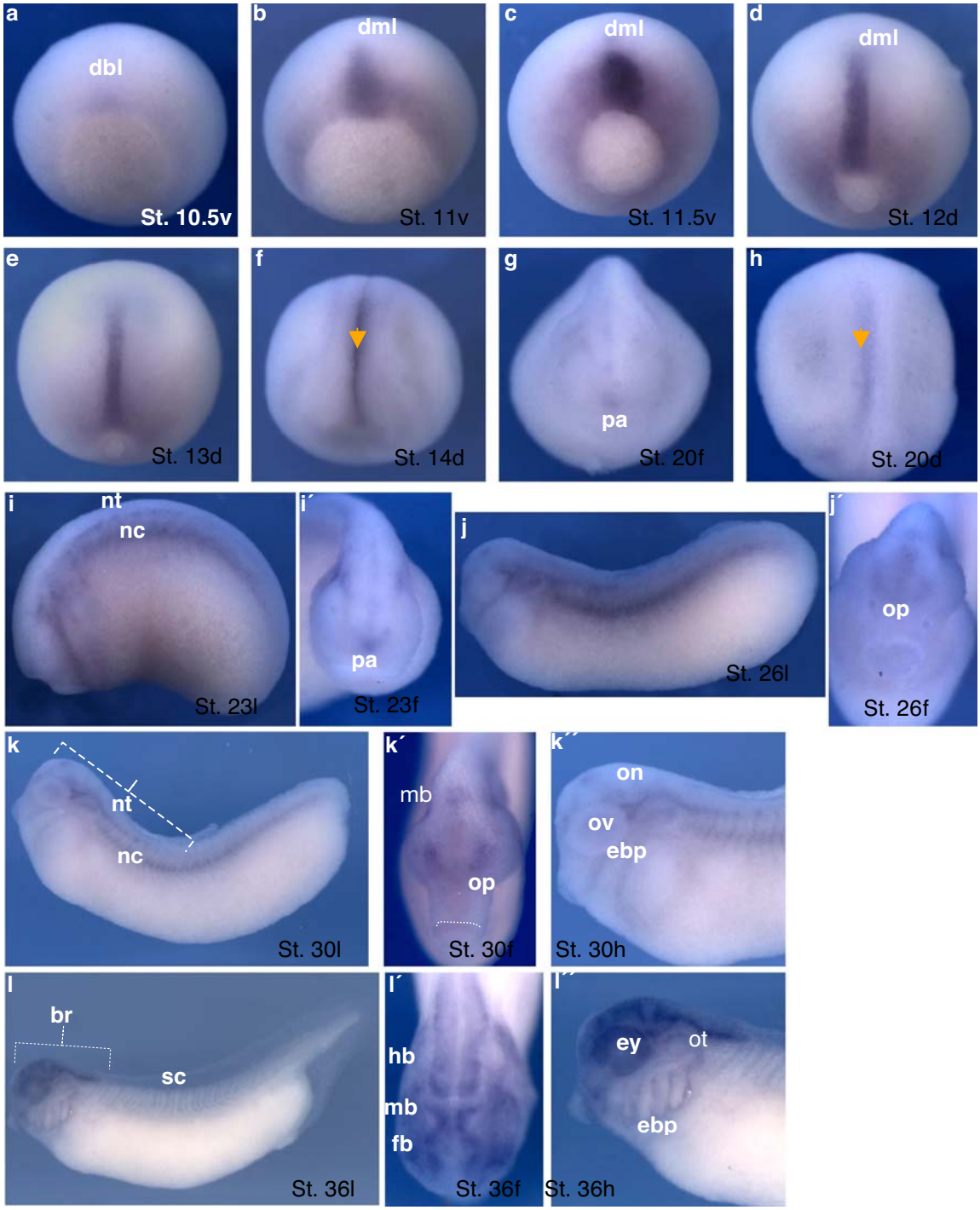

Figure 10: Overview of the WMISH analysis of Xdhcr7 expression

a - c: vegetal view (dorsal up) of gastrula stage embryos; d and e: dorsal view (anterior up) of late gastrula stage embryos; f and h: dorsal view (anterior down) of neurula stage embryos; i, j, k and l: lateral view (dorsal up, anterior to the left) of stage 23, 25, 30 and 36 embryos; g, i´, j´, k´´and i´´: frontal view (dorsal up) of stage 20, 23, 25, 30 and 36 embryos; k´and l´: magnifications of the head portions of k and l. During gastrulation and neurulation, Xdhcr7 transcripts are first visible in the dorsal blastopore lip (dbl) by stage 10.5, then in the forming dorsal midline (dml) by stage 12 – 13, and later in the floor of the neural groove (orange arrows) by stage 14 - 20. By early tailbud stage (st.25 – 30), the expression can be seen in the notochord (nc), the neural tube (nt), the epibranchial placodes (ebp), the olfactory placodes and the optic nerve (on). By late tailbud stage (st.36) this expression is more restricted to head structures. The following structures are also shown: pituitary anlage (pa), optic vesicle (ov), cement gland (cg), forebrain (fb), midbrain (mb), hindbrain (hb), eye (ey) and spinal chord (sc).

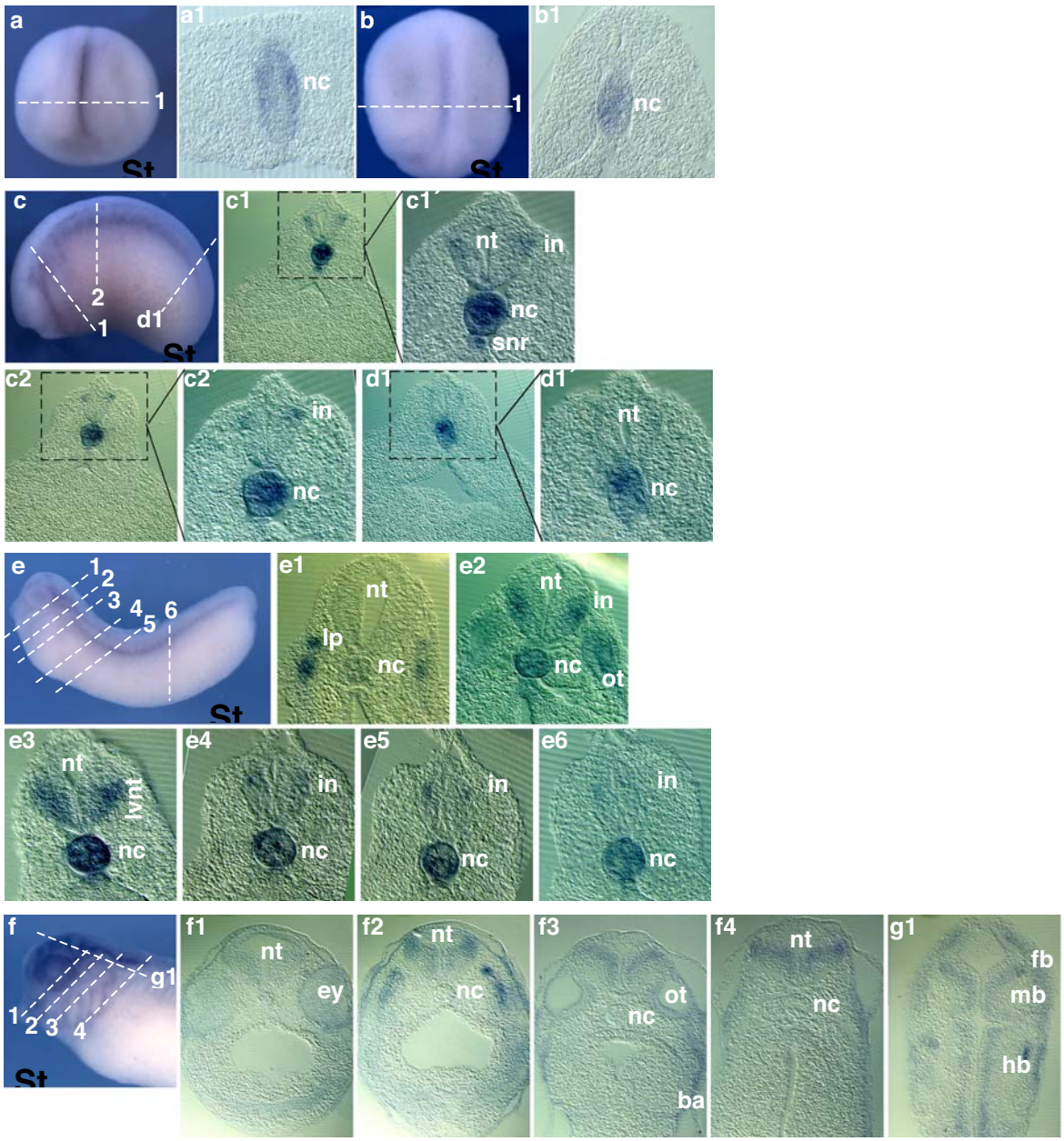

Figure 11: Sections of selected stages of Xdhcr7 expression

a1-f4: transversal sections of stage 14 (a1), 20 (b1), 23 (c1 – d1), 30 (e1 – e6) and 36 (f1 – f4) embryos. Sections are arranged from anterior to posterior, with dorsal side up. Section d1 is from a different embryo of the same stage as the embryo shown on c (st. 23). c1´, c2´ and d1´: magnification of c1, c2 and d1. g1: horizontal section (anterior up) of a stage 36 embryo showing the expression of xdhcr7 in the three lobes of the brain.

The staining demarcates the whole notochord (nc) at neurula stages (14 – 20: a1 and b1); during early tailbud stages (23 – 30: c and d), additional staining can be seen in dorsal neural tube (nt), at the position corresponding to inter neurons (in) at stage 23 (c1´and c2´), the lateral ventral neural tube at stage 30 (lvnt, e3). The subnotochordal rod (snr, c1´), the lateral placode (lp, c1) and the otic vesicle (ot, e2) are stained as well. With development, the expression in the spinal chord decreases from anterior to posterior. At late tailbud stage (36: f), the Xdhcr7 stains most of the head structures, comprising the brain and the eye (ey, f1). The expression is severely reduced in the notochord (nc, f2-f4) at this stage.

The active form of the morphogene protein Sonic hedgehog (SHH) is cholesterol-modified (Mann and Beachy, 2000); the steroidogenic acute regulatory (STAR) protein regulates steroid hormone biogenesis by binding and translocating cholesterol to the inner mitochondrial membrane of steroidogenic cell (Petrescu et al., 2001; Christenson and Straus, 2000; Tsujishita and Hurley, 2000). A *Xenopus* StAR-like cDNA (*XstAR*) has been isolated in our group by Souopgui and colleagues (2004, unpublished data) in a screen for neurally enriched transcripts. A comparative look at the expression pattern of *Xdhcr7*, *Xenopus* shh (*Xshh*; Ruiz i Altaba et al., 1995) and *Xenopus* stAR (*XstAR*) could then bring new insights into the correlation between cholesterol biosynthesis and function.

Like *Xshh*, *Xdhcr7* is expressed in the dorsal midline at neural folds stage (Fig. 12a and a´); however, this expression is excluded from the prechordal plate where *Xshh* is highly expressed. A section of a stage 30 embryo (Fig. 7b and b´) shows *Xshh* and *Xdhcr7* expression in close vicinity, but in a partially overlapping manner. Hence, while *Xdhcr7* is expressed in the notochord and in motor neurons, *Xshh* is expressed in the notochord and floor plate. The early expression (late gastrula and early neurula stage) of *XstAR* is localised bilaterally in the presomitic mesoderm, at a time when *Xdhcr7* expression domain is restricted to the dorsal midline (Fig. 12c-d and 12c´- d´). At stage 20 (Fig. 12e and e´), the anterior domain of *XstAR* expression comprises two bilateral strips at the inner boarders of the neural folds (red arrows), whereas *Xdhcr7* is expressed in the pituitary anlage (pa), the neural groove and the deuterencephalon (red arrowheads). At tailbud stage (Fig. 12f and f´) the facial expression domain of *Xdhcr7* comprises the olfactory placode, and a ring around the cement gland (red arrowhead); on the other hand, *XstAR* is revealed in a domain between the two expression domains of *Xdhcr7*, at the level of the stomodeal-hypophyseal anlage. Unlike *Xshh*, *XstAR* does not seem to co-express with Xdhcr7; however, their expression domains are distributed in interestingly tight vicinity.

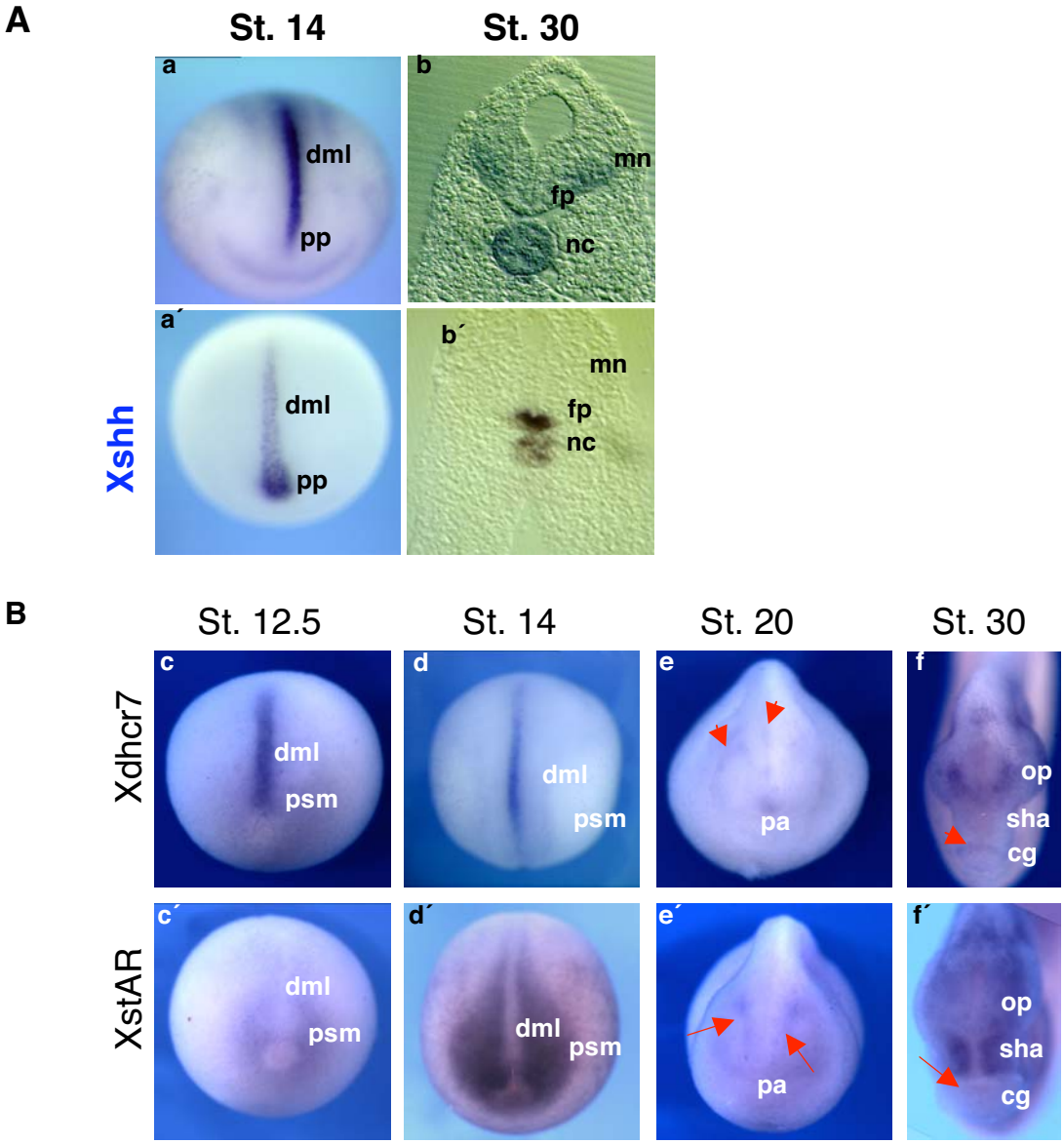

Figure. 12: WMISH analysis of *Xdhcr7* expression in comparison with *Xshh* and *XstAR*.
a and a´: anterior view (dorsal up) of stage 14 embryos showing the expression of *Xdhcr7* and *Xshh* respectively. b and b´: transversal sections of stage 30 embryos showing the expression of *Xdhcr7* and *Xshh* respectively. c-d, and c´-d´: dorsal view (anterior up) of late gastrula and early neurula stage embryos showing the expression of *Xdhcr7* and *XstAR* respectively. e-f, and e´-f´: dorsal view (anterior up) of late neurula (e and e´) and tailbud (f and f´) stage embryos showing the expression of *Xdhcr7* and *XstAR* respectively.
At stage 14, *Xdhcr7* stains the dorsal midline, the same as for *Xshh*. But unlike *Xshh*, no *Xdhcr7* staining is revealed in the prechordal plate (pp). A section of a stage 30 embryo shows *Xshh* expression in the notochord and floor plate, whereas expression of *Xdhcr7* is revealed in the notochord and in motor neurons.
Unlike *Xdhcr7*, the *XstAR* transcript is expressed in the presomitic mesoderm (psm), and not in the midline during gastrula and early neurula stages. An anterior view of stage 20 embryos (e and e´) shows the expression of *XstAR* in two bilateral strips at the inner boarders of the neural folds (red arrows in e´), and *Xdhcr7* expression in the pituitary anlage (pa), the neural groove and the deuterencephalon (red arrowheads in e). A facial view of stage 30 embryos (f and f´) shows the expression of *XstAR* in the stomodeal-hypophyseal anlage (sha); *Xdhcr7* is revealed in the olfactory placodes (op), and in a ring around the cement gland (red arrowhead in f), from where the expression of *XstAR* is excluded (red arrow in f´).

II.3. Functional characterisation dhcr7 in *Xenopus*.

II.3.1. Gain-of-function analysis of dhcr7

The Xdchr7 is expressed in the Spemann organizer and the notochord, which are important organising centers. This suggests a potential role for XDHCR7 in pattern formation and / or organogenesis. The expression of Xdhcr7 in the eye points at this organ as a suitable candidate for analysing the role played by dhcr7 during *Xenopus* development. To address this issue, the three Xdhcr7 isoforms (L, M and S) were subcloned into pCS2+ vector as EcoRI / XbaI fragments. Beside, the ORF of the mouse dhcr7 (Mdhcr7) was cloned as a pCS2+ recombinant plasmid. The constructs were tested in transcription translation (TnT) assays for DHCR7 proteins synthesis. Results obtained (Fig. 13, lanes 1-7) confirmed the synthesis of proteins of expected molecular weight in TnT. In order to investigate the activity of dhcr7 during development, the pCS2+ recombinant plasmids were linearized and used as templates to prepare cap-mRNAs, which were microinjected into one (or two) blastomere(s), of two-cell stage *Xenopus* embryos.

The injections were optimised by testing different concentrations of each cap-mRNA (results not shown), and the following amounts were found to be optimal: 2 ng per embryo for Xdhcr7-L, Xdhcr7-M and Mdhcr7, and 750 pg per embryo for Xdhcr7-S. Each tested cap-mRNA was injected in combination with nuclear-β-galatosidase (n-β-Gal) cap-mRNA, as linage tracer.

For phenotypic analysis purpose, injected (pigmented) embryos were fixed at tadpole stage (NF st. 43 / 44), stained with X-gal, and scored for eye phenotypes. For WMISH analysis purpose, injected (albino) embryos were fixed at open neural plate (NF st. 14 / 15) and tailbud (NF st. 32 / 34) stages, stained with X-gal and analysed with selected molecular markers.

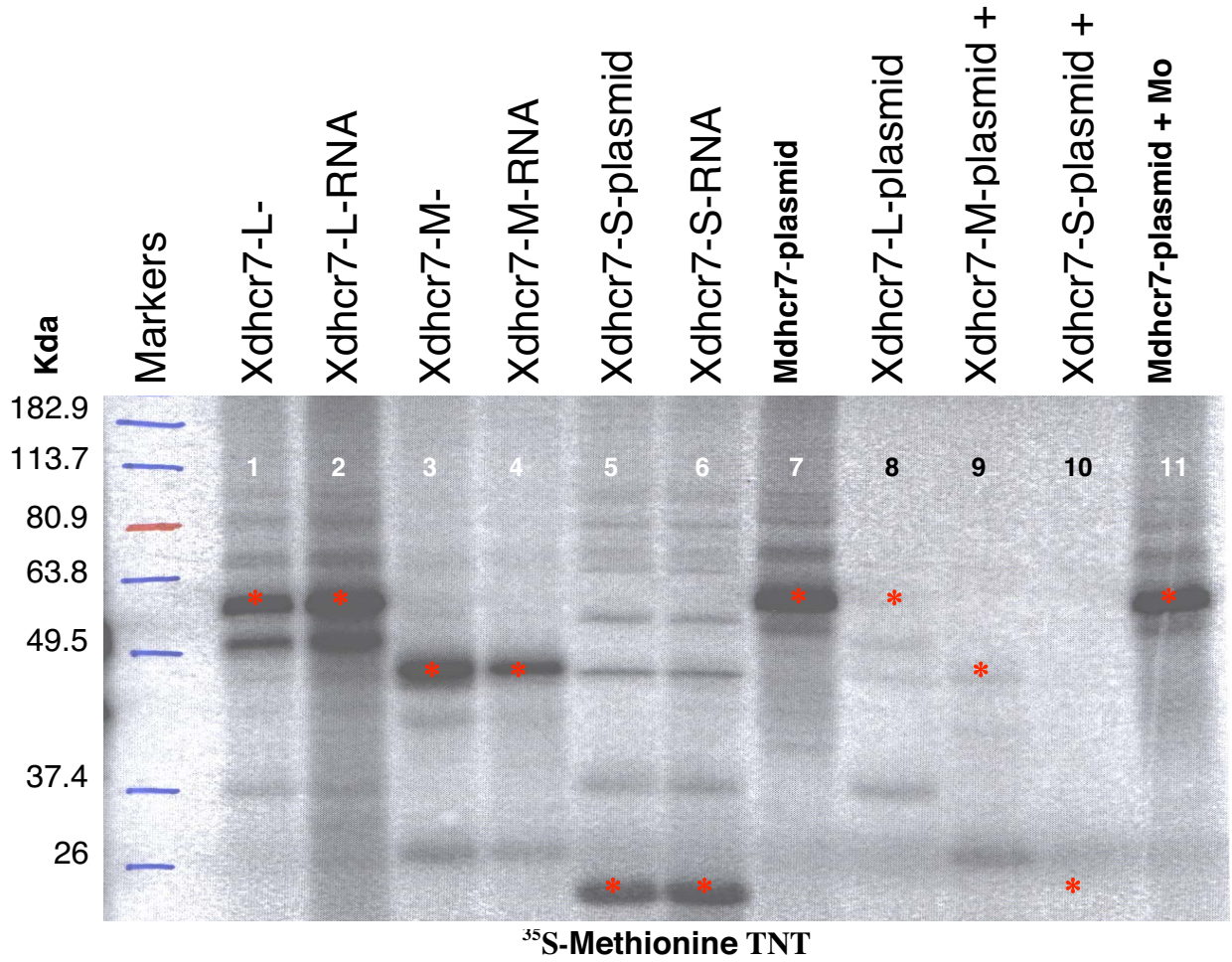

Figure 13: Control of dhcr7 expression constructs in the transcription and translation (TnT) system
500 pg of pCS2+ construct (plasmid) or capped-RNA (RNA) of each Xdhcr7 isoforms, as well as the mouse homolog was incubated in the TnT reaction system (Promega) containing a supplement of radio-labeled methionine (^{35}S-Methionine). Alternatively, 500 pmol of Xdhcr7-morpholino (Mo) oligos were incubated in combination with the plasmid to control the XDHCR7 protein synthesis inhibitory activity of the morpholino. The TnT reaction was resolved on a 12 % polyacrylamide gel, along with a prestained marker set. After separation, the gel was dried and scanned by mean of a phosphoimager. The positions of the Kda markers were identified by direct tracing from the dried gel.
Lanes 1-6 show the synthesis of XDHCR7-L (54 Kda), XDHCR7- M (49 Kda) and XDHCR7-S (21 Kda) proteins both from RNA and plasmid. The mouse construct can also drive the synthesis of a 54 Kda protein in the system (lane 7).
Lanes 8-10 show the inhibition of the protein from synthesis of all three Xdhcr7 plasmid constructs by the Xdhcr7-morpholino. The specificity of the morpholino to the Xdhcr7 is proven by an absence of inhibitory activity on the mouse dhcr7 construct (lane 11).

,II.3.1.1. The overexpression of Xdhcr7 interferes with eye development.

Upon overexpression, the Xdhcr7 isoforms show differential effects on eye development. Up to 2 ng of Xdhcr7-M cap-mRNA causes no visible developmental defect (n = 200) (Fig. 14a – a´´). Apart from massive gastrulation defect, higher amount (3 ng) did not show any characteristic effect. When overexpressed at a concentration of 1 ng per embryo, Xdhcr7-S caused almost 100 % death by stage 9, with a characteristic cell proliferation arrest activity (not shown). At a concentration of 750 pg of Xdhcr7-S RNA per embryo, (37.5 %, n = 75 / 200) of the injected embryos showed a reduced eye phenotype (Fig. 14 b – b´´). The small eyes were medially shifted (30 %, n = 60 / 200), but transversal section through the control and injected eyes did not show any structural difference (Fig. 14 b´1 and b´2). The small eye phenotype was also observed in 39.5 % (n = 79 / 200) of the embryos injected with 2 ng of Xdhcr7-L (Fig. 14c – c´´). Although no structural difference was seen between the control and injected eyes in most of the cases (Fig. 14c´1and c´2), 25 % (n = 50 / 200) of the injected embryos showed in addition a thickened and retinal-pigmented eye stalk on the injected side (Fig. 14d). The injection of 2 ng of mouse dhcr7 (Fig. 14e – f) resulted in the same phenotypes as for Xdhcr7-L. However, Mdhcr7 caused more severe and more frequent phenotypes. (55%, n = 110 / 200) showed small eye phenotype, with 20 % (n = 40 / 200) severe; 30 % (n = 60 / 200) showed a retinal pigmentation of the eye stalk. For a significant number of embryos, more pigment was seen on the injected side of the head compared to the control side (not shown). Overall the truncation of the most of the c-terminus end of the XDHCR7 renders the protein toxic, whereas the lost of the 6^{th} and 7^{th} TMDs renders it rather less active.

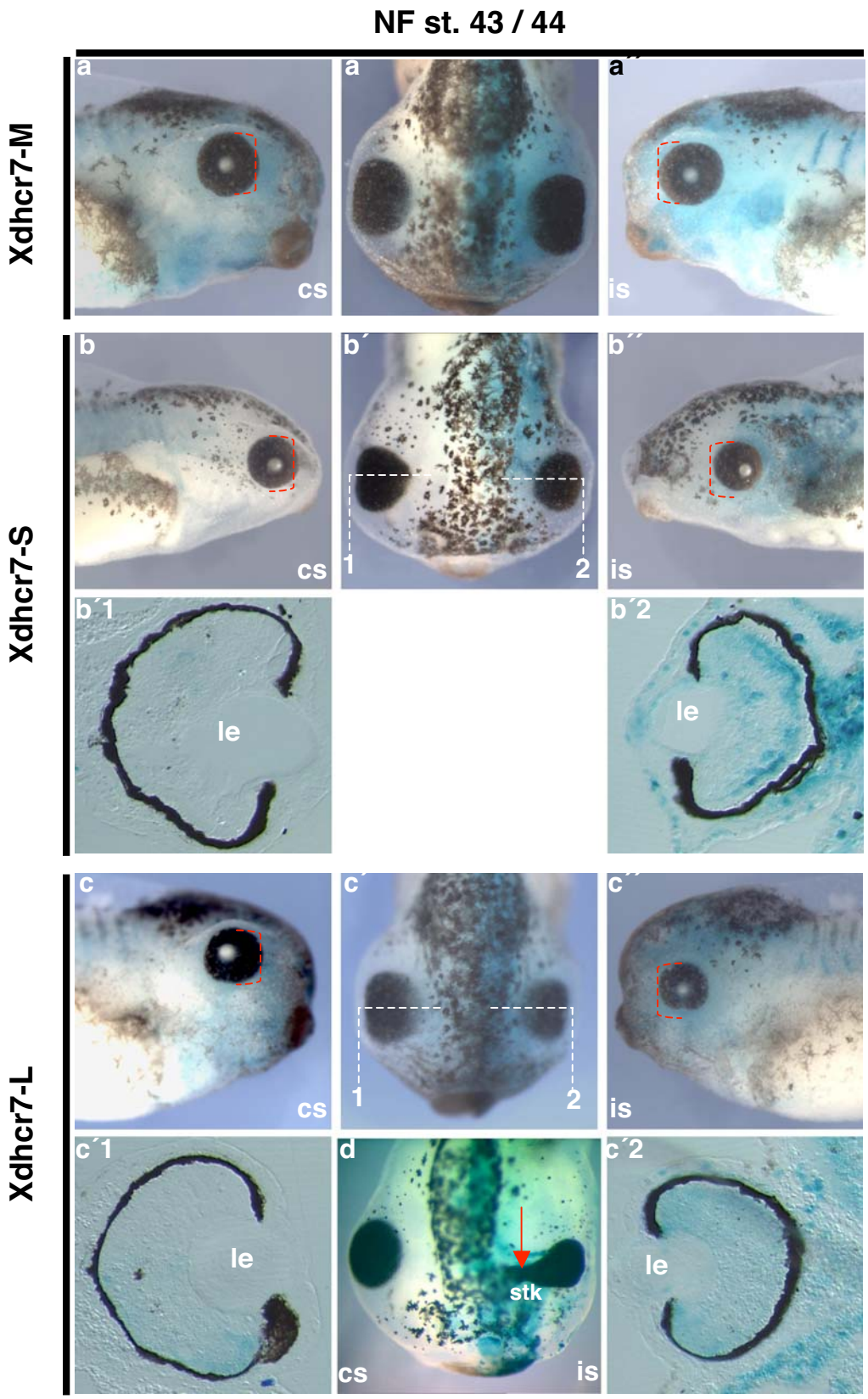
NF st. 43 / 44
Xdhcr7-M
Xdhcr7-S
Xdhcr7-L
a
a´
a´´
cs
is
b
b´
b´´
1
2
b´1
b´2
le
c
c´
c´´
c´1
c´2
d
stk

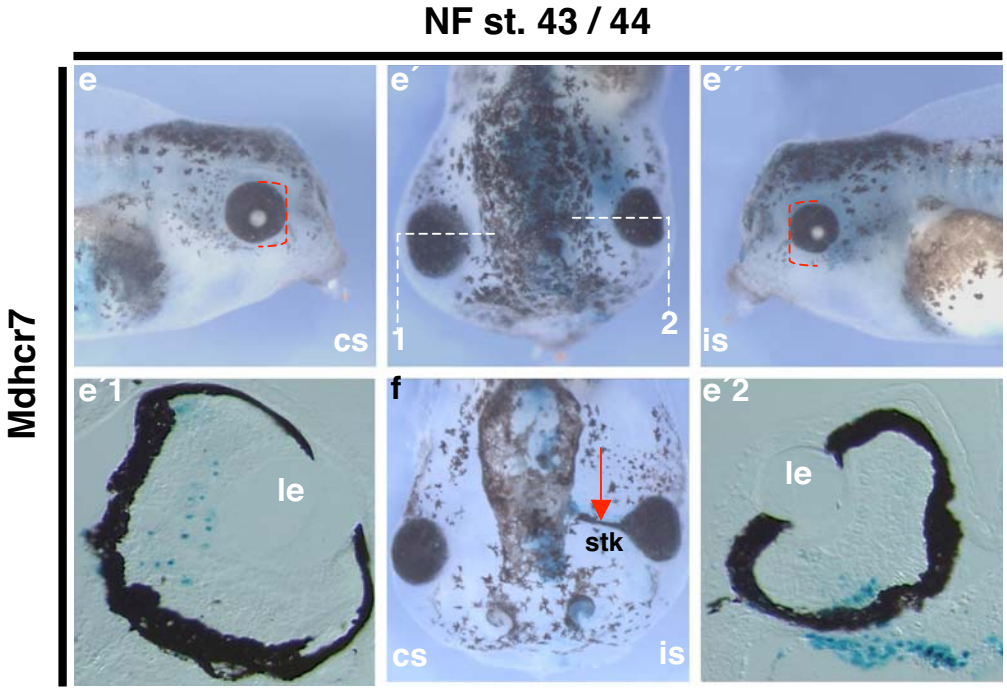

Figure 14: The overexpression of Xdhcr7 interferes with eye development.
a, b , c, e, a´´, b´´, c´´, and e´´: side view (head region) of tadpole stage injected embryos.
a´, b´, c´, d, e´ f: dorsal view of injected embryos. "is" indicates the injected side (blue staining), and "cs" indicates the control (non injected) side of the same embryo. b´1, b´2, c´1, c´2, e´1and e´2: magnification of the eyes as viewed on transversal section.
Two-cell stage pigmented embryos were injected (in one of two blastomers) with 2 ng of Xdhcr7-M, 750 pg of Xdhcr7-S, 2 ng of Xdhcr7-L or 2 ng of Mdhcr7 capped RNA, combination with 200pg of n-β-Gal capped RNA as linage tracer. Injected embryos were cultured in 0.1 X MBS until tadpole stage (NF st. 43 / 44), fixed in MEMFA, and recorded for eye phenotypes after X-gal staining (blue colour).
Injection of 2 ng of dhcr7-M (a – a´´) did not result in any visible eye phenotype.
Injection of 750 pg of Xdhcr7-S resulted in small eye phenotype (b – b´´), with no obvious structural defect.
In addition to small eye phenotype, injection of 2 ng of Xdhcr7-L (c – d) resulted in retinal pigmentation of the optic stalk (red arrow in d). On transversal section (c´1 and c´2), no obvious structural defect can be seen in the small (injected) eye as compared to the control eye. The same phenotypes were obtained upon injection of 2 ng of mouse dhcr7 (e – f). The following structures are indicated: eye stalk (stk), lens (le) and retina (re).

II.3.1.2.The overexpression of Xdhcr7 interferes with the late expression of eye marker genes.

In summary, apart from the medium version, which showed no phenotype, the Xdhcr7 isoforms as well as the mouse homolog impaired eye development upon overexpression. Since the eye develops as part of the brain, we hypothesised that these phenotypes could result either from an impairment of the development of the whole brain, or from a specific effect on the development of the eye. To assess this hypothesis, we perform WMISH analysis on neurula and tailbud stage injected embryos, using *Xrx1* (Fig. 15, red arrowheads) and *Xsix3* (Fig. 16) as eye markers, and *Xen2* (Fig. 15, green arrowheads)

and *Xkrox20* (Fig. 15, white arrowheads) as brain boundaries markers. As could be expected with regard to the phenotypic analysis, the overexpression of Xdhcr7-M (Fig. 15a – b´´) did not interfere with the expression of any of these markers. The overexpression of Xdhcr7-S did not cause any change to the early expression of *Xrx1*, *Xen2* and *Xkrox20* (Fig. 15c). At tailbud stage (Fig. 15d – d´´), Xdhcr7-S injected embryos displayed a significant reduction of *Xrx1* expression domain (29.6 %, n = 8 / 30), with no change on the expression of *Xen2* and *Xkrox20.* Although Xdhcr7-L (Fig. 15c – c´´) and Mdhcr7 (Fig. 15d – d´´) caused a minor reduction of *Xkrox20* expression in the 5th rhombomere, at neurula stage (20 %, n = 5 / 25 and 24 %, n = 6 / 25 respectively), no significant changes could be seen either of the later expression of *Xkrox20* or of the expression of *Xen2*. The expression domain of Xrx1 was reduced in 40 % (n = 12 / 30) of embryos injected with Xdhcr7-L (Fig. 15f – f´´), and in 43.33 % (n = 13 / 30) of those injected with Mdhcr7 (Fig. 15h – h´´). Like for *Xrx1*, *Xsix3´*s expression did not show any change upon overexpression of Xdhcr7-M (Fig. 16a – b´´). Upon overexpression of Xdhcr7-s, the early expression of *Xsix3* (Fig. 16c) did not show any significant change. However, when analysed at tailbud stage (Fig. 16 d – d´´), the Xdhcr7-S injected embryos showed a severe reduction of *Xsix3* expression level (61.5 %, n = 16 / 26). A significant number (19.2 % n = 5 / 26) of Xdhcr7-L injected embryos displayed a minor ectopic expression of Xsix3 in the presumptive lens placode at neural plate stage (red arrowhead in fig. 16e). However, at tailbud stage (Fig. 16f – f´´), the Xdhcr7-L injected embryos showed rather a severe reduction of *Xsix3* expression (48 %, n = 12 / 25). Mdhcr7 caused no change to *Xsix3* expression at neurula stage (Fig. 16g), but a severe reduction of *Xsix3* expression (60 %, n = 18 / 30) was noted for the injected embryos that were analysed at tailbud stage (Fig 16h – h´´).

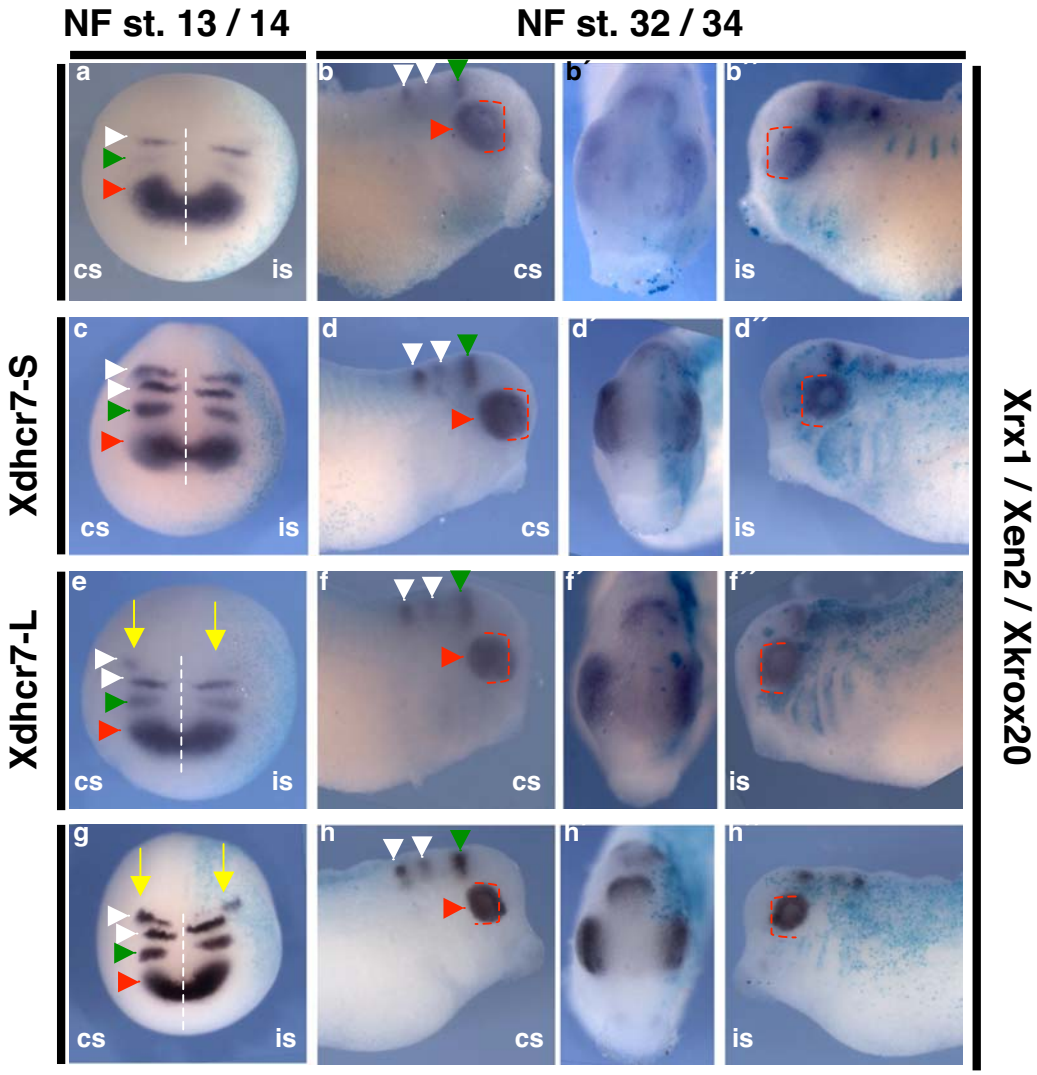

Figure 15: The overexpression of Xdhcr7 causes a reduction of *Xrx1* expression domain.
WMISH of *Xrx1* (red arrowheads), *Xen2* (green arrowheads) and *Xkrox20* (white arrowheads) are shown. a, c, e, and g: anterior views (dorsal up) of stage 14 embryos ; the white dashes indicate the position of the midline. b, b´´, d, d´´, f, f´´, h and h´´ : side views of stage 32 embryos. The frontal views are shown in b´, d´, f´ and h´. All embryos are shown with the non injected control side (cs) to the left and injected side (is, blue staining) to the right.
Two-cell stage albino embryos were injected (in one of two blastomers) with 2 ng of Xdhcr7-M, 750 pg of Xdhcr7-S, 2 ng of Xdhcr7-L or 2 ng of Mdhcr7 capped RNA, in combination with 200pg of n- -Gal capped RNA as linage tracer. Injected embryos were cultured in 0.1 X MBS until opened neural plate (NF st. 13 / 14) or tailbud stage (NF st. 32 / 32), fixed in MEMFA, and hybridized with a mixture of Dig-labelled *Xrx1*, *Xen2* and *Xkrox20* antisense RNAs, after X-gal staining (blue color). Injection of 2 ng of Xdhcr7-M (a – b´´) did not interfere with either the expression of *Xrx1,* or with that of *Xen2* or *Xkrox20.* As shown with red dashed in b and b´´, the expression domain of *Xrx1* on the injected side (is) was of the same size as that of the control side (cs). Upon injection of 750 pg of Xdhcr7-S capped RNA, the expression of *Xrx1* showed no disturbance at neural plate stage (c). However, at tailbud stage, the injected side (is, c´´) showed a smaller *Xrx1* expression domain, as compared (red dashes) to the control side (cs, c). The expression of *Xen2* and *Xkrxo20* showed no change at either of the analysed stages. No significant effect on *Xrx1* expression at neurula stage could be seen upon injection of 2 ng of Xdhcr7-L (e) and Mdhcr7 (g) capped RNA as well. At tailbud stage both Xdhcr7-L (f – f´´) and Mdhcr7 (h – h´´) induced a significant reduction of *Xrx1* expression domain. A slight reduction of the early expression of *Xkrox20* (e and g) could be noted in the 5th rhombomer (yellow arrows in e and g), but there was no effect on either late *Xkrox20* expression, or *Xen2* expression.

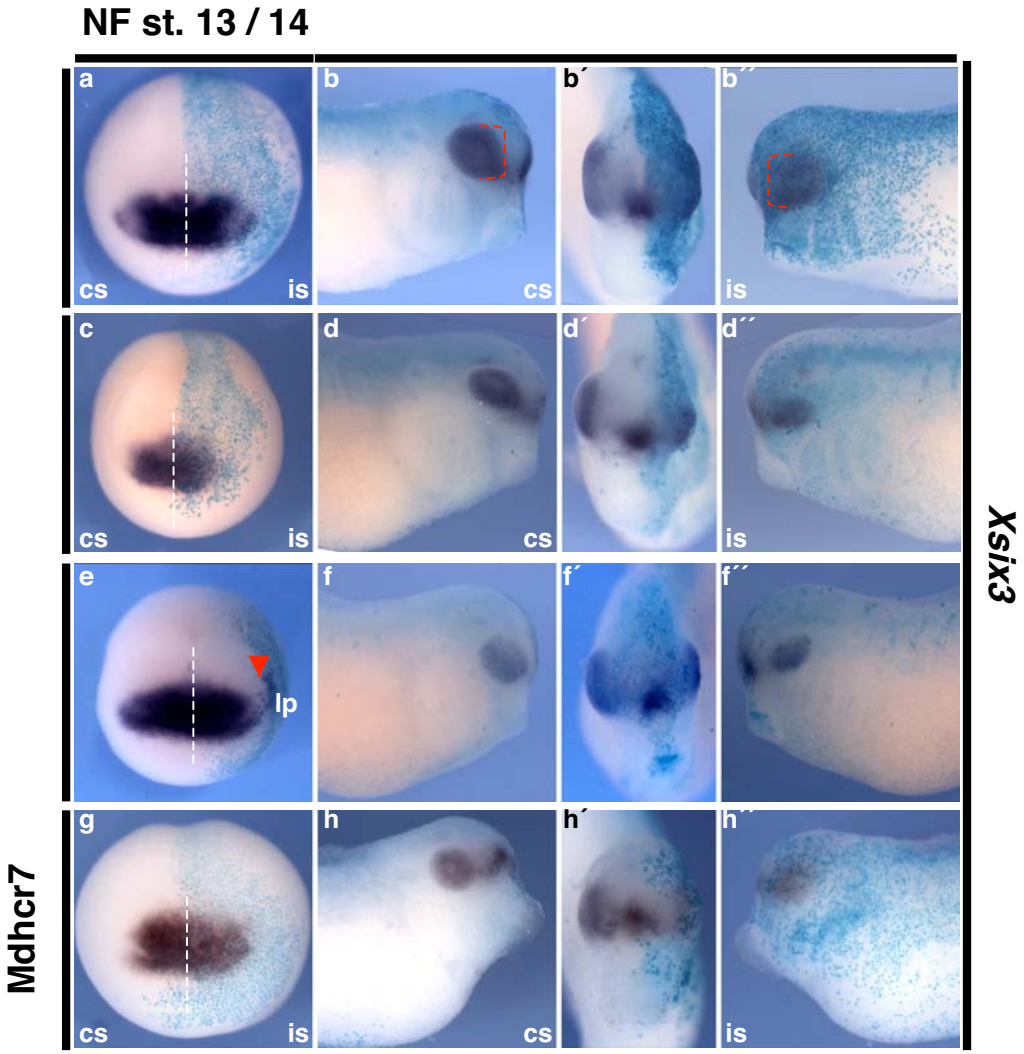

Figure 16: The overexpression of Xdhcr7 causes a severe reduction *Xsix3* expression.

a, c, e, and g: anterior views (dorsal up) of stage 14 embryos ; the white dashes indicate the position of the midline. b, b´´, d, d´´, f, f´´, h and h´´ : side views of stage 32 embryos. The frontal views are shown in b´, d´, f´ and h´. All embryos are shown with the non injected control side (cs) to the left and injected side (is, blue staining) to the right.

Two-cell stage albino embryos were injected (in one of two blastomers) with 2 ng of Xdhcr7-M, 750 pg of Xdhcr7-S, 2 ng of Xdhcr7-L or 2 ng of Mdhcr7 capped RNA, in combination with 200pg of n-β-Gal capped RNA as linage tracer. Injected embryos were cultured in 0.1 X MBS until opened neural plate (NF st. 13 / 14) or tailbud stage (NF st. 32 / 32), fixed in MEMFA, and hybridized with a Dig-labelled *Xsix3* antisense RNA, after X-gal staining (blue color).

Same as for *Xrx1*, the injection of 2 ng of Xdhcr7-M (a – b´´) did not interfere with *Xsix3* expression. Xdhcr7-S caused no significant change to the early expression of *Xsix3* (c) but a severe reduction of the expression could obviously be noted at tailbud stage (d – d´´). Upon injection at 2 ng per embryo, Xdhcr7-L caused a minor ectopic expression of *Xsix3* in the presumptive lens placode (arrowhead in e) at neurula stage. However, at tailbud stage (f – f´´), the expression of *Xsix3* was rather severely reduced on the injected side, as compared to the control non injected side. Mdhcr7 caused no significant effect on *Xsix3* expression at neurula stage (g). However, later (tailbud) stage injected embryos showed a severe reduction of *Xsix3* expression domain (h – h´´)

The overexpression of the Xdhcr7-L and and Xdhcr7-S caused a reduction of eye size, as major phenotype. This phenotype was confirmed by a reduction of the expression domain of the eye field markers *Xrx1* and *Xsix3*. Moreover, overexpression of the mouse dhcr7 showed the same phenotypes as the *Xenopus* homolog. To detect the endogenous Xdhcr7, we made use of the mouse dhcr7 for further overexpression experiments. To further analyse the dhcr7 eye phenotypes, we analysed the expression of the ventral anterior homeobox 1 (*Xvax1*) and the pituitary homeobox 3 (*Xpitx3*), which stain the optic stalk and the late lens epithelium respectively. As a lens epithelium marker, *Xpitx3* was a good candidate to answer the question whether the small eye phenotype was limited to retinal structures or also included lens tissues. For 31 % (n = 9 / 29) of the injected embryos, the expression domain of *Xpitx3* was reduced. Close analysis indicated that the injected and non-injected sides showed no apparent difference in the expression pattern of *Xpitx3*. The lens expression domain in the injected side appeared smaller, but regular (Fig. 17a – a´´). When analysed for *Xvax1* expression, 45.4 % (n = 15 / 33) of the Mdhcr7-injected embryos showed a noticeable (but not dramatic) reduction of its expression domain (Fig. 17b). On a horizontal section through the eyes-midline, the expression domain of *Xvax1* does not appear shortened on the injected side (is), but rather thinned as compared to the control non-injected side (cs). Furthermore, no structural alteration of the stalk was seen visible on the section (Fig. 17b1).

Taken together, the results of the phenotypic and molecular analysis of the dhcr7 activity suggest an inhibitory potential in the context of eye development. Although no dramatic effect was seen on the expression of brain markers *Xen2* and *Xkrox20*, it remained unclear whether the small eye phenotype was due to the failure of the eye territory to differentiate from the nervous system, or rather the consequence of a general inhibition of neural development. It then appeared reasonable to further analyse the phenotypes at the level of neurogenesis.

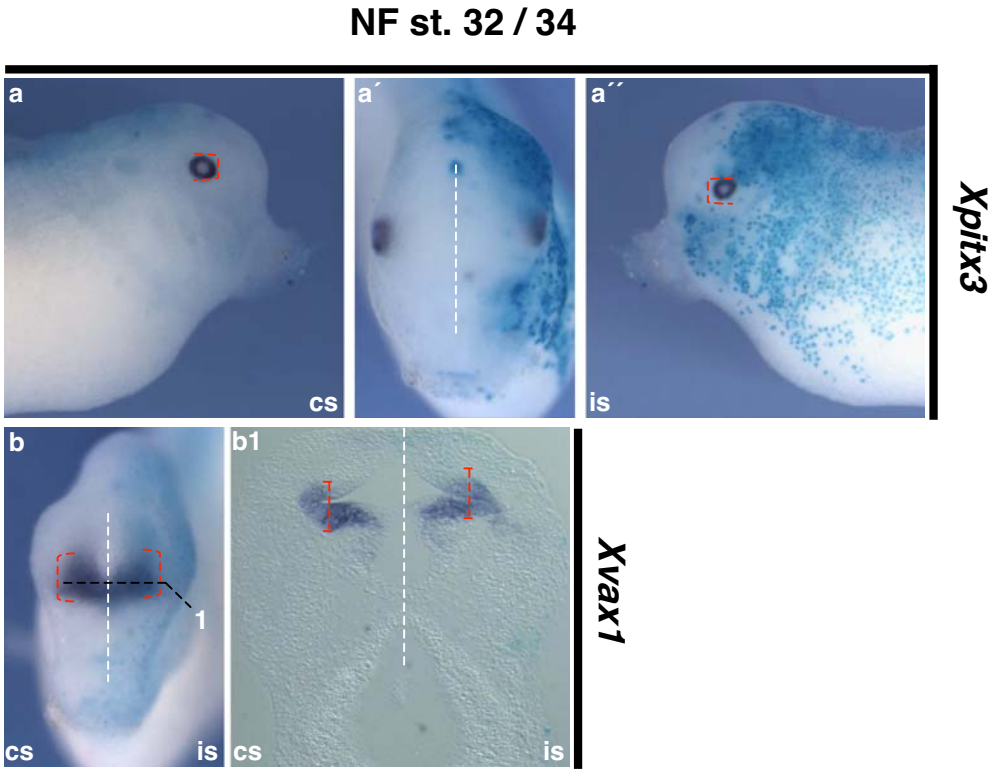

Figure 17: The overexpression of Mdhcr7 interferes with the expression of *Xvax1* and *Xpitx3*.
a and a´´: lateral views (dorsal up) of a tailbud stage Mdhcr7-injected embryo showing the expression of Xpitx3. the frontal view of the same embryo is shown in a´. White dashes indicate the position of the midline.
b: frontal view (dorsal up) of a tailbud stage Mdhcr7-injected embryo showing the expression of Xvax1.
b1: horizontal section (anterior up) in the head region of (b).
Two-cell stage albino embryos were injected (in one of two blastomers) with 2 ng of Mdhcr7 capped RNA, in combination with 200pg of n-β-Gal capped RNA as linage tracer. Injected embryos were cultured in 0.1 X MBS until tailbud stage (NF st. 32 / 32), fixed in MEMFA, and hybridized with a Dig-labelled *Xpitx3* (a – a´´) or *Xvax1* (b) antisense RNA, after X-gal staining (blue color).
The overexpression of Mdhcr7 resulted in the reduction of the expression domain of *Xpitx3* (a – a´´). However, although reduced, the expression domain of Xpitx3 on the injected side (is) was similar in appearance to that of the control side (cs). The expression of Xvax1 (b) was also reduced upon injection of Mdhcr7. On a horizontal section through the eyes (b1), the expression domain of Xvax1 appeared obviously not shortened on the injected side (is), but rather thinner, as compared to the expression domain on the control side (cs).

II.3.1.3. The overexpression of dhcr7 mostly interferes with placodal development in *Xenopus*.

Since the eye develops as part of the central nervous system, we hypothesised that the dhcr7-induced eye phenotype could be the consequence of an alteration of neural development. To test this possibility, we used the Sex-Determining Region Y Box containing gene 3 (*Xsox3*) as neural marker, neuronal-specific tubulin gene (*Xn-tubulin*) as neuronal marker, the distal-less homeobox-containing gene 3 (*Xdlx3*) as neural boundary marker, the homeobox gene Nkx2.2 (*Xnkx2*.2) as ventral neuronal marker, the genetic screen homeobox gene 1 (*Xgsh1*) as intermediate brain marker. Upon injection of 2 ng of Mdhcr7 capped mRNA, early expression of *Xsox3* (Fig. 18a) was severely reduced in the presumptive lens placode (red arrow in fig. 18a), with a remarkable expansion in the neural plate (40 %, n = 6 / 15). At tailbud stage (Fig. 18 b – b´´) the injected side showed a reduction in the lens (29 %, n = 9 / 31) and branches (45.2 %, n = 14 / 31), as indicated by red arrowheads in b and b´´. When analysed on transversal sections (b´´1-b´´3), the neural tube appeared expanded on the injected side, as compared with the control non injected side (red dashed bars in fig. 18b´´1 – b´´2). The neural plate expression of *Xn-tubulin* (Fig. 18 c) did not show any significant changes upon injection of Mdhcr7, but the placodal expression domain (red arrowheads in fig. 18c) was severely reduced on the injected side at this stage (36 % n = 9 / 25). At tailbud stage, 44,7 % (n = 17 / 40) of the analysed embryos showed a reduction of *Xn-tubulin* staining in the cranial placode (red arrowheads in fig. 18d and d´´). On transversal sections, the expression in the neural retinal (nr in fig. 18 d´´1) also appeared reduced. The dorsal neural tube also appeared expanded on the injected side (red dashed bars in fig. 18 d´´2 and d´´3).

The distal-less homeobox gene 3 demarcates the neural boundary at neural plate stage. This marker was then a suitable tool to answer the question whether the dhcr7 phenotype could also apply to epidermal non-neural structures. When analysed at NF stage 14 (Fig. 19a), 12 % (n = 3 / 25) of the Mdhcr7 injected embryos showed a minor reduction on the injected side, at a position situated just beneath the presumptive lens placode. At tailbud stage (Fig19b – b´´), a reduction of the most posterior pharyngeal pouches (red arrows in j and l) expression domains could be noted for 18.2 % (n = 6 / 33) of the analysed embryos, along with a severe reduction in the olfactory placode (op in fig. 19b´ and b´´1). We further analysed the influence of Dhcr7 on brain development and patterning by means

of positioning markers. Upon Mdhcr7 overexpression, an expansion of the expression domains of *Xgsh1* (Fig. 20 a – a´´) could be noted on the injected side (46.8 %; n = 15 / 32), as compared to the control side (red dashed bars in fig. 20a´´1 and a´´2). The expression domain of *Xnkx2*.2 (Fig. 20 b – b´´) was also expanded (33.33 %; n = 10 / 30). When the expression domain of Xnkx2.2 was analysed on transversal sections (Fig. 20b´´1 – b´´2), the dorso-ventral position of the expression domains was the same on the injected side, as compared to the control side. Thus, although Mdhcr7 showed an inhibitory activity on placodal development, it seemed to promote brain development; however, the dorso-ventral patterning of the brain is not affected.

Taken together, the expression of *Xsox3*, Xn-*tubulin*, *Xdlx3, Xgsh1* and *Xnkx2.2* suggest that MDHCR7 promotes the development of neural plate at the expense of placodal tissues in *Xenopus*.

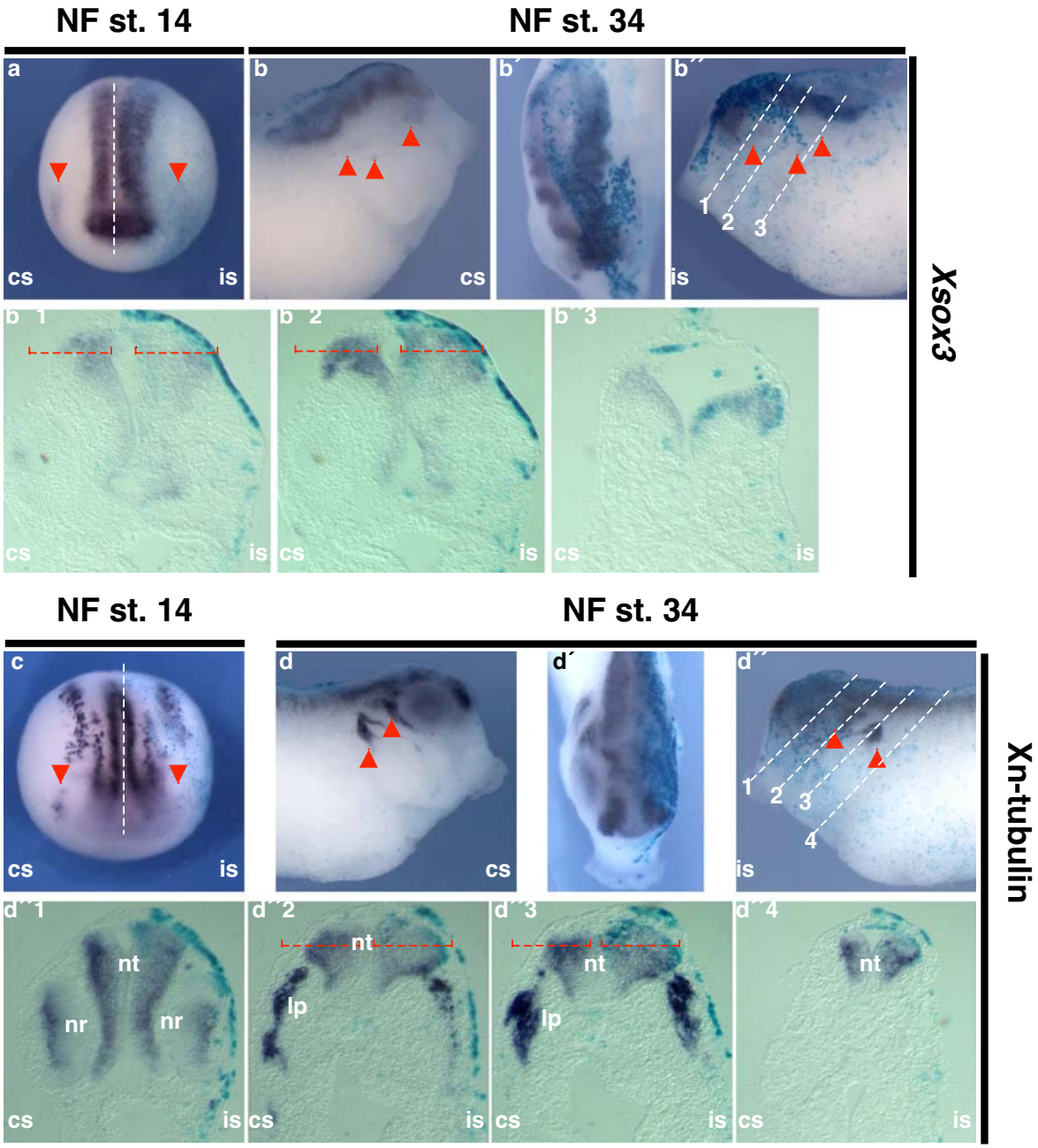

Figure 18: The overexpression of Mdhcr7 results in the reduction of the placodal expression domains of *Xsox3* and *Xn-tubulin*.

a and c: anterior views (dorsal up) of stage 14 embryos; the position of the midline is shown by white dashes. b, b´´, d and d´´: side views of stage 32 embryos. The frontal views are shown in b´ and d´ .

Two-cell stage albino embryos were injected (in one of two blastomers) with 2 ng of Mdhcr7 capped RNA, in combination with 200pg of n-β-Gal capped RNA as linage tracer. Injected embryos were cultured in 0.1 X MBS until opened neural plate (NF st. 13 / 14) or tailbud stage (NF st. 32 / 32), fixed in MEMFA, and hybridized with a Dig-labelled *Xsox3 (a – b´´),* or *Xn-tubulin (c – d´´)* antisense RNA, after X-gal staining (blue colour).

The early expression of *Xsox3* showed an expansion in the neural plate, and a reduction in the presumptive lens placode (red arrowheads in a). At tailbub stage (b – b´´), the Xsox3 staining was less abundant in the lens and branchial placodes of the injected side (red arrowheads in b, and b´´). As can be seen on transversal sections (b´´1 – b´´3, red dashed bars), the neural tube was expanded on the injected side (see also arrowheads in b´). *Xn-tubulin* showed no expansion in the neural plate, but a severe reduction could be noted in lens presumptive lens placode of the injected side (c, red arrowheads). At tailbud stage (d – d´´), the

placodal expression domains were reduced (red arrowheads), however, on transversal sections (d´´1 – d´´4), the neural tube appeared expanded on the injected side, as compared (red dashed bars) to the control side. The following structures are indicated: lateral placode (lp). Lens (le) neural retina (nr) neural tube (nt).

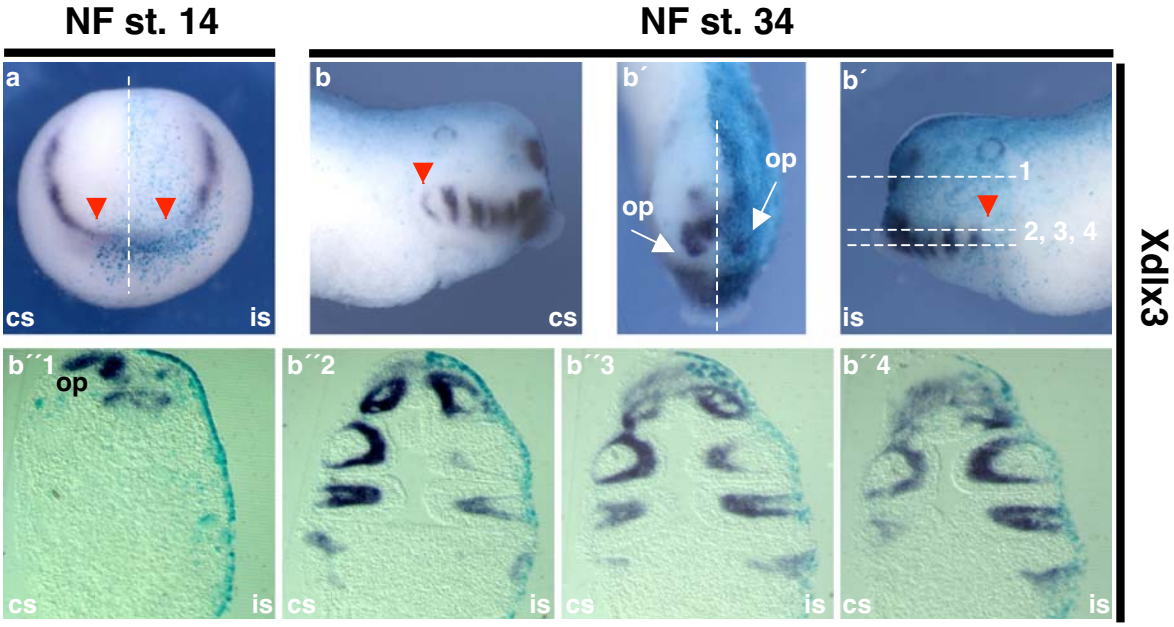

Figure 19: The overexpression of Mdhcr7 results in a minor reduction of the placodal expression domain of *Xdlx3* .

a : anterior view (dorsal up) of stage 14 embryos; the position of the midline is shown by white dashes. b, b´´and b´´: side views of stage 32 embryos. The frontal view is shown in b´.

Two-cell stage albino embryos were injected (in one of two blastomers) with 2 ng of Mdhcr7 capped RNA, in combination with 200pg of n- -Gal capped RNA as linage tracer. Injected embryos were cultured in 0.1 X MBS until open neural plate (NF st. 13 / 14) or tailbud stage (NF st. 32 / 32), fixed in MEMFA, and hybridized with a Dig-labelled *Xdlx3* antisense RNA, after X-gal staining (blue colour).

Apart from a minor reduction in a region beneath the presumptive lens placode (red arrowheads in a), the early expression of *Xdlx3* was not affected. At later stage (b – b´´), a minor reduction could be noted in the posterior pharyngeal pouches (red arrowheads in b and b´´). However, a severe reduction could be noted in the olfactory placode (op in b´´1).

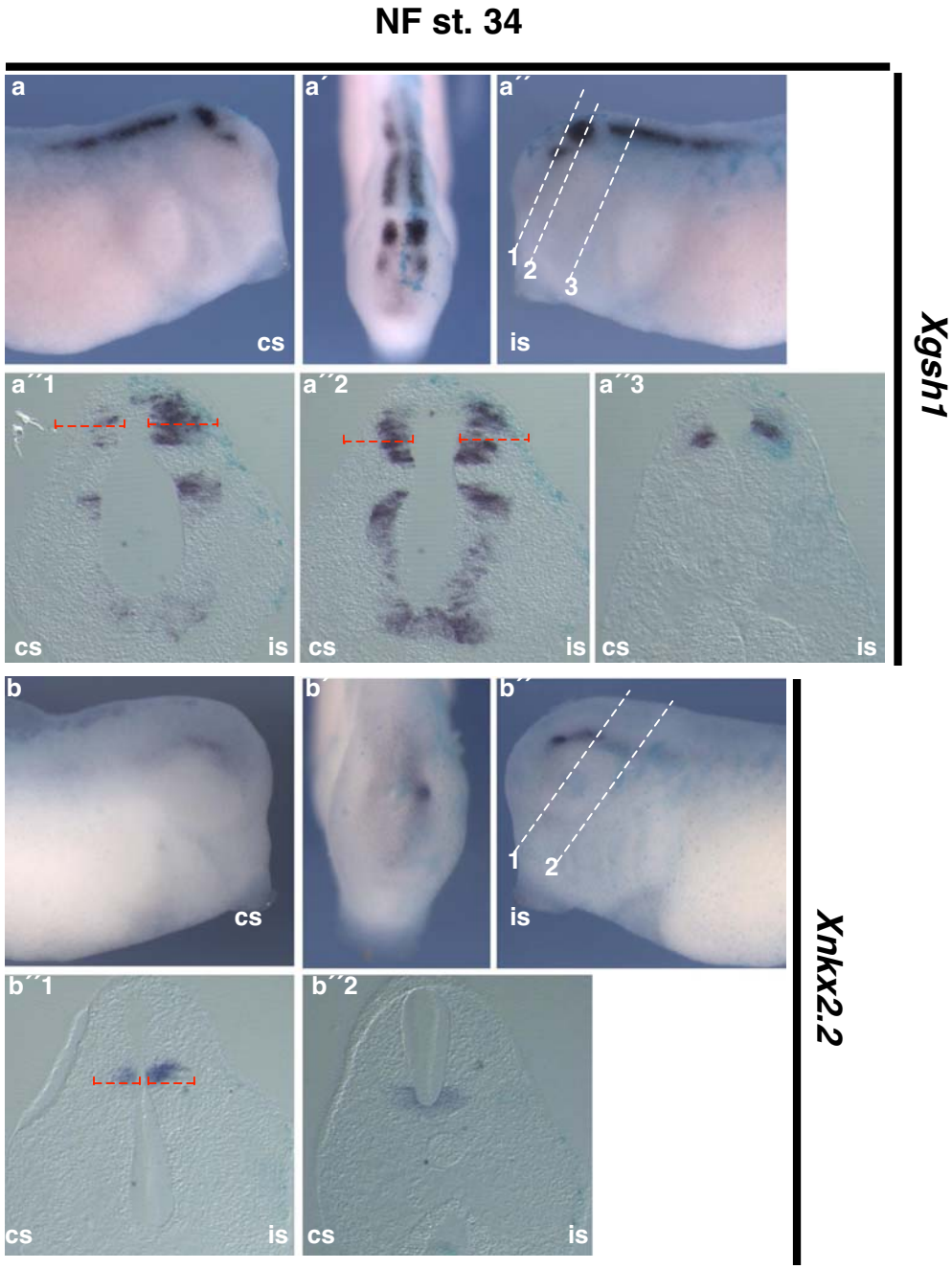

Figure 20: The overexpression of Mdhcr7 results in the expansion of the anterior expression domain of *Xgsh1* and *Xnkx2*.2.
a, a´´, b and b´´ : side views of stage 32 embryos. The frontal views are shown in a´ and b´.
Two-cell stage albino embryos were injected (in one of two blastomers) with 2 ng of Mdhcr7 capped RNA, in combination with 200pg of n- -Gal capped RNA as linage tracer. Injected embryos were cultured in 0.1 X MBS until tailbud stage (NF st. 32 / 34), fixed in MEMFA, and hybridized with a Dig-labelled *Xgsh1* or *Xnkx2.2* antisense RNA, after X-gal staining (blue colour).
The expression domains of both Xgsh1 (a – a´´) and Xnkx2.2 (b – b´´) were expanded upon Mdhcr7 injection. However, this expansion was more pronounced in the forebrain. Moreover, there was no shift in the dorso-ventral position of the expression domains of these markers on the injected side, as they appeared at the same position as the control side.

II.3.1.4. The overexpression of dhcr7 might activate hedgehog signalling in *Xenopus*.

It is known that Sonic hedgehog (Shh) activity promote the patterning of the neural tube. Moreover, the endogenously active sonic hedgehog protein has been shown to be cholesterol modified. Since the DHCR7 protein is involved in cholesterol biosynthesis, we asked if the dhcr7 phenotype could be explained by interference wish the Shh activity. WMISH with dhcr7-injected embryos (result not shown) did not show any change in the expression level of the Shh mRNA. We then supposed that interference could happen at the level of transduction of the signal. To test our hypothesis we analysed the expression of the hepatonuclear factor 3-beta (*Xhnf*-3) gene, which is known to be induced by Shh in the floor plate. When analysed at neural plate stage (Fig. 16a), 72 % (n = 18 / 25) of the Mdhcr7-injected embryos showed an expanded and ectopic expression of Xhnf-3 on the injected side, mostly in the most anterior domain (red arrow in fig. 21a). At tailbud stage (Fig. 21 b-b´), 73,4 % (n = 48 / 66) of the analysed embryos showed a strong ectopic expression of *Xhnf-3β* in the mesoderm. On transversal sections (Fig.21 b´1-b´2X), the endogenous expression domain showed only a slight expansion in the diencephalons (di) and the floor plate (fp). When analysed for the same marker, Xdhcr7-S and Xdhcr7-M-injected embryos did not show any expansion. However, the Xdhcr7-L injected embryos show the same expansion at stage 14, but weaker expansion at tailbud stage. We could also observe an ectopic XlHbox8 expression in the Mdhcr7 injected embryos, but these results are still to be confirmed.

In summary, the gain-of-function analysis of the *Xenopus* Dhcr7 isoforms point to a differential potentiality to induce eye phenotypes, with the medium version showing almost no activity. Furthermore, the activity of the mouse Dhcr7 in *Xenopus* suggests a conservation of the activity of this gene between the two species. The analyses of marker genes expression suggest that the dhcr7 activity might promote the expansion of neural tissues at the expense of non neural tissues, including the eye-field and placodes.

In the context of hedgehog signalling, if confirmed, the dhrc7-induced ectopic expression of *Xhnf-3β* may suggest an activation of the pathway by DHCR7 activity.

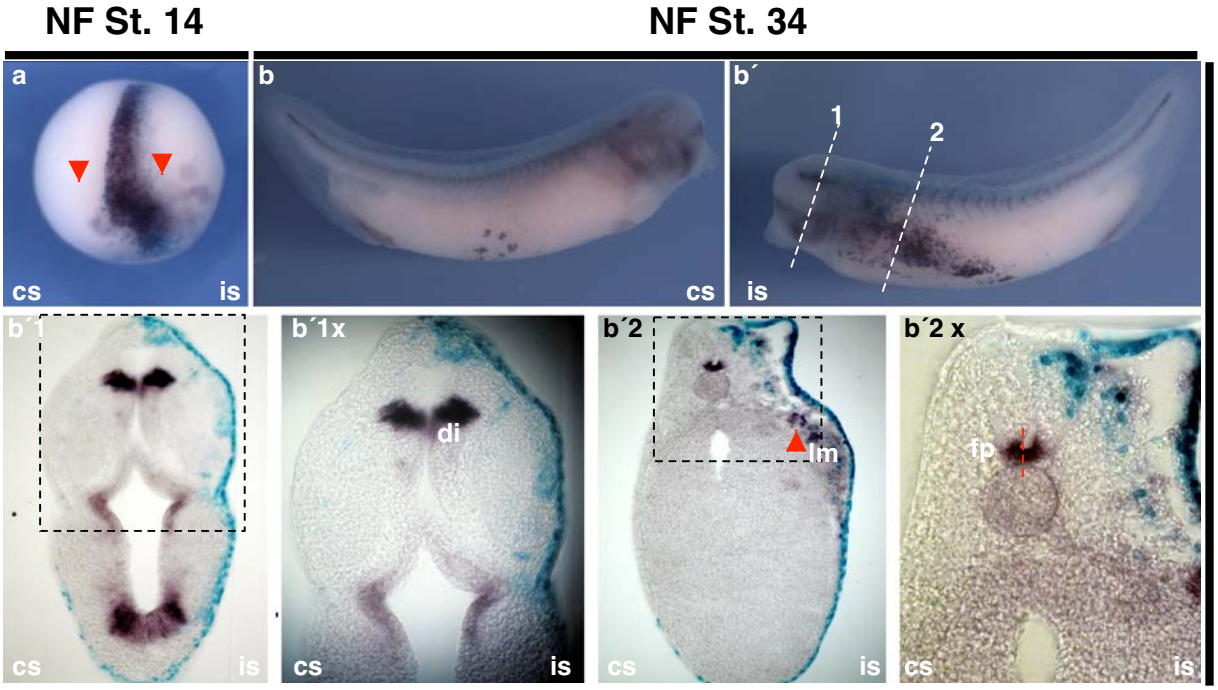

Figure 21: The overexpression of Mdhcr7 results in ectopic induction of Xhnf-3β expression.
a: anterior view (dorsal up) of a stage 14 Mdhcr7-injected embryo.
b and b´ : side view of a stage 34 Mdhcr7-injected embryo. On panels b´1 to b´2x, transversal sections are shown. b´1x and b´2x show a higher magnification of the boxed portion of b´1 and b´2 respectively.
Two-cell stage albino embryos were injected (in one of two blastomers) with 2 ng of Mdhcr7 capped RNA, in combination with 200pg of n- -Gal capped RNA as linage tracer. Injected embryos were cultured in 0.1 X MBS until opened neural plate (NF st. 14) or tailbud stage (NF st. 32 / 34), fixed in MEMFA, and hybridized with a Dig-labelled *Xhnf-3β* antisense RNA, after X-gal staining (blue colour).
At stage 14 (a), although the expression in the midline was expanded in general on the injected side, the most dramatic expansion was seen in the most anterior domain. At tailbud stage, Mdhcr7 caused an ectopic expression of *Xhnf-3β* in the mesoderm (b´). On transversal section, cells that ectopically expressed Xfhn-3b were located in the lateral mesoderm (lm, red arrowhead in b´2). However, the endogenous expression domain (b´1 – b´2X) was only slightly increased in the diencephalons (di) and the floor plate (fp).

II.3.1.5. The overexpression of Mdhcr7 promoted cell survival in the brain, but did not interfere with proliferation rate in *Xenopus*.

Since overexpression of Mdhcr7 seemed to result in the expansion of neural tissues at the expense of non-neural tissue (including the eye-field), we suggested that interference with programmed-cell death (apoptosis), or with cell proliferation could at least partly explain these phenotypes. To test our hypothesis, we made use of the terminal deoxynucleotidyl transferase mediated dUTP nick-end-labeling (TUNEL) assay to analyse apoptosis rate in Mdhcr7 injected embryos. In parallel, in order to analyse cell proliferation rate, we performed a whole mount immunostaining using antibodies specific for phosphorylated histone H3 (anti-PH3), which detect mitotic cells. Upon Mdhcr7 overexpression, 60 % (n = 9 / 15) of the analysed embryos showed a reduction of TUNEL staining in the injected side of the brain, as compared to the control side (Fig. 22a´´, yellow arrowheads); meanwhile, the staining was increase in several extra-cranial tissues (red arrowed in a, a´, a1 and a´1) on the injected side. This suggests the DHCR7 activity may promote cell survival. When the injected embryos (n = 23) were analysed for mitosis rate (using anti phosphorylated histone H3 antibodies; fig. 22b – b´1), there was no obvious difference in the staining level of the injected side, as compared to the control side. However, more detailed analysis (by sectioning) may bring more light to these results.

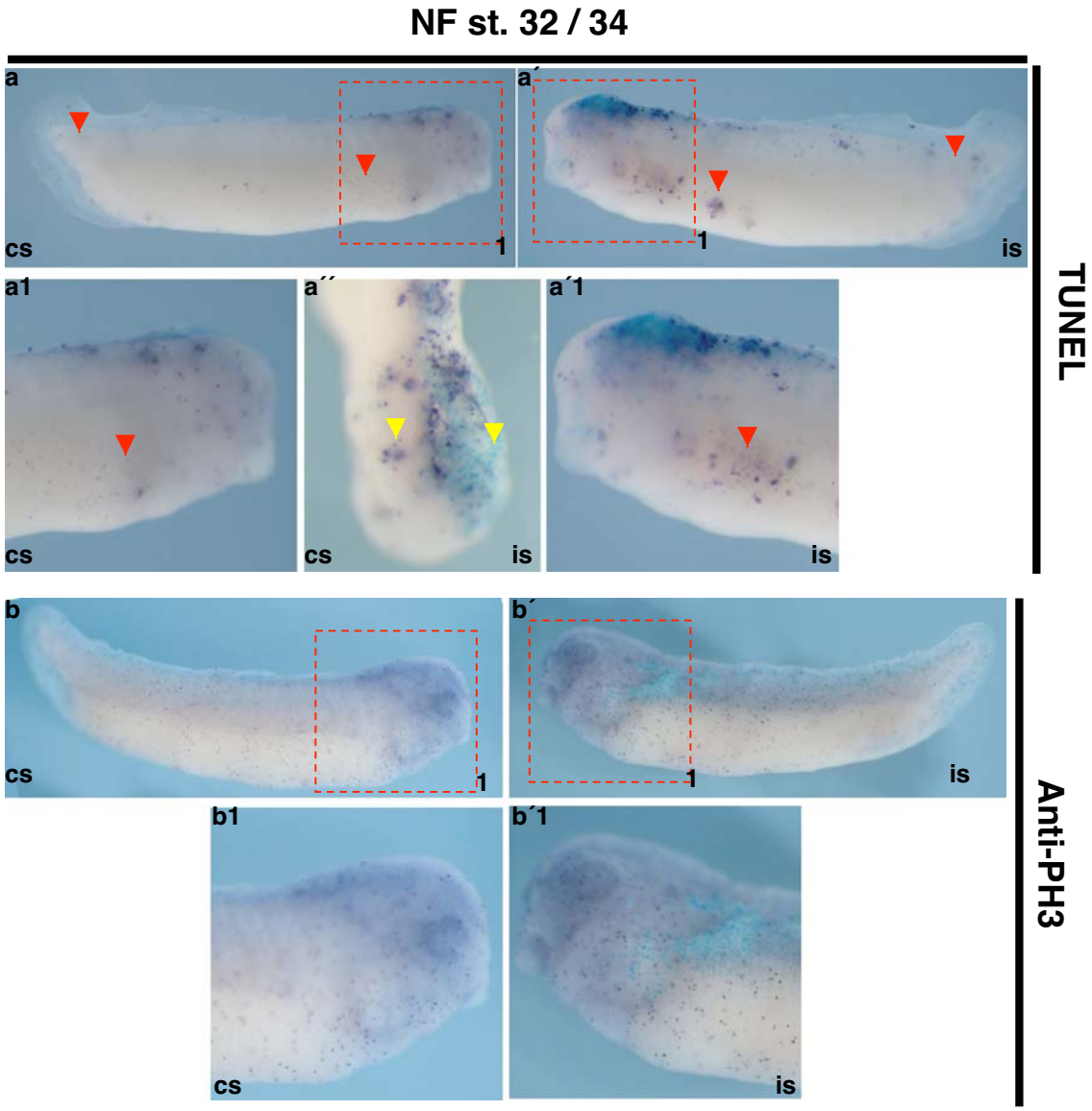

Figure 22: Overexpression of Mdhcr7 resulted in reduced apoptosis in the brain, but had no effect on proliferation rate.

a and a´: side views (dorsal up) of the control side (cs) and injected side (is) of a NF st. 32 embryo showing the staining for apoptotic cells (TUNEL). a1 and a´1 show a higher magnification of the head portion of a and a´ respectively. The frontal view of the same embryo is shown in a´´. b and b´: side views (dorsal up) of the control side (cs) and injected side (is) of a NF st. 34 embryo showing the staining for mitotic cells (Anti-PH3 immunostaining). b1 and b´1 show a higher magnification of the head portion of b and b´ respectively.

Two-cell stage albino embryos were injected (in one of two blastomers) with 2 ng of Mdhcr7 capped RNA, in combination with 200pg of n- -Gal capped RNA as linage tracer. Injected embryos were cultured in 0.1 X MBS until tailbud stage (NF st. 32 / 34), fixed in MEMFA, and stained with X-gal to identify the injected side (blue colour). After refixation, embryos were dehydrated in ethanol, permeabilised by incubation in the DENT´s fixative (-20 °C, overnight), and further processed for TNUEL assay or Anti-PH3 immunostaining.

Upon Mdhcr7 overexpression, a higher number of apoptotic cells (indicated by red arrowheads in a – a´1) could be noted on the injected side (a, is) as compared to the control side (a´, cs). Interestingly, the number of TUNEL positive cells was rather reduced in the injected side of the brain (yellow arrowhead in b´´), as compared to the control side. On the other hand, no obvious effect was noted on the proliferation rate, as analysed by Anti-PH3 immunostaining. As compared to the control side (cs, b and b1), the injected side (is, b´ and b´1) of the embryo did not show any difference in anti-PH3 staining.

II.3.2. Lost-of-function analysis of *Xenopus* dhcr7

In order to analyse the outcome of *dhcr7* knockdown in *Xenopus*, an antisense morpholino-oligonucleotide (*Xdhcr7-morpholino*) was designed to target the 25 first nucleotides of the *Xdhcr7* open reading frame. The synthetic nucleotide was tested in TnT reaction (see fig. 13), and found to inhibit the in vitro translation of all the three isoforms of XDHCR7. Meanwhile, it was unable to inhibit the in vitro translation of the mouse DHCR7, which was used as specificity control. For optimization, concentrations ranging from 0.5 pmol to 10 pmol per cell were microinjected into one blastomere of two cell-stage *Xenopus* embryos, along with nuclear beta-galactosidase (n-β-Gal) mRNA as linage tracer. When injected with up to 1.5 pmol per cell, embryos showed massive death. The amount of 1 pmol per cell was then chosen as optimal concentration.

Both for phenotypic analysis and for molecular analysis, the injected embryos received the same treatment as for the overexpression experiments.

II.3.2.1. Antisense morpholino-mediated knockdown of Xdhcr7 severely compromised eye development.

Upon injection of the Xdhcr7-morpholino, the injected side of the embryos usually showed a delay in development, which lead to massive gastrulation defects in most of the time. When cultured to tadpole stage, 93 % (n = 279 / 300) of the injected embryos showed a clear reduction of the eye size (Fig. 23). Among them 33,3 % (n = 100 / 300) showed a severe reduction of the eye, which exteriorly resembled an eyeless phenotype (Fig. 23a – a´´). Furthermore, the eye on the injected side was most of the time nearer to the brain, as compared to the control side (93 %, n = 279 / 300) (red dashed bars fig. 23b´). In some cases (40 %, n = 120 / 300), the lens viewed from outside looked opaque, and seemed to fill most of the volume of the eye. However, on sections through the eye midline, although smaller, the lens appeared normal on the injected side, both for the mild (Fig. 23 b´2) and the apparent eyeless (Fig. 23 a´2) phenotypes. Meanwhile, retinal stratification appeared severely disorganised with almost no visible retinal-pigmented epithelium (rpe, a´1 – a´2; b´1 – b´2) layer on the injected side. A ventral coloboma (yellow arrow in b´´) was also a common characteristic of the small eyes.

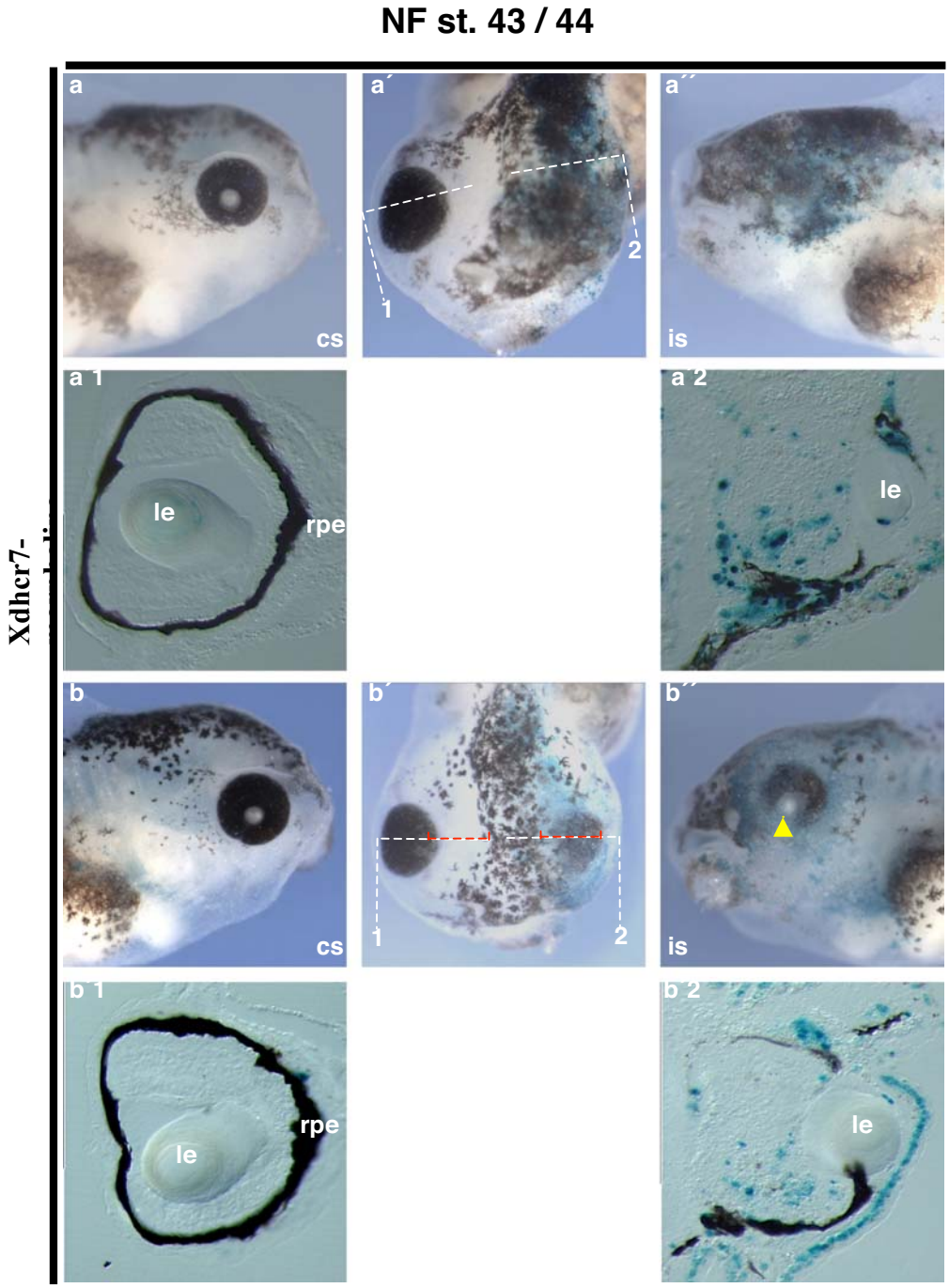

Figure 23: The antisense morpholino-mediated knockdown of Xdhcr7 severely compromised eye development.
a, b ,a´´ and b´´: side view (head region) of tadpole stage injected embryos.
a´ and b´: dorsal view of injected embryos.
"is" indicates the injected side (blue staining), and "cs" indicates the control (non injected) side of the same embryo. a´1, a´2, b´1 and b´2: magnification of the eyes as view on transversal sections.
Two-cell stage pigmented embryos were injected (in one of two blastomers) with 1pmol of Xdhcr7-morpholino, in combination with 200pg of n- -Gal capped RNA as linage tracer. Injected embryos were cultured in 0.1 X MBS until tadpole stage (NF st. 43 / 44), fixed in MEMFA, and recorded for eye phenotypes after X-gal staining (blue colour).
Upon injection of 1pmol of Xdhcr7-morpholino, a significant number of embryos showed a severe reduction of eye size on the injected side (a – a´´). When analysed by histological section, reduced eye showed a severe disorganisation of the retinal stratification, with almost no visible pigmented epithelium layer in the injected eye (a´2). Even when mildly reduced, the injected eye was closer to the brain than the control one

(b – b´´), and showed the same disorganised retinal stratification (b´2) as the severely reduced one. A failure of the optic vesicle to close (eye coloboma, yellow arrow in b´´) was also a common phenotype.

In an attempt to rescue the morpholino phenotypes, 1pmol of Xdhcr7-morpholino was injected into one blastomere of two cells stage embryos in combination with 2 ng Mdhcr7 capped RNA. This combination resulted in more than 40 % death (76 survivors / 143 injected). However, a severe reduction of the eye size was recorded for only 9.2 % (n = 7 / 76) of the survivors; 39.4 % (n = 30 / 76) showed a minor reduction of the eye size, and 50 % showed medially shifted eyes. However, no eye coloboma phenotype was recorded. This indicated that mdhcr7 could at least partially rescue the phenotype of Xdhcr7-morpholino.

II.3.2.2 Antisense morpholino-mediated knockdown of Xdhcr7 severely interfered with the expression of eye marker genes.

To further characterise the Xdhcr7-morpholino eye phenotypes, we made used of *Xrx1* and *Xsix3* as eye field markers, *Xen2* and *Xkrox20* as brain boundaries markers, *Xvax1* and *Xpitx3* as stalk and late lens epithelium markers respectively.

When analysed at neurula stage, 48 % (n = 12 / 25) of the Xdhcr7-morpholino-injected embryos showed an expansion of *Xrx1* (Fig. 24a, red arrowhead). At this stage, the expression Xen2 (Fig. 24a, green arrowhead) and Xkrox20 (Fig. 24a, white arrowheads) was remarkably reduced for 40 % (n = 10 / 25) of the analysed embryos. At tailbud stage, the expression of *Xrx1* (Fig. 24 b – b´´) was reduced for 56 % (n = 18 / 32) of the analysed embryos; in addition, the expression domain appeared shifted towards the midline. On a horizontal section through the eye (Fig. 24b´´1), the reduced expression domain of *Xrx1* appeared diffused on the injected side, reminiscent of the disorganised retinal stratification phenotype. The expressions of *Xen2* (Fig. 24 b – b´´; green arrowhead) and Xkrox20 (Fig. 24b – b´´; white arrowheads) were severely reduced at this stage (65 %, n = 21 / 32 and 53 %, n = 17 / 32 respectively). The early expression of *Xsix3* was expanded for 56 % (n = 14 / 25) of the analysed embryos (Fig. 24c). At tailbud stage, *Xsix3* expression (Fig. 24d-d´´) was in general reduced on the injected side, but severely reduced for 60.7 % (n = 17 / 28). For 89.3 % (n = 25 / 28) of the analysed embryos, the expression domain was shifted towards the midline. The shift was more obvious on a horizontal section (Fig. 244d´´1, red arrowhead), where the expression domain of *Xsix3* appeared reduced and diffused in the eye, and the forebrain (fb).

From the analysis of *Xrx1*, *Xsix3*, *Xen2* and *Xkrox20* expression, the Xdhcr7-morpholino seemed to interfere not only with the early establishment of the eye field and later development of the eye, but also with the establishment of brain boundaries.

When analysed for stalk and lens markers (*Xvax1* and *Xpitx3* respectively; fig. 25), Xdhcr7-morpholino showed a less striking effect as compared to *Xrx1* and *Xsix3*.

For 42.4 % (n = 14 / 33) of the analyzed embryos, the lens expression domain of Xpitx3 was reduced on the injected side; one half of these embryos (21.2 %, n = 7 / 33) displayed a diffused expression domain, as compared to the control side (Fig. 25a – a´´). The expression domain of *Xvax1* was reduced for 30 % (n = 9 / 30) of the analysed embryos (Fig. 25b); on a horizontal section, the expression domain appeared thinner on the injected side (Fig. 25b1).

In summary, Xdhcr7-morpholino interfered with the expression of eye marker genes, both at early and late stages. We were therefore interested in investigating the Xdhc7-morpholino phenotype in the context of neurogenesis.

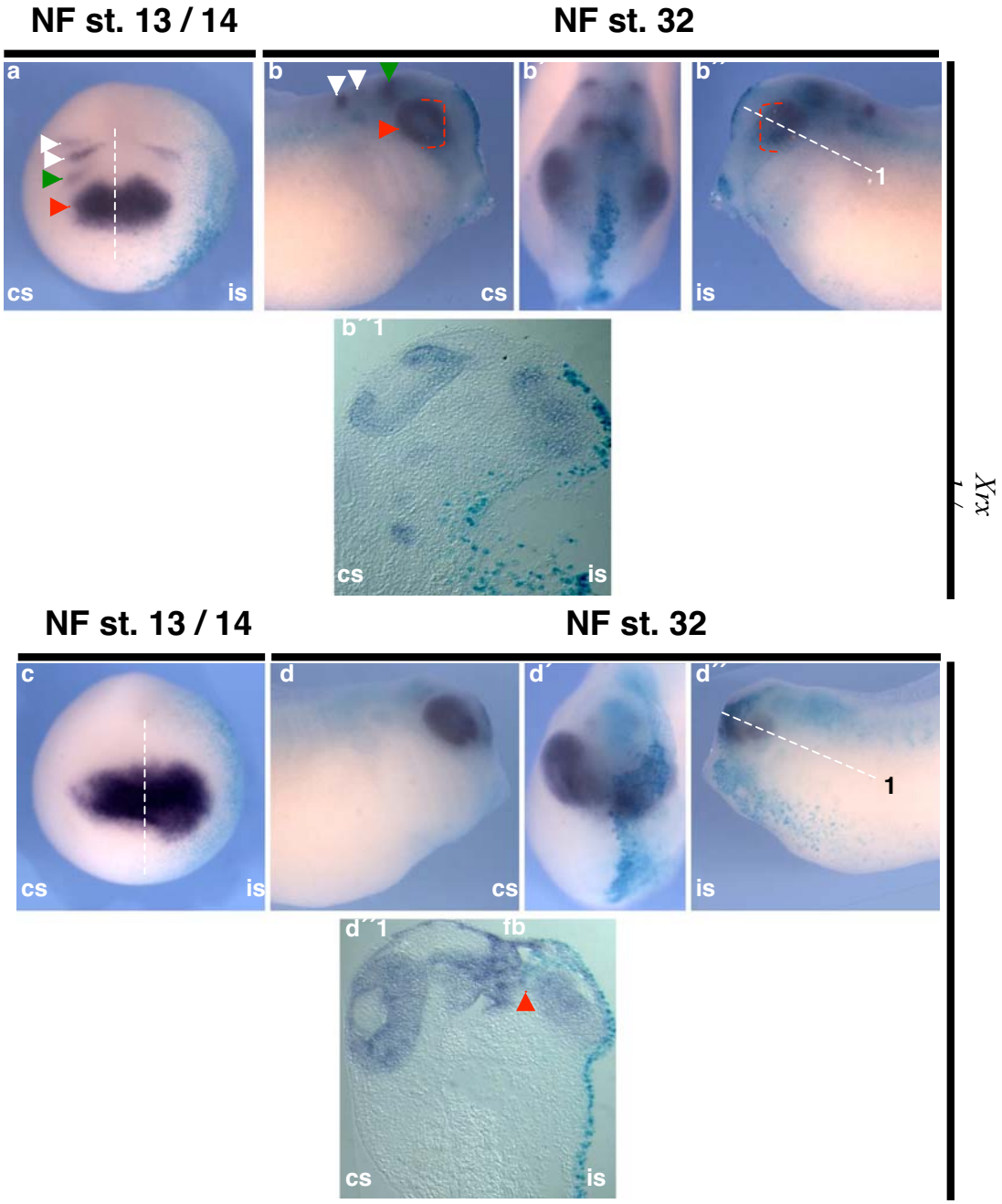

Figure 24: The antisense morpholino-mediated knockdown of Xdhcr7 induced an early expansion and a late reduction in the expression of eye-field markers genes.
a – b´´: WMISH of *Xrx1* (red arrowheads), *Xen2* (green arrowheads) and *Xkrox20* (white arrowheads).
c – d´: WMISH of *Xsix3*
a and c: anterior views (dorsal up) of stage 14 embryos ; the white dashes indicate the position of the midline. b, b´´, d and d´´: side views of stage 32 embryos. The frontal views are shown in b´ and d´.
Two-cell stage albino embryos were injected (in one of two blastomers) with 1 pmol of Xdhcr7-morpholino, in combination with 200pg of n- -Gal capped RNA as linage tracer. Injected embryos were cultured in 0.1 X MBS until opened neural plate (NF st. 13 / 14) or tailbud stage (NF st. 32 / 32), fixed in MEMFA, and hybridized with a mixture of Dig-labelled *Xrx1*, *Xen2* and *Xkrox20* antisense RNAs (a – b´´) or Dig-labelled *Xsix3* antisense RNA alone (c – d´´), after X-gal staining (blue colour).
The Xdhcr7-morpholino induced and expansion of the expression domains of *Xrx1* (a) and *Xsix3* (c) at opened neural plate stage (stage 14). However, the expression of brain markers *Xen2* and *Xkrox20* is severely reduced. The later (tailbud stage) expression of both *Xrx1* (b – b´´) and *Xsix3* (d – d´´) showed rather a severe reduction on the injected side. On transversal sections the appearance of the expression pattern of both *Xrx1* (b´´1, is) and *Xsix3* (d´´1, is) indicate a disorganisation of the retinal stratification. Note that the expression domain of *Xsix3* appeared almost sticked to the brain (red arrowhead in d´´1).

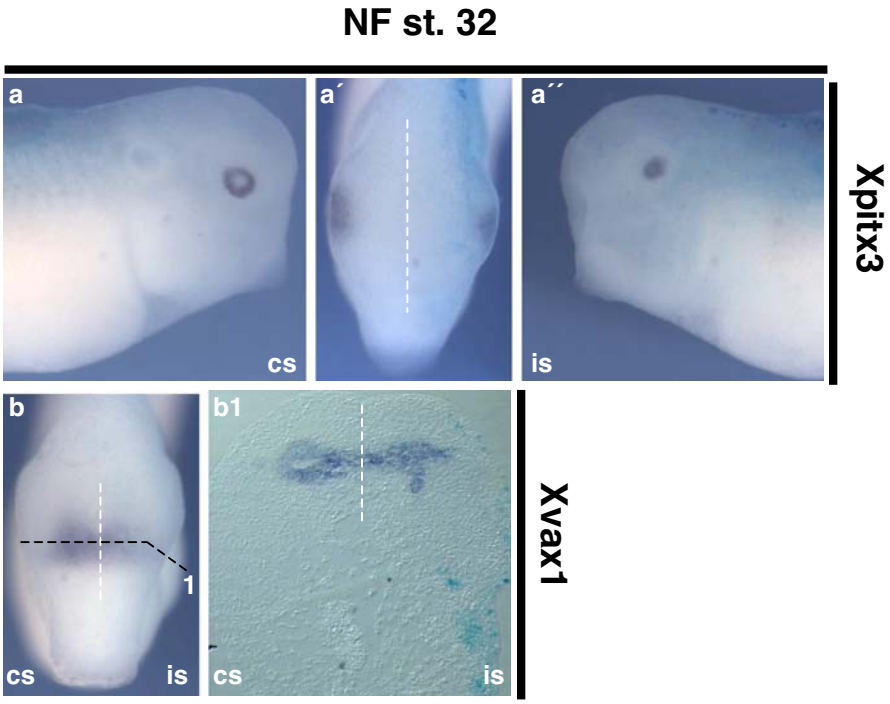

Figure 25: The antisense morpholino-mediated knockdown of Xdhcr7 interferes with the expression of *Xvax1* and *Xpitx3*.
a and a´´: lateral views (dorsal up) of a tailbud stage Mdhcr7-injected embryo showing the expression of Xpitx3. The frontal view of the same embryo is shown in a´. White dashes indicate the position of the midline.
b: frontal view (dorsal up) of a tailbud stage Mdhcr7-injected embryo showing the expression of *Xvax1*.
b1: horizontal section (anterior up) in the head region of (b).
Two-cell stage albino embryos were injected (in one of two blastomers) with 1pmol of Xdhcr7-morpholino, in combination with 200pg of n-β-Gal capped RNA as linage tracer. Injected embryos were cultured in 0.1 X MBS until tailbud stage (NF st. 32 / 32), fixed in MEMFA, and hybridized with a Dig-labelled *Xpitx3* (a – a´´) or *Xvax1* (b) antisense RNA, after X-gal staining (blue color).
Xdhcr7-morpholino injection caused the reduction of the lens expression domain of *Xpitx3* (a – a´´). It is interesting to note that the expression domain of Xpitx3 is not only reduced, but also diffused on the injected side (is) as compared to the control side (cs). The expression of *Xvax1* (b) was also reduced upon injection of Xdhcr7-morpholino. On a horizontal section through the eyes (b1), the expression domain of *Xvax1* appeared severely thinned on the injected side (is), as compared to the expression domain on the control side (cs).

II.3.2.3. Antisense morpholino-mediated knockdown of Xdhcr7 severely compromised both placodal and neural development.

In order to investigate the effect of Xdhcr7-morpholino on neurogenesis, we analysed the expression of *Xsox3*, *Xn-tubulin*. *Xdlx3*, *Xgsh1* and *Xnkx2*.2. At neurula stage, the Xsox3 expression (Fig. 26a) was severely reduced (65 %, n = 13 / 20) in the neural plate and more severely in the presumptive lens placode (red arrowheads in Fig. 26a). The expression domain around the eye field was usually expanded on the injected side, (55 %, n = 11 / 20), but compared to the control side, the staining was clearly weaker (Fig. 26a). At tailbud stage, the expression was severely reduced in the brain and lens (55.55 %, n = 15 / 27), and in the branches (red arrows in fig. 26b and b´´) as well (70.3 %, n = 19 / 27). On transversal sections (Fig. 26b´´1 – b´´3), the expression appeared scattered (less organised as compared to the control side) in the forebrain, and the neural tube appeared reduced in size on the injected side (b´´1). When analysed for *Xn-tubulin* expression, the neurula stage Xdhcr7-morpholino injected embryos showed severe reduction of the transcripts level on the injected side (Fig. 26c; 72,4 %, n = 21 / 29), both in neural and placodal domains. At tailbud stage, 57.1 % (n = 20 / 35) of the analysed embryos showed a severe reduction of *Xn-tubulin* expression in the brain and cranial placodes (red arrowheads in fig. 26d and d´´). On transversal sections (Fig. 26d´´1 – d´´4), the expression appeared almost absent in the neural tube and neural retina of the injected side. Hence, with regard to the expression of *Xsox3* and *Xn-tubulin*, no discrimination was observed between neural and non neural effect of Xdhcr7-morpholino. For *Xdlx3* expression (Fig. 27), a severe reduction was observed at neural plate stage, mostly in the posterior domain (Fig. 27a). At this stage, 48 % (n = 12 / 25) of the analysed embryos displayed a severely reduced expression of *Xdlx3*. At tail bud stage (Fig. 27b – b´´) 55.9 % (n = 19 / 34) of the analysed embryos showed a severe reduction of the pharyngeal pouches expression domain of *Xdlx3* (red arrowheads in Fig. 27b and b´´). On serial horizontal sections (Fig. 27b´´1 – b´´4), the expression appeared also reduced in the olfactory placode (op in fig. 27b´´1). The analysis of *Xdlx3* expression then suggested that the Xdhcr7-morpholino´s effect was not restricted to neural structures only. Our next interest was then to answer the question as to whether Xdhcr7-morpholino could also interfere with brain patterning.

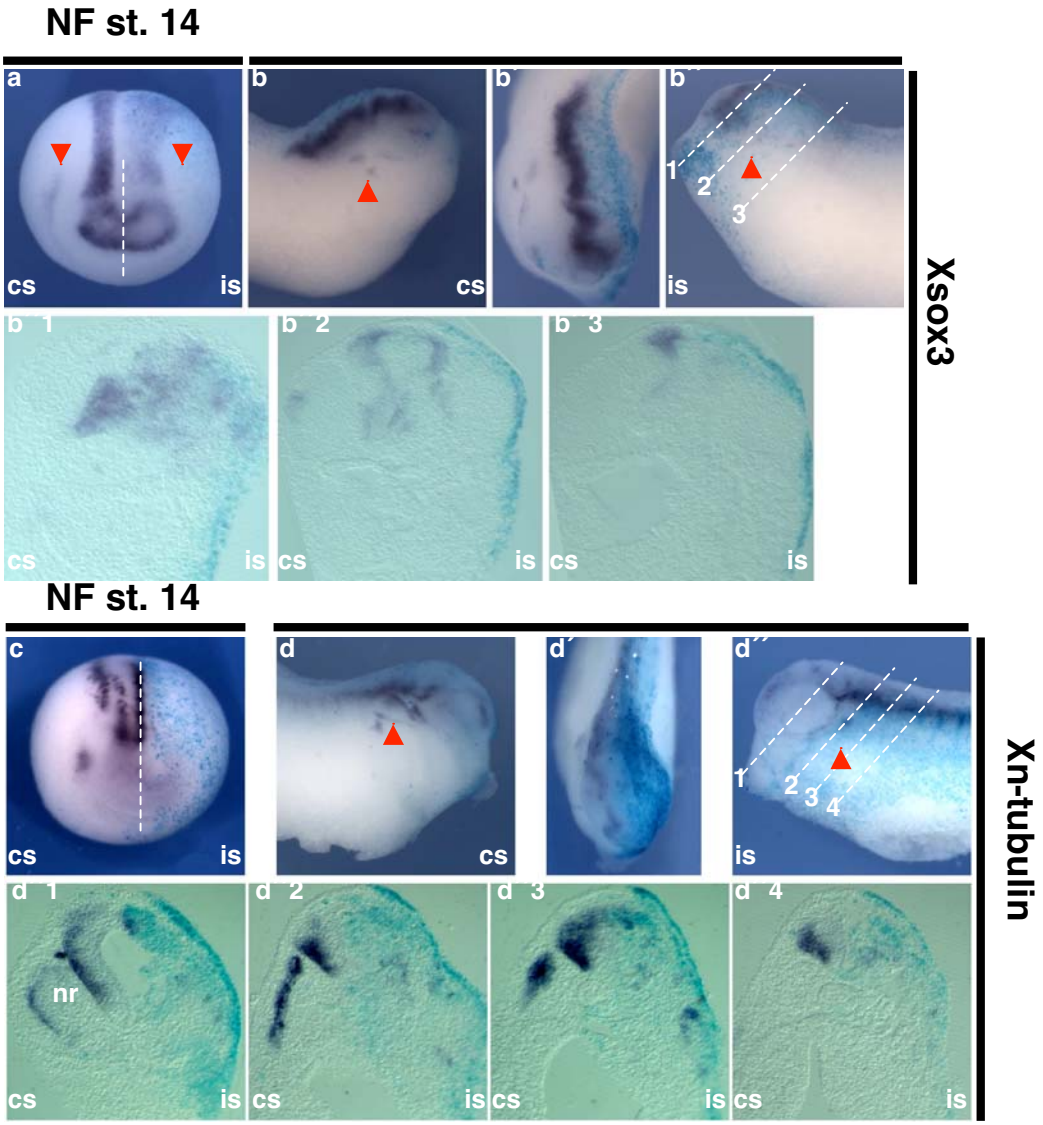

Figure 26: The antisense morpholino-mediated knockdown of Xdhcr7 severely interferes with neural and neuronal markers expression.

a and c: anterior views (dorsal up) of stage 14 embryos; the position of the midline is shown by white dashes. b, b´´, d and d´´: side views of stage 32 embryos. The frontal views are shown in b´ and d´.

Two-cell stage albino embryos were injected (in one of two blastomers) with 1pmol of Xdhcr7-morpholino, in combination with 200pg of n-β-Gal capped RNA as linage tracer. Injected embryos were cultured in 0.1 X MBS until opened neural plate (NF st. 13 / 14) or tailbud stage (NF st. 32 / 32), fixed in MEMFA, and hybridized with a Dig-labelled *Xsox3 (a – b´´),* or *Xn-tubulin (c – d´´)* antisense RNA, after X-gal staining (blue colour).

At neural plate stage (a), although the staining was less on the injected side, the anterior expression domain of *Xsox3* was expanded as compared to the control side. The expression in the presumptive lens placode was completely abolished (red arrowheads in a). When analysed at tailbud stage (b – b´´), the expression of *Xsox3* was severely reduced all along the neural tube, and showed a “scattered” feature in the forebrain (b´´1). The lens and branchial placodes expression domains were almost absent on the injected side (red arrowhead in b and b´). The expression of Xn-*tubulin* (c – d´´) was in general severely reduced, both at early and late stage. At early stage (c), the expression was almost abolished both in the placode and neural plate. When analysed at later stage (d – d´´), the placodal expression domain was severely reduced, (red arrowheads in d and d´´). On transversal sections, the neural tube expression domain appeared severely reduced on the injected side (d´´1 – d´´4).

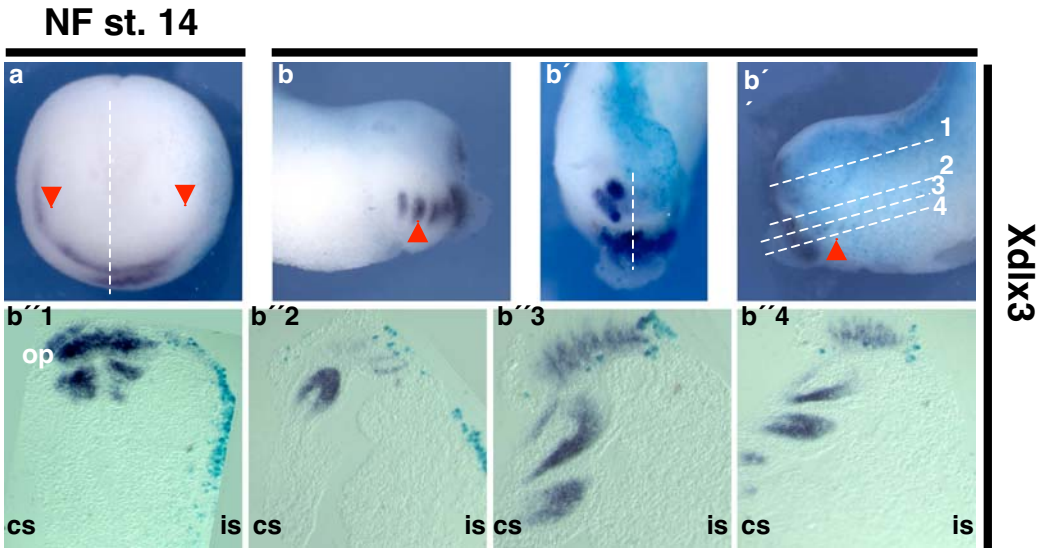

Figure 27: The antisense morpholino-mediated knockdown of Xdhcr7 resulted in a severe reduction of *Xdlx3* expression.
a : anterior view (dorsal up) of stage 14 embryos; the position of the midline is shown by white dashes. b, b´´and b´´: side views of stage 32 embryos. The frontal view is shown in b´.
Two-cell stage albino embryos were injected (in one of two blastomers) with 1pmol of Xdhcr7-morpholino, in combination with 200pg of n- -Gal capped RNA as linage tracer. Injected embryos were cultured in 0.1 X MBS until opened neural plate (NF st. 13 / 14) or tailbud stage (NF st. 32 / 32), fixed in MEMFA, and hybridized with a Dig-labelled *Xdlx3* antisense RNA, after X-gal staining (blue colour). Xdhcr7 morpholino caused a severe reduction of *Xdlx3* expression both at early (a) and late (b – b´´) stages of development. At neurula stage, almost no *Xdlx3* staining could be detected on the injected side (is, red arrowhead in a). The same reduction was observed at tailbud stage, but the pharyngeal pouches expression domain appeared more severely reduced (see red arrowheads in b and b´´, and is in b´´2 – b´´4).

When embryos were analysed for *Xgsh1* and *Xnkx2.2* expression (Fig. 28), the results were more in line with the gain-of-function activity.

The forebrain expression domain of Xgsh1 (Fig. 28a – a´´) was reduced for 63.3 % (n = 19 / 30) of the analysed embryos. On transversal sections (Fig. 28 b´´1 – b´´3), this reduction appeared more pronounced in the forebrain. Moreover, the expression domains on the injected and control side were not symmetrical, suggesting an effect on the dorso-ventral patterning of the brain. When hybridized with the ventral brain marker *Xnkx2.2* (Fig. 28b – b´´), 59.4 % (n = 19 / 32) of the embryos displayed a reduction of the expression. Same as for *Xgsh1*, the reduction was more severe in the forebrain, and the expression domain was ventrally shifted on the injected side (Fig. 28b´´1 – b´´2).

In summary, the antisense morpholino-mediated knockdown of Xdhcr7 severely compromised eye development, and interfered with the expression of both eye and neural marker genes.

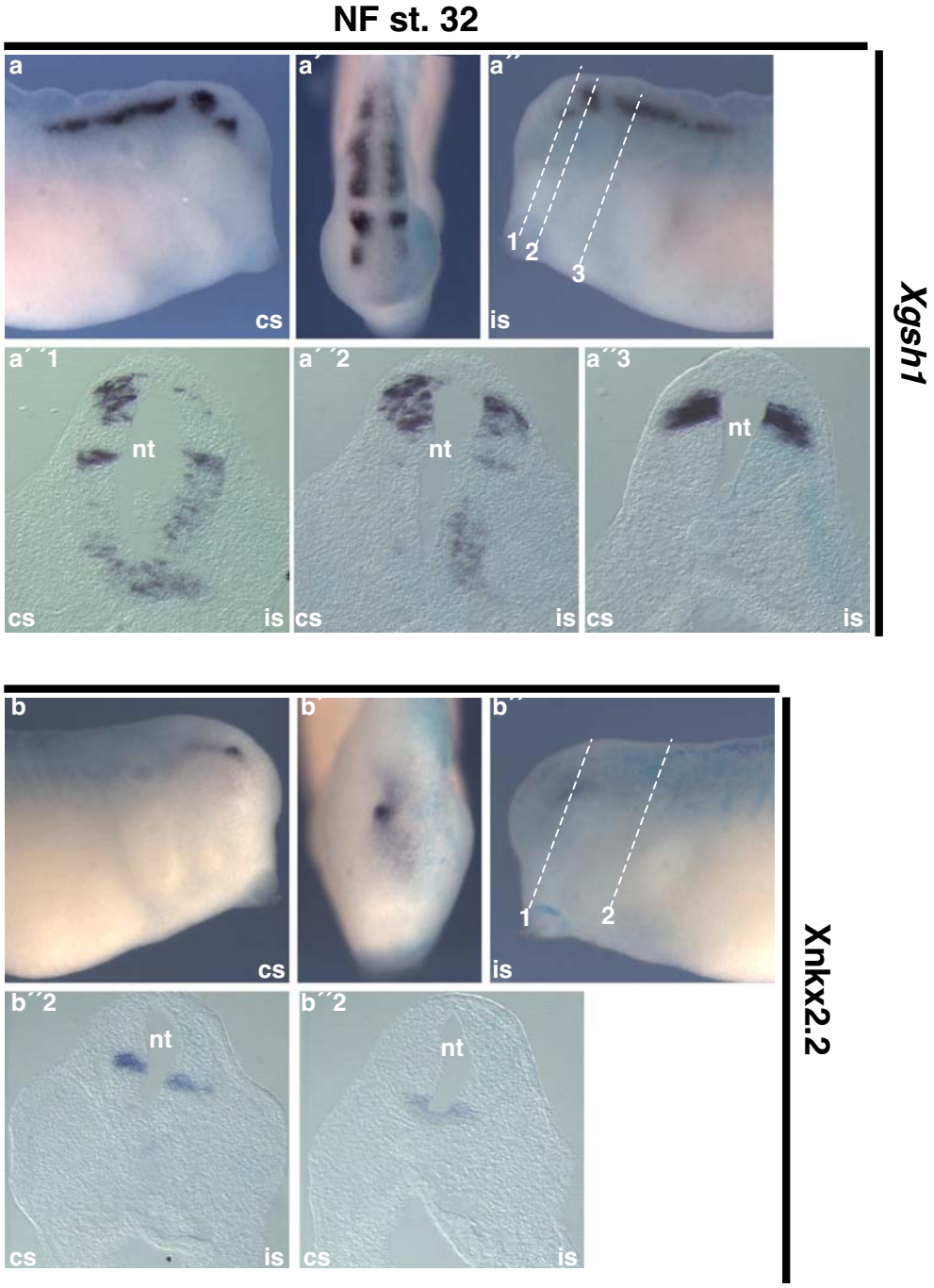

Figure 28: The antisense morpholino-mediated knockdown of Xdhcr7 resulted in the reduction of the anterior expression domain of *Xgsh1* and *Xnkx2*.2.
a, a´´, b and b´´ : side views of stage 32 embryos. The frontal views are shown in a´ and b´.
Two-cell stage albino embryos were injected (in one of two blastomers) with 1 pmol of Xdhcr7-morpholino, in combination with 200pg of n- -Gal capped RNA as linage tracer. Injected embryos were cultured in 0.1 X MBS until tailbud stage (NF st. 32 / 34), fixed in MEMFA, and hybridized with a Dig-labelled *Xgsh1* or *Xnkx2.2* antisense RNA, after X-gal staining (blue colour).
The expression domain of *Xgsh1* (a – a´´) appeared reduced on the injected side. On transversal sections (a´´1 – a´´3), the dorso-ventral patterning of the brain seemed to be affected, as the expression domain of Xgsh1 appeared ventrally shifted on the injected side. Same as for *Xgsh1*, the expression domain of *Xnkx2*.2 (b – b´´2) was reduced and ventrally shifted (see b´´2). However, a general observation was that the reduction of both *Xgsh1* and *Xnkx2*.2 expression was more pronounced in the forebrain.

II.3.2.4. Antisense morpholino-mediated knockdown of Xdhcr7 mildly interfered with sonic hedgehog signalling.

As Xdhcr7-morpholino seemed to interfere with the eye development and dorso-ventral patterning of the brain, we were interested in knowing whether these phenotypes could be due to an interference with hedgehog signalling. When hybridized with *Xshh* Dig-RNA, the Xdhcr7-morpholino injected embryos did not show any clear phenotype, suggesting that the expression of *Xshh* was not influenced. When analysed for *Xhnf-3β* expression, unlike for the overexpression experiment, the injected embryos did not show any striking phenotype at the first sight (Fig 29 a – a´). However, a detailed analysis (Fig. 29 a1 – a´1) showed a minor, but significant reduction (51.7 %, n = 15 / 29) of the expression in the branchial arches at tailbud stage (red arrowheads in a1 an a´1). When analysed on transversal section, the expression domain appeared reduced on the injected side, mostly at the dorsal edge, suggesting a shift in the dorso-ventral distribution of the signal. Although this phenotype was not further confirmed, it appeared to be in line with the analysis of the expression of *Xgsh1* and *Xnkx2.2.*

Taken together, the results of the lost-of-function analysis suggested that XDHCR7 activity is needed for eye development. Consistent with the gain-of-function analysis (which showed increased pigmentation), the lost of XDHCR7 function resulted in severe reduction of pigments cells, comprising the retinal-pigmented epithelial layer. In the context of neural development, Xdhcr7-morpholino induced a reduction of the neural tube, and seem to interfere with the dorso-ventral patterning of the brain. As monitored by the expression of *Xhnf-3β*, the effect on sonic hedgehog signalling was not striking, by a significant minor interference could be noted.

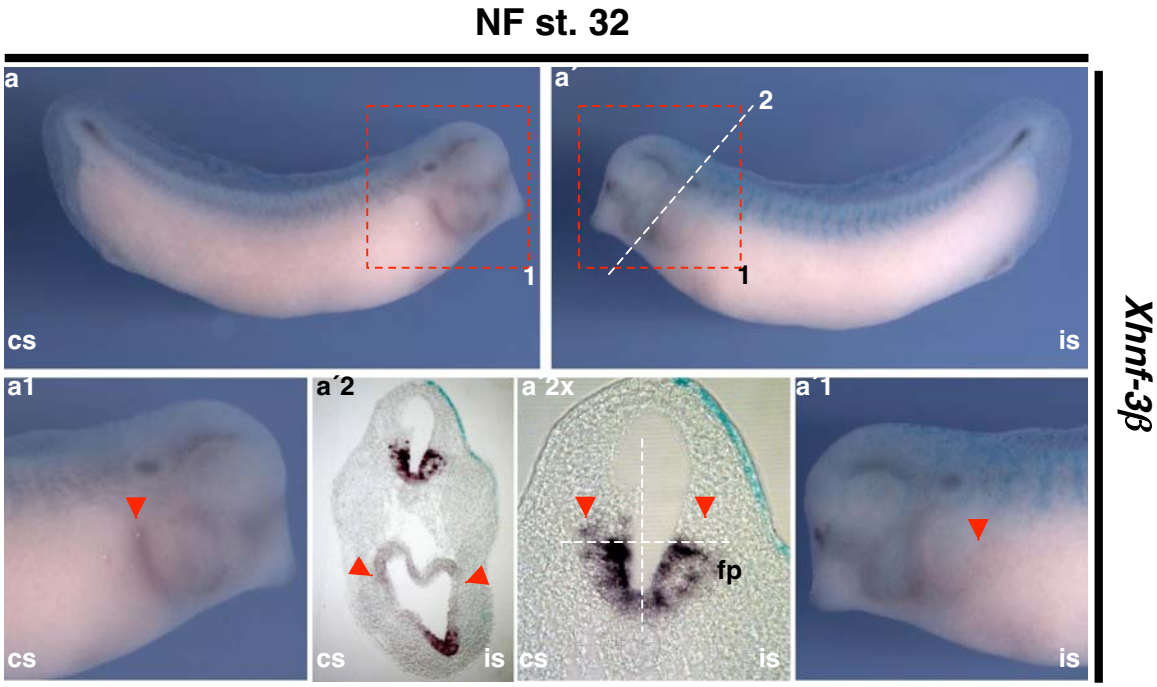

Figure 29: The antisense morpholino-mediated knockdown of Xdhcr7 resulted in a minor, but significant reduction of *Xhnf*-3β expression.
a and a´´ : side view of a stage 32 Xdhcr7-morpholino injected embryo. On panels a´2 and a´2x, transversal sections are shown. a´2x shows a higher magnification of the boxed portion of a´2 respectively, whereas a1 and a´1 show a higher magnification of the boxed portion of a and a´ respectively.
Two-cell stage albino embryos were injected (in one of two blastomers) with 1 pmol of Xdhcr7-morpholino, in combination with 200pg of n-β-Gal capped RNA as linage tracer. Injected embryos were cultured in 0.1 X MBS to tailbud stage (NF st. 32 / 34), fixed in MEMFA, and hybridized with a Dig-labelled *Xhnf-3β* antisense RNA, after X-gal staining (blue colour).
Upon injection of Xdhcr7-morpholino, no dramatic effect could be noted on the expression of *Xhnf-3β* (a – a´). However, for a significant number of embryos, the expression appeared reduced in the branchial arches on the injected side, as compared to the control side (red arrowheads in a1 and a´1). When closely analysed by transversal section, the floor plate (fp) expression domain appeared reduced on the injected side, mostly at the dorsal edge (red arrowheads in a´2x).

II.3.2.5. Antisense morpholino-mediated knockdown of Xdhcr7 resulted in increased apoptosis and reduced proliferation

To test whether the Xdhcr7-morpholino eye and brain phenotype could be explained by an influence on programmed-cell death or on proliferation rate, injected embryos were analysed by TUNEL assay to detect apoptosis, and by anti-PH3 immunostaining, to detect mitotic cells.

Upon Xdhcr7-morpholino injection, 85,7 % (n = 18 / 21) of the analysed embryos showed an increased TUNEL staining in the injected side of the brain, as compared to the control side (Fig. 30a´´, red arrowheads); meanwhile, the staining was reduced in several extra-cranial tissues (yelloow arrowed in a, a´, a1 and a´1) on the injected side. This was in line with the overexpression experiment, which suggested a need of DHCR7 activity for cell survival in the brain, but not in extra-cranial tissues. When the injected embryos were analysed for mitosis rate (using anti phosphorylated histone H3 antibodies; fig. 30b – b´1), a significant number of embryos (29.4 %, n = 5 /17) showed a general reduction of the number of positive cells on the injected side, as compared to the control side

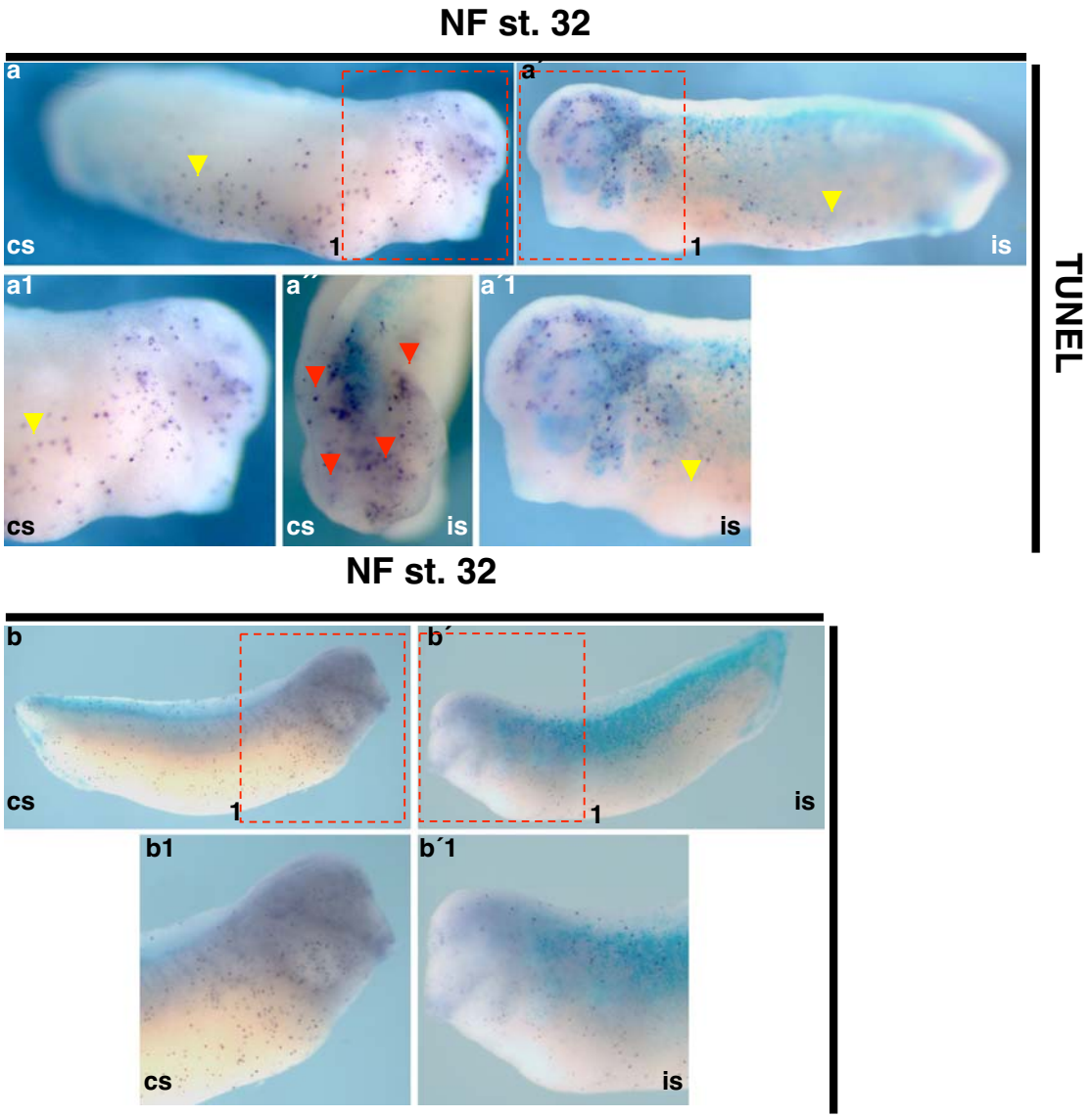

Figure 30: The antisense morpholino-mediated knockdown of Xdhcr7 resulted increased apoptosis in the brain, and reduced proliferation rate.
a and a´: side views (dorsal up) of the control side (cs) and injected side (is) of a NF st. 32 embryo showing the staining for apoptotic cells (TUNEL). a1 and a´1 show a higher magnification of the head portion of a and a´ respectively. The frontal view of the same embryo is shown in a´´.
b and b´: side views (dorsal up) of the control side (cs) and injected side (is) of a NF st. 34 embryo showing the staining for mitotic cells (Anti-PH3 immunostaining). b1 and b´1 show a higher magnification of the head portion of b and b´ respectively.
Two-cell stage albino embryos were injected (in one of two blastomers) with 1 pmol of Xdhcr7-morpholino, in combination with 200pg of n- -Gal capped RNA as linage tracer. Injected embryos were cultured in 0.1 X MBS to tailbud stage (NF st. 32 / 34), fixed in MEMFA, and stained with to identify the injected side (blue colour). After refixation, embryos were dehydrated in ethanol, permeabilised by incubation in the DENT´s fixative (-20 °C, overnight), and further processed for TNUEL assay or Anti-PH3 immunostaining.
Upon xdhcr7-morpholino injection, a higher number of apoptotic cells (indicated by red arrowheads in a´´) could be noted on the injected side (is) of the brain, as compared to the control side (cs). Interestingly, the number of TUNEL positive cells was rather reduced in non cranial tissues of the injected side (yellow arrowhead in a, a1, a´ and a´1), as compared to the control side. On the other hand, a general reduction of the proliferation rated was noted, as analysed by Anti-PH3 immunostaining. As compared to the control side (cs, b and b1), the injected side (is, b´ and b´1) of the embryo showed less anti-PH3 staining positive cells.

II.3.2.6. Chemical inhibition of cholesterol synthesis caused comparable phenotypes as Xdhcr7 morpholino-mediated knockdown.

In order to analyse the effect of the direct inhibition of cholesterol biosynthesis on *Xenopus* development, we made used of two well-characterised chemical inhibitors of enzymes of the Kandutsch-Russel cholesterol biosynthesis pathway. Lovastatin (mevinolin) is an inhibitor of the hydroxymethylglutaryl-coA reductases (HMGR), the catalyser of the rate limiting step of the pathway), and the trans-1,4 bis-(2-dichlorobenzylaminomethyl) cyclohexane dihydrochloride (AY9944) blocks the synthesis by inhibiting the direct DHCR7-catalysed conversion of 7-dehydrocholesterol (7-DHC) to cholesterol (CHO).

Two cell stage or blastula stage (St. 8) embryos were continuously treated with AY9944 (250 μM in 0.1 X MBS) or Mevinolin (125 μM in 0.1 X MBS) and recorded for survival and phenotype. When treatment was started at two cells stage, all the AY9944-treated embryos died short after complete neurulation (Fig. 31a). Those that were treated from stage 8 on developed until early tadpole stage (Fig.31c), and failed to grow further (died massively). They all showed growth retardation, smaller body size, smaller eyes and shortened head, as compared with the control embryos from the same batch. A striking observation was that the treated embryos first lost their head structures before they died (example is the case of the cement gland which is absent in c (red arrow)). Whether treated from two cells stage or from stage 8, the Mevinolin-treated embryos were developmentally comparable to the control ones (no striking growth retardation). However, they all showed a severe reduction of the eye and body sizes, and a severely pronounced eye coloboma phenotype. The body axis was most of the time distorted. We were also interested in investigating the effect of a direct application of cholesterol and / or its precursor (7-dehydrocholesterol), but due to the insolubility of these compounds in the embryos culture medium (0.1 X MBS), the experiment was rendered difficult to optimize.

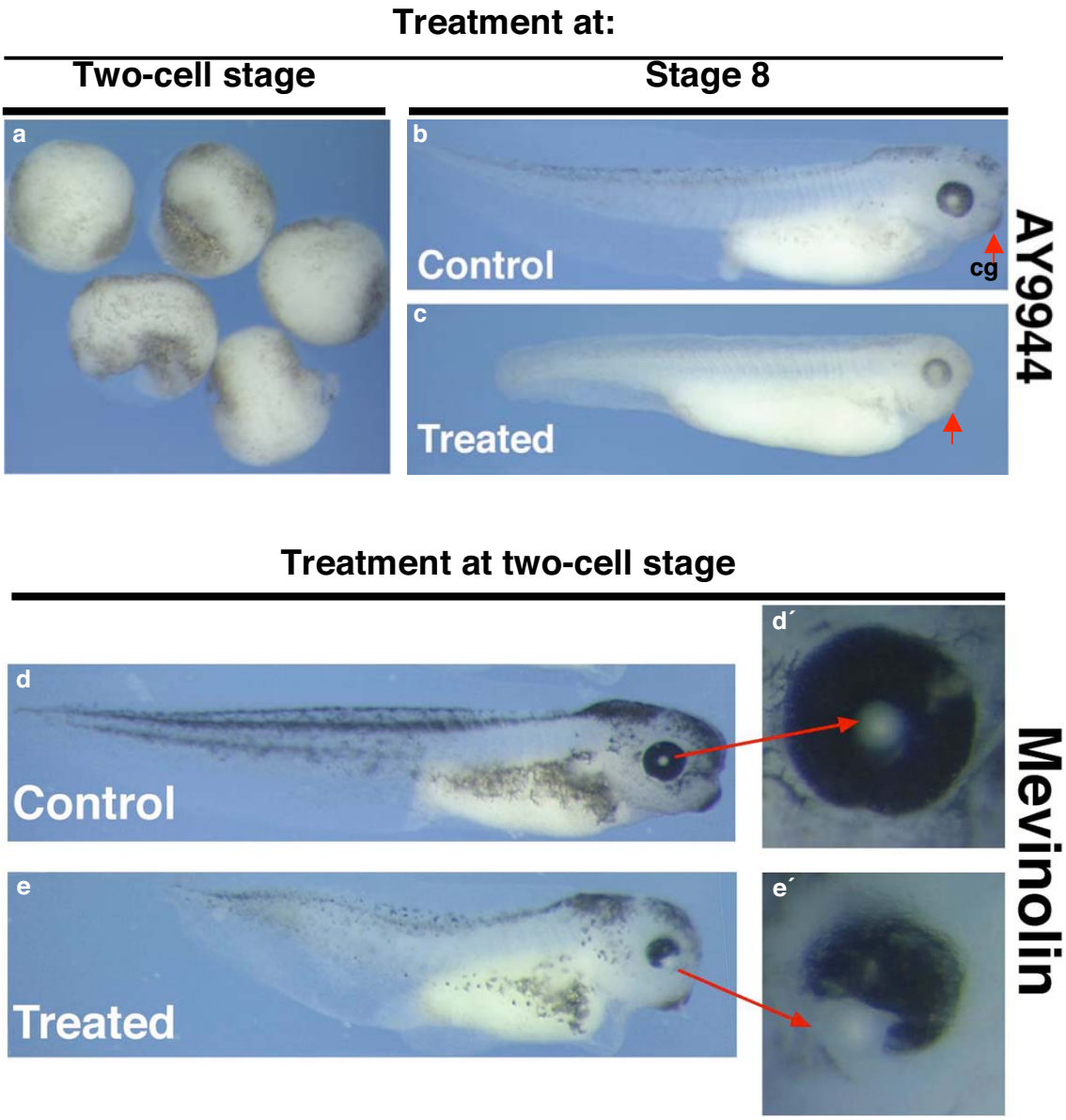

Figure 31: The direct chemical inhibition of cholesterol biosynthesis impaired development.

a: late neurula stage AY9944-treated embryos showing severe necrosis.
b: tadpole stage control embryo.
c: tadpole stage AY9944-treated embryo.
d: tadpole stage control embryo.
d´: higher magnification of the eye of (d).
e: tadpole stage Mevinolin-treated embryo.
e´: higher magnification of the eye of (e).

Early AY9944 treatment caused massive death (a). When applied later, AY9944 caused growth retardation, and reduced body size (b-c). Note that the embryo shown here had already started losing head structures; the cement gland (cg) is not visible in this case (red arrows).
When applied at two-cell stage, Mevinolin caused reduced body size and severe eye phenotype (d-e´).

II.4. Heterologous expression of XDHCR7 proteins in the yeast *Saccharomyces cerevisiae*.

In order to further analyse the activities of the three XDHCR7 isoforms, we carried out a heterogous expression in yeast. Xdhcr7-L, - M and – S cDNA were subcloned in the 2 μ yeast vector pYX212 (R & D System), as EcoRI / MluI fragments. Each isoform was inserted in frame (et the 3´-end) or not with the haemagglutinin (HA) tag contained in the plasmid, with or without a 5´-flag tag. These constructs were transformed into *Saccharomyces cerevisiae* strain ABYS (protease deficient). Cells were grown on appropriate medium and assayed for DHCR7 protein synthesis. For western blot analysis, microsomal proteins fractions (100,000 g pellets) were prepared from transformed cells and fractionated by SDS-PAGE. Using the HA-tagged constructs, the western blot analysis confirmed the synthesis of proteins of expected sizes, which were enriched in the microsomal fractions (not shown).

To investigate whether the three XDHCR7 proteins had the same cellular localisation pattern, we performed an in situ immunostaining of the transformed cell, using and anti-HA primary antibody and a Cy5 coupled secondary antibody. Despite their different molecular topology (as was shown in fig. 7B), there was no difference in their subcellular localisation pattern. They all localised to the ER when expressed in yeast (Fig. 32, and not shown). The actual aim of the heterologous expression was to perform in vitro kinetic studies of the three XDHCR7 isoforms. Preliminary results pointed to a necessity for an intact c-terminus end of the protein for XDHCR7 enzymatic activity. In fact, the S version, the M version and the HA-tagged L version showed no activity as compared to the non modified L version. However, due to optimization difficulties, this experiment is still going on.

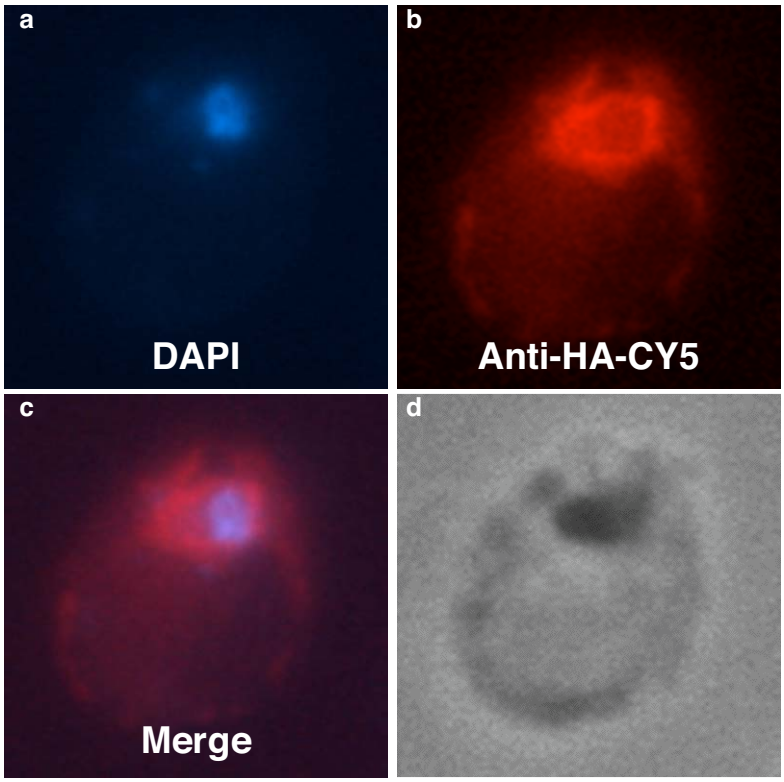

Figure 32: The XDHCR7 proteins localised to ER structures when expressed in yeast.

a: DAPI staining of the chromatin.
b: Anti-HA-CY5 staining of the HA-tagged XDHCR7-L protein.
c: Merge image of a and b.
d: same cell view with normal light.
The heterologously expressed XDHCR7-L protein localised around the nucleus and beneath (b and c), which correspond to ER structures in yeast.

III. DISCUSSION

Cholesterol is one of the biochemical compounds with the most controversy in the history of its physiological properties. From the first isolation of cholesterol in the late 1700s (Nwokoro et al., 2001) to the discovery of mevalonic aciduria as the first disorder of its biosynthesis (Berger et al., 1985; Hoffmann et al., 1986), most of the discussion about cholesterol was centered on its possible involvement in coronary heard diseases (Steinberg, 2004). Since the identification of DHCR7 mutations as cause of the Smith-Lemli-Opitz syndrome (SLOS; Tint et al., 1994), the dhcr7 gene has been isolated in mouse, rat and human, but the amphibian dhcr7 has not yet been described. Furthermore, most of the studies intended at describing the molecular background of the SLOS have made used of mutant mice or cell lines (Yu et al., 2004; Cooper et al., 2003). No partial knockdown experiment has been carried out, neither has it been the case for an overexpression experiment. In the present project, our main gaol was not only to make a breakthrough in the study of sterol metabolism in amphibians, but mostly to bring new insights into the understanding of the disorders of cholesterol metabolism, by analysing the molecular mechanisms underlying the reported phenotypes.

In our experimental approach, the description of the dhcr7 expression pattern was a suitable tool to understand the spatial and temporal distribution of endogenous cholesterol biogenesis potential, which could help in predicting the sensitivity of different tissues and developmental stages to perturbations in the cholesterol balance, as well as some pathways in which cholesterol may have a potential role. Recent data by Laubner et al. (2003) have reported that embryonic cholesterogenic genes expression is restricted in distinct domains and colocalizes with apoptotic regions in mice, but no detailed histological description of the embryonic expression pattern of the dhcr7 transcripts had been shown. Moreover, their study did not consider the very early expression. Here we have reported the expression pattern of Xdhcr7, starting from the very beginning of gastrulation. The functional characterisation was not only intended at understanding the role of cholesterol in development, but mostly to understand the very role of the dhcr7 gene in both development and cholesterol homeostasis.

III.1. Molecular cloning of the xdhcr7 cDNA and structural features of the XDHCR7 protein.

Cloning by metabolic interference was the strategy used by Lecain and colleagues (1996) to isolate the first known Sterol Δ7-reductase cDNA from *Arabidopsis thaliana*. In our study, we took advantage of the existence of previously isolated vertebrate Δ7-sterol reductase cDNAs with high sequence homology, and the availability of a *Xenopus* expressed sequence tagged (EST) database. In a database search, we were able to identify three clones with homology to the human dhcr7 cDNA, but no full-length open reading frame (ORF) of the *Xenopus* dhcr7 (Xdhcr7) cDNA was available. In our attempt to isolate the full-length Xdhcr7 cDNA, we were able to isolate three alternatively spliced isoforms (Xdhcr7-L, Xdhcr7-M and Xdhcr7-S), which shared the same ORF. This feature of the dhcr7 transcripts to be present as alternatively spliced isoforms, had also been reported in rat by Lee and colleagues (2002), who could also show that the five alternatively spliced transcripts were differentially expressed between tissues. This could also be the case in *Xenopus*, but we failed to clearly rule it out in our study.

The *Xenopus* dhcr7 protein (XDHCR7) shares high homology with vertebrates DHCR7 (more than 75 % identity in average), but very low homology with plants Sterol Δ7-reductases (less than 35 % identity). This is not only a consequence of the evolutionary distance between vertebrates and plants, but is biochemically meaningful with regard to the natural substrates of the enzymes in these species (7-dehydrocholesterol and 7-dehydrositosterol respectively). As other DHCR7 proteins already described (Fitzky et al., 1998; Bae et al., 1999), the predicted amino acids sequence of XDHCR7 point to a membrane protein with 9 putative transmembrane domains. This is a general feature of proteins involved in the later stages of sterol biosynthesis, as intermediate substrates are generally lipophilic and likely to be trafficked within the membrane lipid bilayer.

The amino acids composition of XDHCR7 comprises a total of 4.4 % serine (21 residues) and 4.6 % threonine (22 residues) distributed throughout the backbone. This is close to the serine / threonine contents of rat DHCR7 (4.8 % / 4.7 %; Bae et al., 1999), *nasturtium* sterol Δ7-reductase (4.6 % / 5.1 %; Acc Nr.: AAR29980) and *Arabidopisis* sterol 7-reductase (5.1 % / 5.6 %; Lecain et al., 1996). Thus, despite their differences in amino acids composition, plants and vertebrates sterol Δ7-reductase proteins seem to share the

same susceptibility to phosphorylation by serine / threonine kinases (Hanks and Hunter, 1995). Three putative N-linked glycosylation sites (positions 8-11, 253-256 and 410-413) as well as a highly conserved N-myristylation site (position 127-132) are present in the XDHCR7, which suggest a possible posttranslational golgi-maturation and membrane anchoring of the protein (Farazi et al., 2001; Dennis et al., 1999; Masaki et al., 1996). This feature is shared by rat DHCR7, but is not obvious in plant sterol Δ7-reductases. The SSD content of XDHCR7 is a general feature of most of the proteins involved in sterol metabolism and / or homeostasis, and those involved in sterol-linked signal transduction (Kuwabara and Labouesse, 2002). Interestingly, all the four vertebrates DHCR7 compared here share almost 100 % sequence identity in their 9 transmembrane domains. This suggests that the transmembrane domains might play an important role in the activity of the protein, probably in their membrane targeting, and substrate binding. In fact, in SLOS patients, most of the mutations with severe pathology are located in transmembrane domains or at the c-terminal end of the DHCR7 protein (Shim et al., 2004; Nowaczyk et al., 2003; Jira et al., 2003; Witsch-Baumgartner et al., 2001). The membrane anchoring may not only be important for allowing a suitable folding of the protein, but also in the way that it may favour the clustering of the enzymes involved in the sterol biosynthesis pathway, since most of these enzymes are located in the peroxisomes or in the endoplasmic reticulum membrane (ER) (Liscum, 2002). The XDHCR7 shares homolog structural features with other vertebrates DHCR7s, suggesting a conserved activity of the dhcr7 gene between these species.

III.2. Expression pattern of *Xdhcr7*

By RT-PCR a baseline maternal *Xdhcr7* transcripts level can be detected in the unfertilized egg (Fig. 9A). This suggests a requirement for *de novo* cholesterol biosynthesis from the very early stages of *Xenopus* development. With regard to the role of cholesterol as membrane constituent, and considering the need for membrane biogenesis during early developmental stages of *Xenopus*, which mainly comprise cleavages, a very early requirement for DHCR7 activity appear just understandable. This may not be the case in mammals (human for example), since the transplacental receptor-mediated lipoprotein transfer may satisfy this very early cholesterol demand (Witsch-Baumgartner et al., 2004). The level of *Xdhcr7* expression greatly increases by stage 11-13, which corresponds to the starting of neurulation processes in *Xenopus*. This points to a role for cholesterol in cellular

events taking place at this stage of development. This activation is gradually shut down by stage 28, at which most of the tissue identities have already been established. This then suggests that XDHCR7 activity might be mostly critical for neurulation and tissue induction processes. In the adult frog, *Xdhcr7* transcripts also show a differential tissue distribution (Fig. 9B), being mostly expressed in the brain, eye, spinal cord, skin, kidney, lung, liver stomach and testis. The human dhcr7 transcripts have been reported to be ubiquitously expressed (Moebius et al., 1998), but with higher expression in the adrenal gland, liver, testis and brain. This suggests a relatively conserved tissue distribution in frog and human. However, unlike for human, the expression in *Xenopus* ovary was hardly detectable. This suggests that endogenous cholesterol biosynthesis may be less necessary for female than for male sex formation. However, this does not explain the expression in the non-fertilized egg. In fact, several SLOS medical screens have reported sex abnormally (genitalia) in males (46 XY Karyotype with female external genital phenotype) but no genitalia have yet been reported in female SLOS patients (Lin et al., 1997; Lachman et al., 1991; Pinsky et al., 1965). The increase in the level of the developmental expression of *Xdhcr7* transcripts coincides interestingly with the beginning of *Xshh* expression; the tissue expression of *Xshh* transcripts also follows the same pattern as for Xdhcr7. A possible link between cholesterol metabolism and hedgehog signalling has already been suggested by previous reports. Inborn errors of cholesterol biosynthesis share the same holoprosencephaly phenotype as mutations affecting the hedgehog signalling pathway, and the cholesterol modification of the hedgehog protein is important both for the sending, the receiving and the graded distribution of the signal (Jira et al., 2003; Cooper et al., 2003; Kelley and Herman, 2001 Lewis et al., 2001; Mann and Beachy, 2000). Our finding that *Xdhcr7* and *Xshh* are expressed in overlapping temporal and spatial patterns is then in line with these previous findings.

Although less sensitive than RT-PCR, analysing expression pattern by mean of WMISH has a greater advantage in the way that, technically, it makes it possible to describe both the spatial and temporal distribution of the transcripts, at the same time. By this technique, the first expression of Xdhcr7 appears around stage 10 – 10.5 (Fig. 10a), which corresponds to the stage at which increase of the RT-PCR product is noted (Fig. 9A). The Xdhcr7 appears in the dorsal blastopore lip (dbl in fig. 10a), which corresponds, to the Spemann organizer; the maintenance of the expression in the forming dorsal midline

(notochord; Fig. 10b – h) is meaningful, since this corresponds to an important signalling center. This suggests a role for cholesterol biosynthesis in pattern formation, since many patterning activities are secreted from the notochord during vertebrate development (Fleming et al., 2004; De Robertis et al., 2000; Cleaver et al., 2000).

During neurulation and organogenesis (Fig. 10f – l), Xdhcr7 shows an interestingly dynamic expression pattern. After the notochord, the expression is activated in several neural and placodal tissues. As shown on sections (Fig. 11a-e), apart from ectodermal tissues (neural and placodal derivatives), the expression of Xdhcr7 can only be seen in the notochord (Fig. 11a-d) and the hypocord (subnotochordal, fig. 11c1´). With regard to the ubiquitous need for cholesterol in cell structure, this restricted expression pattern of Xdhcr7 suggests that the need for *de novo* cholesterol biosynthesis may not be the same for every *Xenopus* embryonic cell types. In mice, uptake of LDL cholesterol from blood circulation does not contribute to growth and differentiation of the central nervous system (Dietschy and Turley, 2001; Hanaka et al., 2000). If the situation were similar in *Xenopus*, neural cells may then need to synthesize their own cholesterol because of an inability to use extracellular cholesterol, whereas midline cells (notochord) may produce cholesterol not only for their proper use, but also probably for export to surrounding cell. In fact, de novo synthesised cholesterol is transported from the ER to the plasma membrane (PM) via caveolae; once at the exoplasmic face of the PM, cholesterol diffuses laterally and becomes available for efflux into the extracellular environment (Tabas, 2002; Garver and Heidenreich, 2002; Schmitz and Orsó, 2001; Hoekstra and Ijzendoorn, 2000). The expression pattern of *XstAR* transcripts as compared to *Xdhcr7* expression (Fig. 12B) can fit into this model. *XstAR* and *Xdhcr7* are expressed in an interestingly complementary feature. Since the STAR protein is a cholesterol transporter (Petrescu et al., 2001; Christenson and Straus, 2000; Tsujishita and Hurley, 2000), this suggests that cells that do not synthesize cholesterol by themselves may satisfy their cholesterol need by transporter-mediated uptake from the neighbouring. It is also interesting to note that *Xdhcr7* and *Xshh* are coexpressed in the notochord, but not in the neural tube (Fig. 12A). Hence, at stage 30, while Xdhcr7 is expressed in the notochord and in the motor neurons area (but not in the floor plate, fig. 12Ab), *Xshh* is expressed in the notochord and the floor plate but not in the motor neurons area (Fig. 12Ab´). Evidence of a cholesterol modification of the hedgehog protein has been established since 1996 (Mann and Beachy, 2000).

Since then, this modification has been suggested to be important for the protein to elicit long-range activity, and for a proper sequestration of the protein by its receptor patched (Lewis et al., 2001; Ingham, 2000). In sending cell, the export of the Shh signal is facilitated by the membrane-bound protein Dispatched, which like Patched, contains a sterol-sensing domain. Moreover, graded Shh activity (from the floor plate) has been proven to trigger different cell fates along the dorso-ventral axis of the neural tube (Marti and Bovolenta, 2002). The vicinity between *Xshh* and *Xdhcr7* expression areas is interestingly in line with these previous findings. Since signals (Shh and others) from the notochord are known to pattern the mesoderm, the expression of *XstAR* (Fig. 12Bd´) in the presomitic mesoderm (psm, where *Xshh* is not expressed) is also in line with the need for cholesterol in Shh receiving cells, for long-range signalling.

At later stage (Fig. 10I-I´´and fig. 11e) the expression of Xdhcr7 is more restricted to head structures; this is in accordance with the decrease of the RT-PCR product at late stage (Fig. 9A), and the higher levels in the brain and eye, as compared to the rest of tissues (Fig. 9B). This is likely to be physiologically, meaningful in the way that compared to other tissues, the brain structures need more cholesterol and are dependant on the *do novo* cholesterol biosynthesis for the whole life. In fact, the highly selective blood-brain barrier does not allow the uptake of cholesterol-rich lipoproteins from the blood stream. However, the size of sterol pool in the central nervous system increases disproportionately as brain size increases, and nearly 25 % of the human total body free cholesterol is present in the brain, mainly in the myelin (Bjorkhem and Meany, 2004; Pfrieger, 2003). The brain cholesterol is important not only for the structure of the brain, but also for its normal function. It has been suggested that low level of cholesterol might be responsible for depression and violent, or even suicidal behaviour. (Dietschy and Turley, 2004). This is also in accordance with multiple craniofacial malformations reported in SLOS patients.

III.3. Functional characterisation of Xdhcr7.

Xdhcr7 is highly expressed in the notochord in early stage, and is later enriched in the central nervous system and its derivatives, including the eye (Fig. 10 and 11). This suggests that XDHCR7 activity might be important for the development of these organs. Moreover, mental retardation and microphtalmia are among the most common symptoms reported in SLOS patients (Bataille et al., 2001; Bataille and Steiner, 2000; Porter, 2000; Wassif et al., 1998; Honda et al., 1998). In the functional characterisation of Xdhcr7, we

use the eye as our principal model organ, not only because of its endogenous expression of the Xdhcr7 transcripts, but also because accumulating evidence indicates that Shh activity is involved in pattern formation of the vertebrate eye (Cornesse et al., 2004; Zhang and Yang, 2001). In fact, since graded hedgehog signalling is dependent on the cholesterol modification of the hedgehog protein (Ingham and McMahon, 2001), studying cholesterol homeostasis in the context of eye development could bring new insights in the molecular background of cholesterol metabolism disorders.

III.3.1. Gain-of-function study.

III.3.1.1. Overexpression of Xdhcr7 isoforms differentially affected eye development.

The injection of Xdhcr7-M did not cause any obvious phenotype in tadpole stage embryos, neither did it interfere with eye field marker genes (*Xrx1* and *Xsix3*) expression during neurulation (Fig. 14a – a´´; fig. 15a – a´´; Fig. 16a – a´´). Structurally (Fig. 33), XDHCR7-M protein differs from the L version by the truncation of amino acids residues 278 – 323 (TMD6 and TMD7; fig. 7A – B). In the human DHCR7, these amino acids are part of the region encoded by the exon 9, which is highly conserved and is reported to be mutated in a high proportion of SLOS patients (Shim et al., 2004; Kelley and Herman, 2001). The lack of activity of XDHCR7-M may be due to an inefficient substrate binding capacity, since the truncated portion is part of the predicted sterol-binding domain. Unlike the M version, Xdhcr7-S caused massive embryonic lethality, and small eye phenotypes (Fig. 14b – b´´). The small eyes did not show any stratification disturbance (Fig. 14b´1 and b´2), and when analysed for eye field marker genes expression, a reduction of the late expression domain of *Xrx1* and *Xsix3* could be noted (Fig. 15b – b´´; fig.16b – b´´). In some cases, a slight enlargement of the early expression domain of these markers could be noted, suggesting an interference with the evagination of the eye primordium. This was reminiscent of the effect of Xdhcr7-morpholino. With regard to its structure (Fig. 33), XDHCR7-S may potentially act as a dominant negative protein, since it lacks the whole sterol-binding domain, as well as the NADPH binding domain. The preliminary data from kinetics study suggested that this version lacks enzyme activity, but this is still to be confirmed. Since XDHCR7-S might localise in the same subcellular compartment as XDHCR7-L (Fig. 32), it may potentially interfere with the clustering of the active protein on the ER membrane. However, it is still unclear why the M version did not show the same phenotype, although it is truncated and probably lacks enzyme activity to. Upon overexpression, Xdhcr7-L caused

small eyes phenotype (Fig. 14c – c´´), and a transdifferentiation of optic stalk cells into retinal-pigmented cells (pigmented eye stalk, fig. 14d), which suggests an impairment of both the development and the proximo-distal patterning of the eye primordium. However, histological analysis of the small eyes did not show any obvious alteration of the retinal stratification, suggesting that XDHCR7-L activity reduced the eye territory, but did not disturb cell identity in the retina. When analysed for eye field marker genes expression, Xdhcr7-L did not cause any drastic change to the early expression, but caused a reduction of the expression domains of *Xrx1* and *Xsix3,* at late stage (Fig. 15c – c´´). This suggests that the observed eye phenotypes may not be due to the impairment of the early establishment of the eye field, but rather to an interference with the later development of the established eye primordium. A schematic interpretation of the differential activities of XDHCR7 isoforms in shown in figure 33. When overexpressed in *Xenopus*, the mouse dhcr7 (Mdhcr7) caused the same eye phenotypes (Fig. 14e – f), and the same effects on the expression of eye field marker genes (Fig. 15d – d´´; fig. 16d – d´´) as Xdhcr7-L. This is an indication that the observed phenotypes may be due to a conserved activity of vertebrate Δ7-sterol reductases. Since the NADPH-dependent reduction of the C_6-C_7 double bond of 7-dehydrocholesterol (to cholesterol) or 7-dehydrodesmosterol (to desmosterol, which is isomerised to cholesterol) is the only function that has clearly been assigned to the vertebrate DHCR7 proteins so far (Jira et al., 2003; Nowaczyk et al., 2001; Bae et al., 1999; Moebius et al., 1998), the Xdhcr7 and Mdhcr7 overexpression phenotypes can be at least partly considered as a reflection of a high cholesterol production. Hence, a high cholesterol input leaded to a reduction of the eye territory, but did not seem to be selective vis-à-vis a particular retinal cell type, as the stratification of the retina did not appear affected. However, a significant proportion of affected eyes showed a retinal pigmentation of the optic stalk. When analysed for the stalk marker *Xvax1* (Fig. 17b – b1), its expression domain was significantly thinned, which may reflect a replacement of part of the stalk cells by pigmented cells. *Xpitx3* is induced in the early lens placode when the eye vesicle is in close contact with the overlaying ectoderm (Pommereit et al., 2001). The expression of *Xpitx3* is then a suitable tool to monitor late development of the lens. Upon overexpression of Mdhcr7 the expression domain of *Xpitx3* was smaller on the injected side, but was morphologically similar to the control side (Fig. 17a – a´´). This fits to the idea that the overexpressed DHCR7 activity may cause a gross reduction of

the eye territory, but does not drastically inhibit the development of a particular cell type.

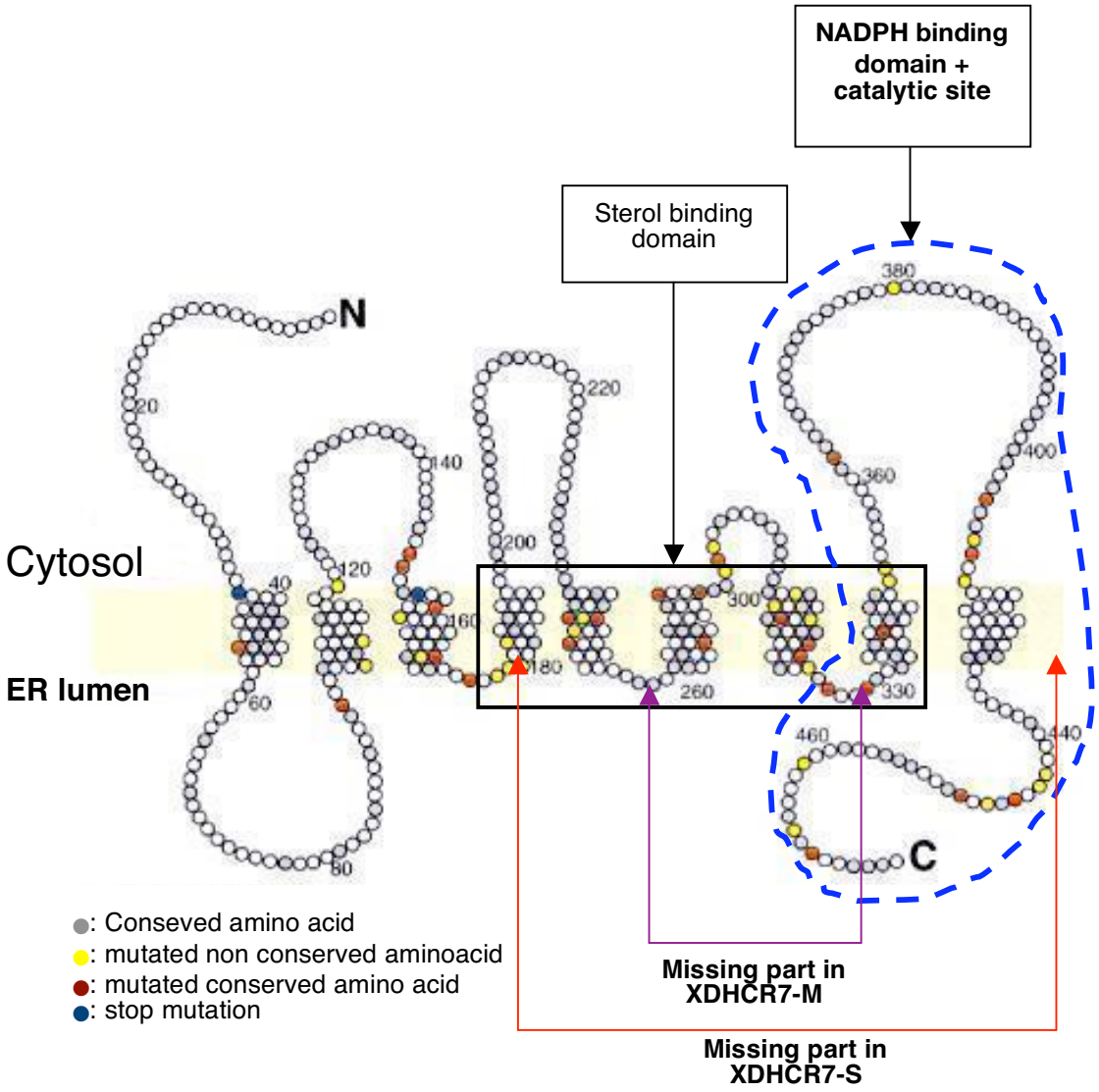

Figure 33: Schematic interpretation of the differential activities of XDHCR7 isoforms.
The topology of human DHCR7 is represented, as proposed by Fitzky et al. (2001).
Black boxed is the sterol binding domain, where the substrate binding probably takes place. Note that this domain contains most of the conserved and non conserved amino acids that are reported to be mutated in SLOS patients.
The blue dashes indicate the fourth large loop, which contains both the NADPH binding domain and the C-terminus catalytic site. The (active) full-length XDHCR7-L is likely to conserve the same topology, with regard to its sequence homology with the human DHCR7. As indicated by purple arrows, XDHCR7-M lacks two transmembrane domains (6^{th} and 7^{th}), which are parts of the sterol binding domain. Although it still contains the entire fourth loop, an inefficient substrate binding may lead to the lack of activity. XDHCR7-S lack both the sterol binding domain and the fourth loop (red arrows). Which predicts that neither sterol binding, nor NADPH binding can be achieved by this isoform. However, it still can be anchored to the membrane, suggesting that it can probably negatively interfere with the active form, due perhaps to its small size which might possibly favour it anchoring as compared to the large isoform.

III.3.1.2. An impairment of cranial placodes development may contribute to the dhcr7-induced small eye phenotype in *Xenopus*.

Since the eye territory is specified as part of the anterior neural plate (Zuber et al., 2003; Chuang and Raymond, 2002), we proposed that the impairment of eye development could result from a miss-patterning of the CNS. Upon overexpression of Mdhcr7, the early expression of the pan-neural marker *Xsox3* was rather expanded in the neural plate, and interestingly severely reduced in the placode (Fig. 18a), the later stage embryos showed and expansion of the neural tube, but the expression of *Xsox3* was reduced in placodal structures, comprising the lens (Fig.18b – b´´2). The analysis of the expression of the neuronal marker *Xn-tubulin* revealed the same expansion of the neural tube, but a severe reduction of the expression in placodal structures (Fig. 18c – d´´4) was significantly displayed. The expression of the neural plate boundary marker *Xdlx3* was also reduced in the vicinity of presumptive cranial placode at early stage (Fig. 19a). However, the late expression did show just a minor reduction in pharyngeal pouches (which are also of placodal – but not cranial – origin). This suggests that the inhibitory activity of DHCR7 may be mainly restricted to cranial placodes. It is well established that reciprocal interactions between the optic cup and the lens placode are essential for the normal development and patterning of the eye (Chow and Lang, 2001; Nguyen and Arnheiter, 2000). Rather than an impairment of the development of the whole CNS, the reduction of the placodal territory (as denoted by the expression analysis of *Xsox3* and *Xn-tubulin*) may be an explanation to the appearance of late small eye phenotype upon dhcr7 overexpression. However, this hypothesis may not account for the stalk transdifferentiation phenotype. The expression of both the dorsal brain marker *Xgsh1* and the ventral brain marker *Xnkx2.2* (Fig.20) was slightly, but significantly expanded, mostly in the forebrain. However, the expression domains of these markers were not shifted. The ectopic expression of *Xhnf-3β* (Fig. 21) could account for an induction of hedgehog signalling upon dhcr7 overexpression; however, although this fits with the expansion of *Xnkx2.2*, which is positively regulated by Shh (Pabst et al., 1999). The expansion of *Xgsh1* would not fit in this hypothesis, since Cornesse et al. (2004) reported a reduction of *Xgsh1* expression upon Xshh overexpression. When analysed for proliferation rate (Fig. 22b1 – b´1), there was no difference between the injected and control sides, suggesting that the expansion of neural structures could not be a result of increased proliferation. The number of apoptotic cells

was generally increased on the injected side as compared to the control one. Meanwhile, the forebrain showed rather the reverse feature, with less apoptotic cells on the injected side (Fig. 22a´´). This suggests that the enlargement of the forebrain may be a result of lost of placodal identity in favour of neural identity and / or an increased cell survival in the forebrain. However, additional analysis will be necessary to better understand the influence of DHCR7 activity on both proliferation and apoptosis. Definitely, the impairment of placodal development may explain the small eye phenotype, whereas increased cell survival may explain the enlargement of the forebrain. As for the stalk transdifferentiation, since the proximo-distal axis is patterned by graded activity of Shh, which promotes proximal structures (like optic stalk) at high dose and distal structures (like retina) at low dose, a possible perturbation of the proximo-distal distribution of the signal may account for such a phenotype (see fig. 34 for explanation).

III.3.2. Loss-of-function study.

Up to date, studies of dhcr7 loss-of-function have been undertaken using exclusive mutant animal model or cell lines (Yu et al., 2004; Cooper et al., 2003). Here we have taken advantage of the well-established antisense morpholino knock-down method to study the loss of dhcr7 function in *Xenopus*. The advantage of this method resides in the fact that, the embryos can be injected on one side, keeping the non injected side as an internal control. The injection of 1 pmol of Xdhcr7-morpholino resulted in severe eye phenotypes (Fig. 23a´and b´), mainly a severe reduction of the eye size, shifting of the injected eye toward the midline (cyclopia-like phenotype) and a failure of the optic cup to close properly (eye coloboma). Interestingly, the same eye phenotype was observed upon chemical inhibition of cholesterol biosynthesis (Fig. 31), suggesting that the Xdhcr7-morpholino phenotypes resulted from a down regulation of cholesterol biosynthesis. When analysed on histological sections (Fig. 23a´1 – a´2 and b´1 – b´2), the reduced eyes showed a severe perturbation of the retinal stratification, with a complete absence of the retinal-pigmented epithelium layer. This suggests that the absence of XDHCR7 activity compromises not only the establishment of the eye territory, but also the establishment of cell identity in the retina; the shifted eye phenotype also suggests a perturbation of the proximo-distal patterning of the eye field. When analysed for neural marker genes, the Xdhcr7-morpholino injected embryos displayed a general severe reduction of neural plate markers *Xsox3* (Fig. 26a – b´´) and *Xn-tubulin* (Fig. 26c – d´´), as well as brain markers

Xen2 and *Xkrox20* (Fig. 24). Histological analysis revealed a size reduction of the neural tube, suggesting an impairment of neural development. On the other hand, an early expansion of the eye field could be noted, as denoted by the expression *Xrx1* (Fig. 24a), *Xsix3* (Fig. 24c) and the anterior domain of *Xsox3* (Fig. 26a). This was a bit in contradiction with the small eyes phenotypes as well as the late expression of *Xrx1* (Fig. 24b – b´´) and *Xsix3* (Fig. 24d – d´´), which was severely reduced. However, this can also account for a delay in the evagination of the optic vesicle; in fact, when analysed closely, the expression domain of these markers do not expand out of the area that should correspond to the eye filed. This probably indicates a situation in which the control side of the eye filed is already engaged in the evagination process, while the injected side is still has not yet started to evaginate. This possible delay of optic vesicle formation can be due to a general delay of the neural folding processes on the injected side. In fact, when analysed closely, the neural plate expression domain of *Xsox3* was broader on the injected side, although the staining was severely reduced. On transversal sections (Fig. 24 b´´1 and d´´1), the expression pattern of *Xrx1* and *Xsix3* denoted an alteration of retinal stratification. When analysed for the lens expression of *Xpitx3* (Fig. 25a – a´´), the expression domain was reduced and diffused on the injected side. This diffused feature of *Xpitx3* expression could also account for a developmental delay, since the normal lens expression domain of *Xpitx3* is first defused before being later restricted to its epithelial layer (Pommereit et al., 2001). The expression of *Xvax1* (Fig. 25b – b1) was reduced on the injected side; this was in accordance with the shifted eyes phenotypes, which could arise from the failure of the optic stalk to develop properly. The expression of *Xgsh1* (Fig. 28a – a´´3) was reduced in the forebrain, and appeared ventrally shifted; the same feature was observed for *Xnkx2*.2 (Fig. 28b – b´´2) as well. This suggests a possible alteration of the dorso-ventral patterning of the neural tube. The reduction of *Xdlx3* (Fig. 27) expression indicated that the effect of Xdhcr7-morpholino was not limited to only neural structures, but could also affect other ectodermal tissues. Furthermore, the Xdhcr7-morpholino did not display any placoldal versus neural selectivity in its effects. When analysed for the expression of the floor plate marker *Xhnf-3β* (Fig. 29a2´x), the injected embryos displayed a dorsal reduction of the floor plate expression domain. Cooper et al. (2003) reported that neural plate explants from cholesterol depleted chick embryos were unable to express HNF3β, but significant HNF3β expression was noted when the explants

were supplied with increasing ShhN, suggesting the cholesterol depleted explants were unable to respond to the endogenous hedgehog signal. Moreover, a cholesterol structural analogue, cyclopamine, has been reported to directly bind to, and inhibit the activity of the Shh signal transducer Smoothened (Frank-Kamenetsky et al., 2002). It is still not clear whether this idea can apply to our case. However, if we take into consideration the shifted eye phenotype, this could account for a low hedgehog signalling, since Shh is needed to properly split the eye field into two distinct eye primordia (Chow and Lang, 2001). Overexpression of Xshh was reported to reduce the early expression of *Xrx1* and *Xsix3* (Cornesse et al., 2004). Therefore, the early effect of Xdhcr7-morpholino on *Xrx1* and *Xsix3* expression may possibly be correlated to a reduced hedgehog activity; however, the late phenotype may be a combination of multiple factors, including a possible impaired regulation of apoptosis and / or proliferation rates. When analysed for apoptosis and proliferation, Xdhcr7-morpholino injected embryos displayed a significant increase of apoptosis (Fig. 30a – a´´), mainly in head structures. This correlated with a reduced proliferation rate (Fig. 30b – b´1) on the injected side as compared with the control side. This reduced proliferation may also account for the growth retardation reported upon chemical inhibition of XDHCR7 by AY9944 (Fig. 31b – c), meanwhile, the increased apoptosis may also explain the lost of head structures at late stage upon AY9944 treatment. Overall, the Xdhcr7-morpholino-induced small eyes phenotypes may be a consequence of an impairment of the development of the central nervous system, through reduction of cell proliferation, reduction of cell survival, and probably interference with important cholesterol-dependant signalling pathways, including the Shh signalling.

III.3.3. Proposed model for interaction between cholesterol metabolism and eye development.

Overall, the functional analysis of dhcr7 in *Xenopus* suggests a need for a proper regulation of cholesterol metabolism for normal development. Although both overexpression and knock-down resulted in small eye phenotypes, the molecular analysis suggest two different mechanism (Fig. 34A). Hence, high cholesterol input may result in the inhibition of the development of cranial placodes (as denoted by the expression of *Xsox3* and *Xn-tubulin*), including the presumptive lens placode. Therefore, even though the retinal anlage might be normally specified, it may later interact with a reduced lens competent area in the surface ectoderm, leading to the formation of a reduced eye. In fact,

it is known that Chx10, a factor essential for the proliferation of retinal progenitor cell, is induced in the presumptive neural retina by secreted factors (probably FGFs) produced by the overlaying lens ectoderm (Nguyen and Arnheiter, 2000). Therefore, a defective lens placode formation may lead to a defective lens and retina development, leading finally to a reduced eye. On the other hand, the morpholino-mediated knock-down results in a reduced number of neural cells (as denoted by early expression of *Xsox3* and *Xn-tubulin*); as part of the CNS, the eye forming area may consequently be reduced, leading to small eye phenotype. With regard to the proximo-distal patterning of the eye field (Fig. 34B), a gradient of Shh from the midline is believed to establish different cell fates along the proximo-distal (ventro-dorsal) axis of the early optic cup (Zhang and Yang, 2001; Chow and Lang, 2001), with optic stalk arising at a position of high Shh activity, and the retina being formed distally, at a position of low Shh activity. Cholesterol is important not only for the production of the active SHH protein, but also for the proper sequestration of the protein by its receptor Patched (PTC), and the activity of Smoothened (Cooper et al., 2003). Moreover, the cholesterol-modified hedgehog protein can be recruited into raft structures, which restrict its rang of diffusion (Ingham, 2000). We propose that a high cholesterol input (by overexpressing dhcr7) may lead to an abnormal sequestration of the SHH protein near the midline. Although the eye field may be properly splitted into two eye primordia, the over sequestration of the hedgehog protein (by Patched or by retention into rafts) may cause the shift of the gradient towards the midline, leading to the observed transdifferentiation of stalk to retina (pigmented otic stalk). On the other hand, a lowering of cholesterol content (by morpholino injection) may reduce the amount of active Shh necessary to properly split the eye field into two eye primordia. This may then cause the failure of the optic stalk to develop, leading to the shift of the eye towards the midline.

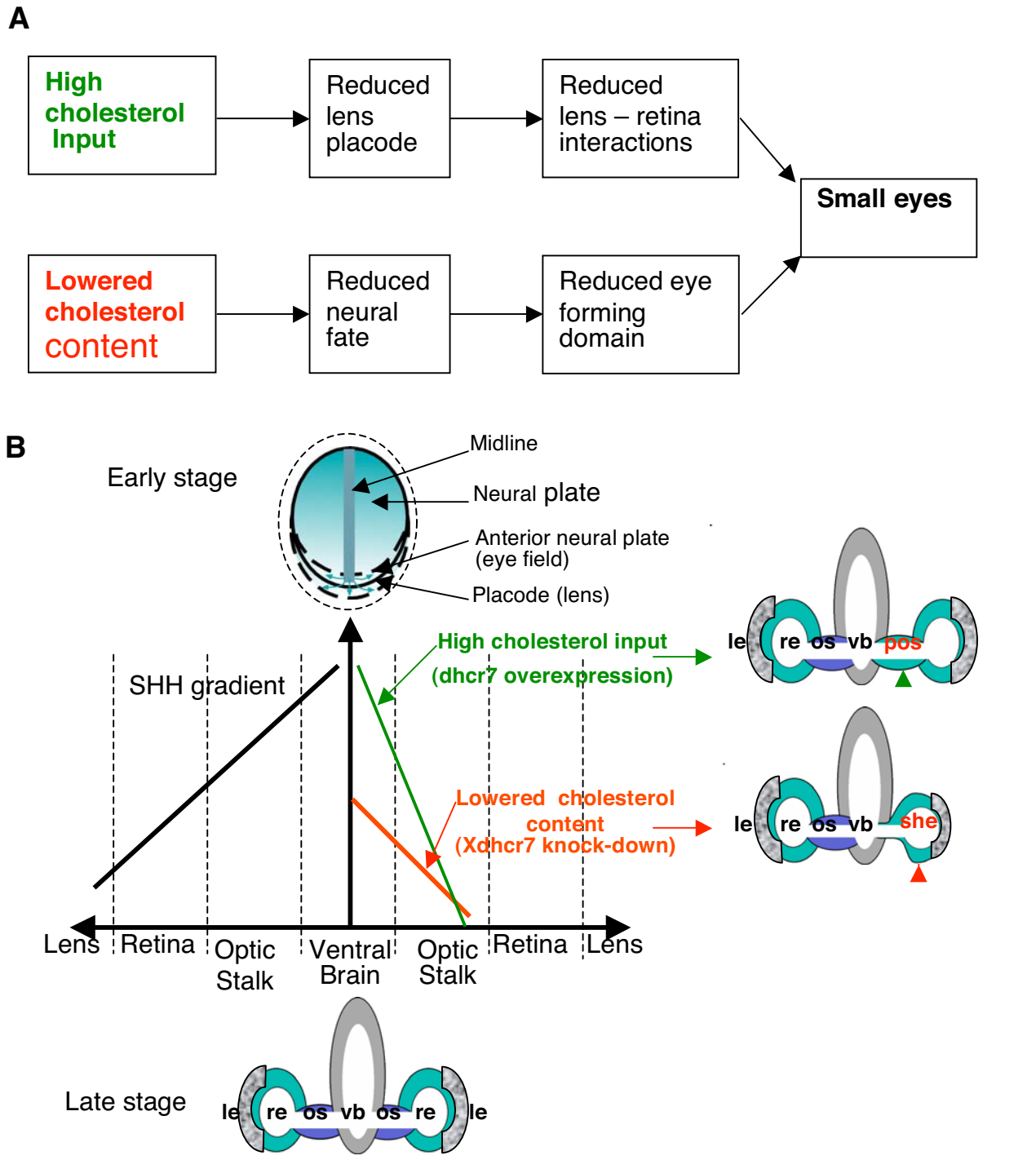

Figure 34: Proposed model explaining the interaction between cholesterol metabolism and eye development and patterning.
The small eyes phenotype (A) may be in relation with placodal versus neural development. Although the retinal anlage might be normally specified, it may later interact with a reduced lens competent area in the surface ectoderm, leading to the formation of a reduced eye. The transdifferentiation and medial shifting phenotypes (B) can be explained by an alteration of Shh gradient along the proximo-distal axis of the eye field. High cholesterol input (by overexpressing dhcr7) may lead to an abnormal sequestration of the SHH protein near the midline. This may cause a shift of the gradient through the midline, leading to the observed transdifferentiation of stalk to retina (pigmented otic stalk). On the other hand, a lowering of cholesterol content (by morpholino injection) may reduce the amount of active Shh necessary to properly split the eye field into two eye primordia. This may then cause the failure of the optic stalk to develop, leading to the shift of the eye towards the midline. Abbreviations: le, lens; re, retina; os, optic stalk; vb, ventral brain; pos, pigmented optic stalk; she, shifted eye.

IV. SUMMARY

Inborn errors of cholesterol biosynthesis are characterised by multiple developmental defects. Among the enzymes involved in the cholesterol biosynthesis pathway, 7-dehydrocholesterol reductase (DHCR7) is the very cholesterol specific enzyme, as it catalyses the last step leading directly to cholesterol. Mutations in the *DHCR7* gene are the major cause of the Smith-Lemli-Opitz syndrome (SLOS), which is a multiple dysmorphogenesis syndrome. Although accumulating data suggest an impairment of sonic hedgehog signalling as possible explanation of the SLOS phenotypes, their molecular mechanism is still a matter of investigations, the very role of cholesterol homeostasis in development as well. By database search, three *Xenopus* EST clones were identified, which shared high homology with the human dhcr7 cDNA. By mean of RT-PCR, three alternative spliced isoforms of Xdhcr7 cDNA were isolated, the products of which shared a common sub-cellular localization (Endoplasmic Reticulum), when expressed in yeast. Expression pattern analysis revealed that the embryonic expression of *Xdhcr7* is restricted to the Spemann organizer, the notochord, and is later mainly revealed in brain structures and derivatives. The temporal expression, as well as the tissue distribution in the adult frog showed that Xdhcr7 transcripts share an interesting correlation with sonic hedgehog, which suggested a role for XDHCR7 activity in pattern formation. Overexpression by injection of 2 ng of the full-length Xdhcr7 capped-mRNA (Xdhcr7-L) leaded to small eye phenotypes, which most likely resulted from a lost of placode structures, as supported by the reduction of the placode expression domains of neural plate markers genes. Knock-down by injection of 1 pmol of Xdhcr7 morpholino leaded to severely reduced eye phenotypes, possibly due to an impairment of the neurulation process, since neural markers gene expression was severely reduced as well. Since the NADPH-dependent reduction of 7-dehydrocholesterol to cholesterol is the only function that has been assigned to DHCR7 proteins so far, these results suggest that the *de novo* cholesterol biosynthesis is essential for organogenesis, and mainly for neural development. Therefore, the homeostatic regulation of cholesterol pool is essential for normal development, since both high cholesterol input and lowered cholesterol content resulted in the impairment of development. This data present the first description of the expression pattern of dhcr7 during early development which,

together with the lost- and gain- of function data strongly suggest a spatially restricted requirement for cholesterol production.

Future Plans

The data presented in this work open additional questions that I will be interested in answering in the near future.

Kinetic analysis of the three XDHCR7 protein isoforms was part of my main goals, but this is still to be optimized. I will also be interested in establishing the sterol profile during *Xenopus* development, by measuring the sterol content of animal cap explants at different embryonic stages. This strategy will also be used to analyse the *in vivo* activity of the XDHCR7 protein isoforms. In the context of cholesterol homeotasis, I intend to implicate the development of other organs; I will then be interested in the pancreas (to better analyse the Xhnf-3β phenotype) and the heart since it is reported to fail in SLOS patients, but the molecular mechanism is still not clear. In addition, analysing the embryonic spatial and temporal distribution of XSHH and XDHCR7 proteins (by means of wholemount immunostaining and western blotting) will be part of my future investigations.

V. ZUSAMMENFASSUNG

Angeborene Störungen der Cholesterol-Biosynthese werden durch eine Reihe unterschiedlicher Entwicklungsdefekte charakterisiert. Unter den Enzymen, die in die Cholesterol-Biosynthese mit einbezogen werden, ist die Reduktase des 7 Dehydrocholesterol (DHCR7) das spezifische Enzym des Cholesterins, da es den letzen Schritt der Synthese katalysiert, der direkt zum Cholesterol führt. Mutationen im Gen für die DHCR7 sind die Hauptursache des Smith-Lemli-Opitz Syndroms (SLOS), das durch die Dysmorphogenese verschiedener Organe gekennzeichnet ist. Obwohl Daten zunehmen, die zeigen, dass der SLOS Phänotyp möglicherweise auf einen gestörten Hedgehog-Signalweg zurückzuführen ist, ist der molekulare Mechanismus weiterhin Gegenstand intensiver Forschung, der die Cholesterol-Homöostase in der Entwicklung mit einschließt. Es konnten drei Xenopus EST Klone über eine Durchmusterung entsprechender Genbanken identifiziert werden, die eine hohe Homologie zur menschlichen dhrc7 cDNA besaßen. Mittels RT-PCR konnten drei Isoformen der Xenopus DHCR7 isoliert werden, die alle gemeinsam im Endoplasmatischen Retikulum lokalisierten, wenn diese in Hefen überexprimiert wurden. Die Analyse der embryonalen Expression zeigte eine Expression im Bereich des Spemann Organisators, dem Notochord und später in bestimmten Bereichen des embryonalen Gehirns. Die zeitlich-räumliche Expression sowie die Verteilung der DHCR7-Transkripte in adulten Geweben zeigte eine auffällige Korrelation mit der lokalen Expression von Sonic Hedgehog. Die Überexpression von 2 ng synthetischer RNA der längsten Isoform von DHCR7 führte in der Folge zu einer Entwicklung kleinerer Augen, was einher ging mit dem Verlust placodaler Strukturen, wie durch die Analyse verschiedener neuraler Markergene gezeigt werden konnte. Die Unterdrückung der Translation ("knock-down") durch die Injektion von 1 pmol Xdhr7-Antisense-Oligonukleotide (Morpholinos) führte ebenfalls zur Ausbildung stark verkleinerter Augenanlagen, wahrscheinlich durch eine teilweise Unterdrückung der Neurogenese.

VI. MATERIALS AND METHODS

VI.1. Materials

VI.1.1. Chemicals

Acetic anhydride	(Sigma)
10 X PCR buffer	(Perkin – Elmer)
Acetic acid	(Merck)
Acetone	(Merck)
Agar	(Difco)
Agarose	(Gibco - BRL)
Ammonium Persulfate	(Serva)
Ampicillin	(Biomol)
Bacto Trypton	(Difco)
Bacto Yeast Extract	(Difco)
BCIP	(Boehringer Mannheim)
Benzyl alcohol	(Sigma)
Boehringer block	(Sigma)
Boric acid	(Merck)
Bovine Albumin	(Sigma)
BSA	(Sigma)
$Ca(NO_3)_2$	(Merck)
$CaCl_2$	(Merck)
CHAPS	(Sigma)
Chloroform	(Merck)
DAB	(Pharmacia)
Dextran sulfate	(Merck)
DMSO	(Merck)
DTT	(Gibco)
EDTA	(Paesel & Lorei)
EGTA	(Sigma)
Entelan	(Merck)
Ethanol	(Merck)
Ethidium Bromide	(Roth)
Ficoll	(Sigma)
Ficoll 400	(Pharmacia)
Formaldehyde	(Merck)
Formamid	(Merck)
Gelatin	(Sigma)
Glutaraldehyde	(Sigma)
Glycerol	(Merck)
Glycogen, Molecular Biology grade	(Boehringer Mannherim)
Goat Serum	Gibco – BRL
H_2O_2	(Baker), (ROTH, N^r 2014)
HCl	(Merck)

Heparin	(Sigma)
HEPES	(Sigma)
Human Chorionic gonadotropin (HCG)	(Sigma)
Isopropanol	(Merck)
$K_3Fe(CN)_6$	(Sigma)
$K_4Fe(CN)_6$	(Sigma)
KCl	(Merck)
L-Cysteinhydrochloride	(Fluka)
LiCl	(Sigma)
Methanol	(Merck)
$MgSO_4$	(Merck)
MOPS	(Sigma)
Mowiol	(Calbiochem)
Na acetate	(Roth)
Na citrate	(Fluka)
Na_2HPO_4	(Merck)
NaCl	(Merck)
NaH_2PO_4	(Merck)
$NaHCO_3$	(Merck)
NaN_3	(Sigma)
NaOH	(Merck)
NBT	(Boehringer Mannherim)
NH_4 acetate	(Merck)
NH_4 sulfate	(Merck)
Nile blue chloride	(Sigma)
Penicillin	(Sigma)
Phenol	(Merck)
Poly-L-lysine solution	(Sigma Diagnostics)
SDS	(Biomol)
(^{35}S)Met	(Amersham)
β-mercaptoethanol	(Sigma)
Streptomycin	(Sigma)
Sucrose	(BRL)
Technovit 7100	(HeraeusKulzer)
TEMED	(Serva)
Triethanolamine	(Sigma)
Tris	Paesel & Lorei)
Triton-X-100	(Sigma)
Tween-20	(Sigma)
Urea	(Pharmacia)

VI.1.2. Solutions, buffers and media

VI.1.2.1. Solutions for embryos and explants

L-Cystein hydrochloride 2 %

L-Cystein hydrochloride 1 X H_2O	: 10 g
dH_2O	: to 500 ml
pH	: 7.8 – 8.0

Ficoll 10 %

Ficoll	: 10 g
ddH_2O	: to 100 ml

Filter through 45µl filter and store at 4 °C.

Human chorionic gonadotropin (HCG) 10.000 U

Resuspend in 5 ml dH_2O to make a stock of 2000 U/ml, aliquot in fractions of 1 ml each, and store at – 20 °C.

Injection buffer

5 X MBS	: 100ml (1 X)
Ficoll 10 %	: 50 ml (1 %)
ddH_2O	: to 500 ml

MBS (Modified Barth Solution) 1 X

NaCl	: 88 mM
$NaHCO_3$	: 2.4 mM
KCl	: 1 mM
HEPES	: 10 mM
$MgSO_4$	: 0.82 mM
$CaCl_2$	: 0.41 mM
$Ca(NO_3)_2$	: 0.33 mM
pH	: 7.4

MBS (Modified Barth Solution) 5 X

NaCl, l5 M	: 88 ml (440 mM)
$NaHCO_3$ 1 M	: 12 ml (12 mM)
KCl, 1M	: 5 ml (5 mM)
HEPES, 1 M, pH 7.0	: 50 ml (50 mM)
$MgSO_4$, 1 M	: 4.1 ml (4.1 mM)
$CaCl_2$, 1 M	: 2.05 ml (2.05 mM)
$Ca(NO_3)_2$, 1 M	: 1.65 ml (1.65 mM)
dH_2O	: to 1 l
pH	: 7.4

Penicillin / Streptomycin

Penicillin	: 100 U / ml
Streptomycin	: 10 mg / ml

Working concentration: Dilute 1 / 1000

VI.1.2.2. Solutions for Wholemount *in situ* hybridization

Alkaline Phosphatase Buffer (APB)

Tris-HCl 1 M, pH 9.5	: 50 ml (100 mM)
$MgCl_2$ 1 M	: 25 ml (50 mM)
NaCl 5 M	: 10 ml (100 mM)
Tween-20, 20 %	: 2.5 ml (0.1 %)
dH_2O	: to 500 ml

Bleaching solution

H_2O_2 (ROTH)	: 1.67 ml (1 %)
Formamid	: 25 ml (50 %)
5X SSC	: to 50 ml

Boehringer Block (BMB) 10 % (autoclaved)

5 X MAB	: 20 ml (1 X)
BMB*	: 10 g (10 %)
dH_2O	: to 100 ml

Takes about 1 h at 60 °C to dissolve.
Autoclave and store at – 20 °C.

Denhart´s 100 X solution

BSA	: 2 g (2 %)
PVP	: 2 g (2 %)
Ficoll 400	: 2 g (2 %)
dH_2O	: to 100 ml

Store at – 20 °C.

Hybridization solution

Deionized formamid*	: 50 ml (50 %)
20 X SSC	: 5 ml (5 X)
Torula RNA 50 mg / ml	: 2 ml (1 mg / ml)
Heparin 10 mg / ml	: 1 ml (100µg / ml)
Denhart´s 100 X	: 1 ml (1 X)
Tween-20, 20 %	: 0.5 ml (0.1 %)
CHAPS 10 %	: 1 ml (0.1 %)
EDTA 0.5 M	: 2 ml (10 mM)
DEPC dH_2O	: to 100 ml

Store at – 20 °C.

***** To deionize formamid: Add 50 g of mixed bead resin (BioRad) to 500 ml formamid, mix on magnetic stirrer for 2 h and filter on Whatman paper. Reuse reusin.

Heparin 10 mg / ml

Heparin	: 100 mg (10 mg / ml)
DEPC dH_2O	: to 10 ml

Store at – 20 °C.

HEPES buffer pH 7.5 (autoclaved)

HEPES	: 238.3 g (1M)
dH_2O	: to 1 l
pH	: 7.5

Autoclave.

5 X MAB solution (autoclaved)

Maleic acid	: 29 g (500 mM)
NaCl	: 21 g (750mM)
dH_2O	: to 500 ml
pH	: 7.5

Autoclave.

$MgCl_2$, 1 M

$MgCl_2$, 6 H2O	: 203.3 g (1 M)
dH_2O	: to 1 l

5 M NaCl (autoclaved)

NaCl	: 292.2 g (5 M)
dH_2O	: to 1liter

Autoclave.

1 X PTw

10 X PBS	: 50 ml (1 X)
Tween-20, 20 %	: 2.5 ml (0.1 %)
dH_2O	: to 500 ml

PTw / Proteinase K solution

PTw	: 20 ml
Proteinase K 20 mg / ml	: 20 µl

2 X SSC / RNase A and RNase T1 solution

20 X SSC	: 1 ml (2 X)
RNase A 10 mg / ml	: 20 µl (20 µg / ml)
RNase T1 20,000 U / ml	: 5 µl (10 U / ml)
dH_2O	: to 10 ml

20 X SSC (autoclaved)

NaCl	: 175.3 g (0.3 M)
Sodium citrate	: 88.2 g (0.3 M)
dH_2O	: to 1 l
pH	: 7.0

Staining solution : NBT / BCIP

APB	: 1 ml
NBT 100 mg / ml in 70 % dimethylformamide	: 1.75 µl
BCIP 50 mg / ml in 100 % dimethylformamide	: 3.5 µl

Torula RNA 10 mg / ml

Torula RNA	: 100 mg (10 mg / ml)
DEPC - dH_2O	: to 10 ml

Store at – 20 °C.

Tris buffer, pH 9.5 (autoclaved)

Tris-HCl	: 121.1 g (1 M)
dH_2O	: to 1 l
pH	: to 9.5

Tween – 20, 20 %

Tween – 20	: 20 ml (20 %)
dH_2O	: to 100 ml

Store at 4 °C, under light protection.

VI.1.2.3. Solutions for histology and immune whole mount staining

DAB 10 mg / ml solution

DAB	: 100 mg (10 mg / ml)
dH_2O	: to 10 ml

Store at – 20 °C.

Dent´s fixative

DMSO	: 20 ml (20 %)
Methanol	: 80 ml (80 %)

Gelatin – albumin medium

10 X PBS	: 45 ml (1X)
Gelatin	: 2.2 g
dH_2O	: to 450 ml

Stir under heating at 60 °C, cool down to room temperature and add:

Albumin	: 135 g

Sucrose : 90 g
Filter through 45 μm filter and store at – 20 °C.
For embedding, add 105 μl of 25 % Glutaraldehyde to 1.5 ml of Gelatin-albumin medium.

$K_3Fe(CN)_6$ solution

$K_3Fe(CN)_6$: 1,65 g (100 mM)
dH_2O : to 50 ml

$K_4Fe(CN)_6$ solution

$K_4Fe(CN)_6$, 3 H_2O : 2,11 g (100 mM)
dH_2O : to 50 ml

10 X MEM (autoclaved)

MOPS : 209.3 g (1 M)
EGTA 0.5 M : 20 ml (20 mM)
$MgSO_4$ 1 M : 5 ml (10 mM)
dH_2O : to 500 ml
Autoclave

1 X MEMFA

10 X MEM : 10 ml (1 X)
Formaldehyde 37 % : 10 ml (3.7 %)
dH_2O : to 100 ml

Mowiol solution

Mowiol : 9.6 g
Glycerine : 19.35 ml
dH_2O : 24 ml
Tris 0.2 M, pH 8.5 : 48 ml
Stir under heating at 50 °C, centrifuge at 5000 rpm for 15 min and store at – 20 °C.

PBT solution

10 X PBS : 10 ml (1 X)
BSA : 200 mg (2 mg / ml
Triton-X-100, 20 % : 0.5 ml (0.1 %)
dH_2O : to 100 ml

X-Gal solution

X-Gal : 1 g (40 mg / ml)
DMSO : to 25 ml
Store at – 20 °C

X-Gal staining solution

10 X PBS : 5 ml
X-Gal 40 mg / ml in DMSO : 1.250 ml (1 mg / ml)

$K_3Fe(CN)_6$ 500 mM	: 0.5 ml (5 mM)
$K_4Fe(CN)_6$ 500 mM	: 0.5 ml (5 mM)
$MgCl_2$ 1M	: 0.1 ml (2 mM)
ddH_2O	: to 50 ml

VI.1.2.4. Solutions for yeast cells transformation

10 X TE buffer: for 500 ml

Tris-HCl 1 M	: 50 ml (0.1 M)
EDTA 0.5 M	: 10 ml (10 mM)
pH	: to 8

Lithium acetate (LiOAc) solution

TE	: 1 X
LiOAc	: 0.1 M

Polyethylene glycol (PEG) solution

TE	: 1 X
LiOAc	: 0.1 M
PEG-4000	: 40 % (w / v)

VI.1.2.5. Solutions for Immunofluorescence in yeast

PBS / Sorbitol (PBSS)

NaCl	: 137 mM
Kcl	: 2.7 mM
Na_2HPO_4	: 4.3 mM
KH_2PO_4	: 1.4 mM
Sorbitol	: 10 % (w / v)
pH	: 7

Fixative

PBSS	: 1 X
Paraformaldehyd	: 3.5 % (w / v)

Zymolyase solution: for 1 ml

PBSS 1X	: 990 μl
Zymolyase 10 mg / ml	: 10 μl
β-mercaptoethanol	: 1.4 μl

Blocking solution: for 10 ml

BSA	: 100 mg (1 % w / v)

Triton-X-100	:	50 µl (0.5 % v / v)
PBSS 1 X	:	to 10 ml

NB: can be stored frozen in 2 ml aliquots.

Mounting solution : for 100 ml

Phenylenediamine	**:**	100 mg (0.1 % w / v)
PBS	**:**	10 ml
pH	**:**	to 8.5 – 9.5 with 0.5 M Na_2CO_3
Glycerin	**:**	to 100 ml

NB: store at – 20 °C, under light protection.

Mounting / DAPI solution: for 1ml

Mounting solution	**:**	1 ml
DAPI 1 mg / ml	**:**	1 µl

VI.1.2.6. Solutions for preparation of yeast microsomal fraction

Lysis buffer: for 25 ml

Tris-HCl, 1 M, pH 7.4	**:**	1.25 ml (50 mM)
EDTA 0.5 M, pH 8	**:**	50 µl (1 mM)
D-Sorbitol 1.2 M	**:**	12.5 ml (0.6 M)
Protease inhibitors complex	**:**	2 tablets
ddH_2O	**:**	to 25 ml

TE-Glycerol: for 10 ml

Tris-HCl, 1 M, pH 7.4	:	1 ml (0.1 M)
EDTA 0.5 M, pH 8	:	10 µl
Glycerol	:	2 ml (20 % v / v)
ddH_2O	:	to 10 ml

VI.1.2.7. Solutions for Molecular Biology

VI.1.2.7.1. Solutions for SDS – PAGE

30 % Acrylamide stock solution

Acrylamide	**:**	29.2 % (w / v)
Bis-acrylamide	**:**	0.8 % (w / v)

10 % Ammonium persulfate (APS) solution

Ammonium persulfate	**:**	10 g (10 %)
dH_2O	**:**	to 100 ml

2 X Laemmli loading buffer

Tris-HCl	: 0.1 M, pH 6.8
SDS	: 2 % (w / v)
Glycerol	: 20 % (w / v)
Bromphenol blue	: 0.002 % (W / v)

VI.1.2.7.2. Solutions for agarose gel electrophoresis of DNA

Ficoll loading buffer

Tris-HCl 1 M, pH 7.5	: 0.5 ml (10 mM)
EDTA 0.5 M	: 0.1 ml (1 mM)
Bromphenol blue	: 0.025 %
Xylencyanol	: 0.025 %
Ficoll 400	: 5 g (10 %)
dH_2O	: to 50 ml

Glycerol loading buffer

Tris-HCl 1 M, pH 7.5	: 0.5 ml (10 mM)
EDTA 0.5 M, pH 8	: 1 ml (10 mM)
Bromphenol blue	: 0.025 %
Xylencyanol	: 0.025 %
Glycerol 99 %	: 15.15 ml (30 %)
dH_2O	: to 50 ml

Formamid loading buffer

EDTA 0.5 M, pH 8	: 0.2 ml (10 mM)
Bromphenol blue	: 0.025 %
Xylene cyanol FF	: 0.025 %
Formamid 99 %	: to 10 ml

10 X TBE buffer

Tris	: 108 g (0.89 M)
Boric acid	: 55 g (0.89 M)
EDTA 0.5 M, pH 8	: 40 ml (20 mM)
dH_2O	: to 1 l

VI.1.2.7.3. Solutions for plasmid DNA preparation

TELT buffer

Tris-HCl 1 M, pH 7.5	: 2.5 ml (50 mM)
EDTA 0.5 M, pH 8	: 0.1 ml (1 mM)
LiCl, 10 M	: 16 ml (3.2 M)
Triton-X-100, 20 %	: 1.25 ml (0.5 %)
dH_2O	: to 50 ml

TE buffer

Tris-HCl 1 M, pH 7.5	: 1 ml (10 mM)
EDTA 0.5 M	: 200 µl (1 mM)
pH	: to 8
dH_2O	: to 100 ml

Lysozym solution

Lysozym	: 100 mg (10 mg / ml)
dH_2O	: to 10 ml
Store at – 20 °C	

Tris buffer (autoclaved)

Tris-HCl	: 121.1 g (1 M)
dH2O	: to 1 l
pH	: to 7.5

Triton-X-100, 20 % solution

Triton-X-100	: 20 ml (20 %)
dH_2O	: to 100 ml

VI.1.2.7.4. Frequently used buffers and solutions

EDTA solution

$Na_2EDTA, 2H_2O$	: 186.12 g (0.5 M)
dH_2O	: to 1 l
pH	: 8

EGTA solution

EGTA	: 190 g (0.5 M)
dH_2O	: to 1 l
pH	: 8

$MgSO_4$ 1 M (autoclaved)

$MgSO_4, 7\ H_2O$	: 246.48 g (1 M)
dH_2O	: to 1 l
Autoclave.	

Dihydrogeno sodium phosphate 1 M

$NaH_2PO_4, 1\ H_2O$	: 137.9 g (1 M)
dH_2O	: to 1 l

Monohydrogeno sodium phosphate 1 M

$Na_2HPO_4, 12\ H_2O$	: 358.14 g (1 M)
dH_2O	: to 1 l

Sodium Phosphate buffer

NaH_2PO_4, 1 M	: 15 ml
Na_2HPO_4, 1 M	: 84.5 ml
pH	: 7.5

10 X Phosphate buffered saline buffer (PBS)

Na_2HPO_4, 12 H_2O	: 36.3 g (0.1 M)
KH_2PO_4	: 2.4 g (20 mM)
NaCl	: 80 g (1.4 M)
KCl	: 2 g (28 mM)
dH_2O	: to 1 l

Sodium acetate 3 M

Sodium acetate, 3 H_2O	: 40.81 g (3 M)
dH_2O	: to 100 ml
pH	: 5.2

SDS 10 %

SDS	: 10 g (10 % w / v)
dH_2O	: to 100 ml

SM buffer

Tris-HCl 1 M, pH 7.5	: 50 ml (10 mM)
$MgSO_4$ 1 M	: 8 ml (8 mM)
NaCl 5 M	: 20 ml (100 mM)
Gelatin 2 %	: 5 ml (0,01 %)
dH_2O	: to 1 l

20 X SSPE (autoclaved)

NaCl	: 174 g (3.6 M)
NaH_2PO_4, 1 H_2O	: 27.6 g (0.2 M)
EDTA	: 7.4 g (20 mM)
dH_2O	: to 1 l
pH	: to 7.4

X-Gal solution

X-Gal	: 0.5 g (20 mg / ml)
Dimethylformamide	: to 25 ml

Isopropylthiogalactoside (IPTG) solution

IPTG	: 238.3 mg (100 mM)
dH_2O	: to 10 ml
Store at – 20 °C	

VI.1.2.7.5. Media and antibiotics

All media were autoclaved for at least 15 min at 120 °C, under 1.5 bar.

LB – medium

Bacto Trypton	**:** 10 g (1 %)
Bacto Yeast Extract	**:** 5 g (0.5 %)
NaCl	**:** 10 g (17.1 mM)
dH_2O	**:** to 1 l
pH	**:** to 7.5

LB –Agar medium

Bacto Trypton	**:** 10 g (1 %)
Bacto Yeast Extract	**:** 5 g (0.5 %)
NaCl	**:** 10 g (17.1 mM)
Agar	**:** 15 g (1.5 %)
dH_2O	**:** to 1 l
pH	**:** to 7.5

Synthetic complete (SC) medium

$(NH_4)SO_4$	**:** 5 g (0.5 %)
Yeast nitrogen base (YNB) without aa	**:** 1.7 g (0.17 %)
Glucose	**:** 20 g (2 %)
Drop-out mix*	**:** 2 g (0.2 %)
ddH_20	**:** to 1l
pH	**:** to 6 – 6.5

For solid medium (agar plates), add 2 % (20 g / l) bacto-agar to the mixture.

**** Drop-out mix***

Drop-out mix is a combination of the following ingredients minus the appropriate selection element (selection marker).

Adenine	:	0.5 g	Leucine	:	4 g
Alanine	:	2 g	Lysine	:	2 g
Arginine	:	2 g	Methionine	:	2 g
Asparagine	:	2 g	*para*-Aminobenzoic acid	:	0.2 g
Aspartic acid	:	2 g	Phenylalanine	:	2 g
Cysteine	:	2 g	Proline	:	2 g
Glutamine	:	2 g	Serine	:	2 g
Glutamic acid	:	2 g	Threonine	:	2 g
Glycine	:	2 g	Tryptophane	:	2 g
Histidine	:	2 g	Tyrosine	:	2 g
Inositol	:	2 g	Uracil	:	2 g
Isoleucine	:	2 g	Valine	:	2 g

Tetracyclin stock solution

Tetracyclin	: 250 mg (25 mg / ml)
Ethanol 100 %	: to 10 ml
Store at – 20 °C	
Working concentration	: 12.5 µg / ml

Ampicillin stock solution

Ampicillin	: 1g (100 mg / ml)
dH_2O	: to 10 ml
Store at – 20 °C	
Working concentration	: 75 µg / ml

VI.1.2.7.6. Solutions for RNA isolation

Diethylpyrocarbonat (DEPC) – dH_2O (autoclaved)

Diethylpyrocarbonat	: 0.5 ml (0.1 %)
dH_2O	: 500 ml

Incubate 2 h at 37 °C and autoclave.

2 X lysis buffer

SDS 20 % (w / v)	: 5 ml (1 %)
EDTA 0.5 M, pH 8.0	: 2 ml (10 mM)
Tris – HCl 1 M, pH 7.5	: 10 ml (100 mM)
NaCl 5 M	: 2 ml (100 mM)

Lysis buffer

2 X lysis buffer	: 5 ml
DEPC – dH_2O	: 4.5 ml
Proteinase K* (20 µg / µl)	: 0.5 ml

*Added immediately before use.

10 X DNase buffer

Tris – HCl	: 400 mM, pH 7.9
NaCl	: 100 mM
$MgCl_2$	: 60 mM
$CaCl_2$	: 1 mM

DNase I digestion mix

10 X DNase buffer	: 5 µl
DTT 20 mM	: 2.5 µl
RNasin (40 U / µl)	: 1 µl
DNase I (10 U / µl)	: 1.5 µl
RNA sample	: 40 µl

Phenol – Chloroform mix

Ratio	: 1 : 1 (v / v)
pH	: 8 – 8.3

Ammonium acetate (NH_4OAc) 7.5 M

NH_4OAc	: 57.8 g (7.5 M)
dH_2O	: to 100 ml

VI.1.3. Bacterial strains, yeast strains and vectors

Escherichia coli Xl1-Blue (Stratagene) and *Saccharomyces cerevisiae* ABYS were used in this study. The following vectors were used: *pGEM-T* (Promega); *pCS2+* (Turner and Weintraub, 1994); pYX212, pYX113 (R&D Systems).

VI.1.4. Plasmid constructs

Below are listed the constructs used for RNA synthesis in this study. The restriction enzymes, used for DNA linearization, and the RNA polymerases used for *in vitro* transcription are indicated:

For the Wholemount *in situ* hybridization

Constructs	Restriction enzyme	RNA polymerase
Xdhcr7-S (pGEM-T)	NcoI	Sp6
Xsox3 (pBSK-)	EcoRI	T3
Xvax1 (pGEM-T)	NcoI	Sp6
Xpax6(pGEM-T)	NotI	T7
Xn-tubulin	BamHI	T3
Xshh ((pBSK)	XbaI	T3
Xrx1	XhoI	T3
Xsix3 (pGEM-T)	NotI	T7
Xen2 (pGEM-T)	NotI	T7
Xkrox20 (pGEM-T)	EcoRI	T7
Xgsh-1 (pGEM-T)	NotI	T7
Xnkx2.1 (pGEM-T)	NotI	T7
Xnkx2.2 (pGEM-T)	Nco I	T7
XHNF-3β (pCS2)	EcoRI	T3

For embryos microinjection

Constructs	Restriction enzyme	RNA polymerase
β-galactosidase (1D1, pCS2+)	NotI	Sp6 (Ambion kit)
Xdhcr7-L (pCS2+)	NotI	Sp6
Xdhcr7-M (pCS2+)	NotI	Sp6
Xdhcr7-S (pCS2+)	NotI	Sp6
Mdhcr7 (pCS2+)	NotI	Sp6

For expression in yeast
Xdhcr7-L, -M and –S cDNAs were sublcloned into the pYX212 vector (R & D System).

VI.1.8. Animals

Wild type (pigmented) and albino *Xenopus laevis* frogs were used.

VI.1.9. Antibodies

Anti-digoxigenin-alkaline phosphatase conjugated (Roche Biochemicals)
Anti-flureseine-alkaline phosphatase conjugated (Roche Biochemicals)
Anti-mouse alkaline phosphatase conjugated (Sigma)
Anti-HA monoclonal antibody (Sigma)

VI.1.10. Enzymes

Restriction enzymes (with supplied buffers)	(NEB, Promega)
Proteinase K	(Merck)
RNase A	(Worthington)
RNase T1	(Sigma)
RNasin (Ribonuclease Inhibitor)	(Promega)
RNase – free DNase I (2000 U / ml)	(Ambion)
Taq polymerase	(Perkin Elmer)
T4 DNA ligase	(Promega)
SP6, T3 and T7 RNA polymerases	(Stratagene)
T4 Polynucleotide kinase	(Boehringer Mannheim)
Terminal Deoxynucleotidyl Transferase (TdT)	(GibcoBRL)
Salmon sperm DNA	(Sigma)
1 kb molecular weight marker mix	(Gibco BRL)

VI.1.11. Sterols and Sterol synthesis inhibitors

Cholesterol	(Sigma)
7-dehydrocholesterol	(Fluka)
Mevinolin	(Mo bi tec)
1,4-Bis(2-Chlorobenzylaminomethyl) cyclohexane dihydrocloride (AY9944)	(Sigma)

VI.1.12. Computers and software

- **Computer**: Apple Macintosh
- **Computer progams** :
  - Adope Photoshop 7.0;
  - DNA-Star software;
  - Free Hand 10.0;
  - Image Quant 2.0;
  - Microsoft Word: mac v.X
  - Microsoft PowerPoint: mac v.X

VI.1.13. Nucleic acids

VI.1.13.1. Nucleotides

dNTPs	(Biomol)
Fluorescein – 12 – UTP	(Boerhinger)
Digoxigenin – 11 - UTP	(Boerhinger)
rNTP solutions (10 mM)	Stratagene
RNA cap structure m7G(5´)ppp(5´)G, sodium salt	(New EnglandBiolabs)
Digoxigenin – 11 - dUTP	(Roche Biochemicals)

VI.1.13.2. Oligonucleotides

For the sequencing:

pYX212-seq-R: 5´-AACCCTCACTAAAGGGAAC-3´
SP6: 5´-GATTTAGGTGACACTATAG-3´
T7: 5´-TAATACGACTCACTATAGGG-3´
T3: 5´-ATTAACCCTCACTAAAGGGA-3´

For the cloning:
DHCR7-RT-F: 5´-GCGAATGGGAGAGCGGAGAAGAGCG-3´
DHCR7-RT-R: 5´-CCGTTAGAATAGTCCGGGGAGTAACC-3´

For the sub-cloning:

DHCR7-EcoRI: 5´-GCGGAATTCAATGGGAGAGCGGAGAAGAGCG-3´
DHCR7-XbaI: 5´-CCGTCTAGATTAGAATAGTCCGGGGAGTAACC-3´

DHCR7-5´-EcoRI-Flag: 5´-
CGGAATTCAATGGACTACAAGGACGACGATGACAAGGGAGAGCGGAG -3´
DHCR7-3´-MluI-STOP: 5´-CACGCGTTTAGAATAGTCCGGGGAGTAACCCG-3´

DHCR7-3´-MluI-Frame: 5´-CCGACGCGTATAGAATAGTCCGGGGAGTAACC-3´
DHCR7-S-3´-MluI-Frame: 5´-ACGCGTCTCGAGCAGCGGTGTTCGTCC-3´

For the loss-of-function:

Xdhcr7 antisense morpholino oligo: 5´-CATTCGCTCTTCTCCGCTCTCCCAT-3´

For the RT-PCR:

dhcr7-int-F: 5´-CAAGTCAACGGACTGCAGGCCTGGACTATT-3´
dhcr7-int-R: 5´-GTTGGTGACCCCGTAGAGCTCTTGCTGTTT-3´

XL-DHCR7-INT2-F: 5´-CTCTTTCCAGGTGTTCCTGTATATGTTCCTTCC-3´
XL-DHCR7-INT2-R: 5´-GCGCTGGTGTAAAGCTTCCAGTCCTTCCCG-3´

Xl-Shh-F: 5´-GGT TGA CCG CGG CCC ATC TAC-3´
Xl-Shh-R: 5´-AGG CGC ATA AGC TCC AGT GTC C-3´

Histone H4-F: 5´-CGGGATAACATTCAGGGTATCACT-3´
Histone H4-R: 5´-ATCCATGGCGGTAACTGTCTTCCT-3´

VI.1.14. Kits

Big dye terminator Cycle sequencing kit	(PE Applied Biosystems)
SP6 Message Mashine *in vitro* transcription	(Ambion)
Qiagen Plasmid Midi kit	(Qiagen)
Qiagen PCR Purification kit	(Qiagen)
RNA PCR Core kit	(Perkin Elmer)
RNeasy mini kit	(Qiagen)
In vitro transcription/translation kit	(Promega)

VI.2. Methods

VI.2.1. Handling and manipulation of embryos

Pigmented and albino *Xenopus laevis* embryos were obtained by hormone-induced egg-laying and *in vitro* fertilization. Eggs were collected from *X. laevis* females, which had been injected with 400 – 800 U of human chorionic gonadotrophin approximately 10 hours prior to eggs collection. Eggs were fertilized with minced testis in 0.1 X MBS, dejellied with 2 % cystein hydrochloride, pH 7.8 – 8.0 and cultured in 0.1 X MBS. Embryos were staged according to Nieuwkoop and Faber (Nieuwkoop and Faber, 1967). For further in situ hybridisation analysis, albino embryos were injected with synthetic RNA along with 30 to 50 pg of NLS β – Galactosidase RNA. The RNA was injected into one blastomere at two-cell stage in a volume of 5 nl, in 1 X MBS solution containing 1 % Ficoll. After injection, embryos were transferred in 0,1 X MBS containing 0.5 % Ficoll, and finally cultured into 0,1 X MBS until the desired stage. For phenotypic analysis, pigmented embryos were injected into one blastomere at two-cell stage.

VI.2.3. Fixation and histological procedures

VI.2.3.1. MEMFA fixation of *Xenopus* embryos

Embryos were transferred in 5 ml glass vials and fixed in 1 X MEMFA for 1 h on the rocking platform, washed twice or more for 5 min in 100 % ethanol and kept at – 20 °C for further analysis by *in situ* hybridization. For X-Gal staining, embryos were fixed in 1 X MEMFA for 30 min, rinsed 2 to 3 times in 1 X PBS, and stored in 1 X PBS at 4 °C.

VI.2.3.2. Gelatine-medium embedding and vibratome sectioning of embryos

Embryos stained by *in situ* hybridization were fixed for 1 h in 1 X MEMFA, washed once with MEM, and transferred into 1 X PBS. Vibratome sectioning was performed essentially as previously described (Hollemann et *al*., 1996). After 20 min equilibration in gelatin-albumin medium, embryos were mounted in gelatin-albumin / glutaraldehyde. Thirty micrometers sections were cut with a vibratome 1000 (Technical Products International Inc.) and mounted in Mowiol solution.

VI.2.4. Wholemount *in situ* hybridization

Whole mount *in situ* hybridization of albino embryos was carried out essentially as described (Harland, 1991) and improved by Hollemann et al., (1998) using digoxigenin-11-UTP- (Dig) or fluorescein-12-UTP (Flu)-labelled antisense RNA probes. For double staining *in situ* hybridization, Fast Red and NBT/BCIP were used as alkaline phosphatase substrates. After first staining reaction with Fast Red, alkaline phosphatase activity was stopped by heating the embryos for 15 min in 1 X MAB + 0.1 M EDTA at 65 °C. the second staining reaction was done using NBT/BCIP.

DAY 1:

Rehydratation of embryos

Reagent(s)	**Temperature**	**Time**
100 % ethanol	RT	5 min
75 % ethanol in water	RT	5 min
50 % ethanol in water	RT	5 min
25 % ethanol in PTw	RT	5 min
100 % PTw	RT	5 min, 4 times

Proteinase K treatment

Embryos in each vial were treated with 2 ml PTw containing 10 µg/ml proteinase K for 15 – 30 min at RT. The treatment time depended on the embryos developmental stage and the value of the real RT. Reasonable time for gastrula stage embryos was 15 – 20 min and longer time (20 – 30 min) for tailbud stage embryos.

Acetylation

After proteinase K treatment, embryos were immediately subjected to the following treatments.

Reagent(s)	**Temperature**	**Time**
0.1 M triethanolamine, pH 7.5	RT	5 min, 2 times
5 ml 0.1 M triethanolamine, pH 7.5 + 12.5 µl acetanhydride	RT	5 min
Above mixture + 12.5 µl acetanhydride	RT	5 min
100 % PTw	RT	5 min, 2 times

Refixation

Reagent(s)	**Temperature**	**Time**
PTw + 4 % formaldehyde	RT	20 min
100 % PTw	RT	5 min, 4 times

* If dealing with pigmented embryos, bleach by the following treatment: 5X SSC + 50 % formamid + 1 % H_2O_2 (ROTH, N^r 2014), 15 – 60 min at room temperature. Wash 4X with 100 % PTw.

Hybridization

Reagent(s)	**Temperature**	**Time**
250 µl PTw + 250 µl hybridization mix	RT	Mix and discard
500 µl hybridization mix	65 °C	10 min
500 µl hybridization mix	60 °C	6 hr
+ probe (1 µg / ml in hybridization solution)	60 °C	Overnight

DAY 2:

Washing

The antisense RNA probes (which can be repeatedly used for several probing cycles), were collected and stored at – 20 °C. the embryos were then wash as follow:

Reagent(s)	**Temperature**	**Time**
500 µl hybridization mix	60 °C	10 min
2 X SSC	60 °C	20 min, 3 times
2 X SSC + 20 µg/ml RNase A and 10 U RNase T1	37 °C	1 hours
2 X SSC	RT	10 min
0.2 X SSC	60 °C	30 min, 2 times

Antibodies incubation

Reagent(s)	**Temperature**	**Time**
1 X MAB	RT	15 min, 2 times
1 X MAB + 2 % BMB	RT	30 min
1 X MAB + 2 % BMB + 20 % serum	RT	60 min
1 X MAB + 2 % BMB + 20 % serum + antidigoxigenin (antifluorescein) antibody (1 : 5000)	RT	6 hours
1 X MAB	RT	15 min, 4 times
1 X MAB in 50 ml corning tubes	4 °C	Overnight

DAY 3:

Colour reaction

Reagent(s)	**Temperature**	**Time**
1 X MAB	RT	15 min, 4 times
APB	RT	5 min, 2 times
APB + NBT / BCIP	4 °C	5 min – 1 week

NBT / BCIP staining solution

APB	**:**	1 ml
100 mg / ml NBT in 75 % dimethylformamide	**:**	1.75 µl
50 mg / ml BCIP in 100 % dimethylformamide	**:**	3.5

After staining, the embryos were clarified in some cases by the following treatment:

Reagent(s)	**Temperature**	**Time**
H_2O	RT	30 sec
100 % MeOH	RT	1 min
75 % MeOH	RT	1 min
50 % MeOH	RT	1 min
25 % MeOH	RT	1 min
H_2O	RT	1 min
MEMFA	4 °C	Store

VI.2.5. Wholemount immunostaining

Wholemount immunostaining was performed as described by Dent *et al*. (1989), with modifications.

Fixation:

After -gal staining, embryos were refixed in 1 X MEMFA, for 1 hr at RT, and permeabilized by incubation in Dent´s fixative, overnight at – 20°C. permeabilized embryos were then transferred in 100 methanol and stored at – 20°C.

Day 1:

Embryos rehydration

Reagents	**Temperature**	**Time**
Ethanol 100 %	RT	5 min
Ethanol 75 % in H_2O	RT	5 min
Ethanol 50 % in H_2O	RT	5 min
Ethanol 25 % in PBS	RT	5 min
PBS	RT	5min
20 % HS in PBS	RT	6 hrs

Primary antibody incubation

Primary antibody was incubated overnight at 4 °C, in 20 % HS / PBS. The anti-PH3 antibody was used at 1 / 1000 dilution.

Day 2:

Washing

Reagents	**Temperature**	**Time**
*PBS-TB	RT	3 X 1.5 hr
**PBS-TBN	RT	1.5 hr
PBS-TB	RT	5 min

* PBS-TB: 1 X PBS containing 0.05 % Tween-20 and 0,2 % BMB

** PBS-TBN: PBS-TB containing 0.3 M NaCl

Secondary antibody incubation

Secondary antibody was incubated overnight at 4 °C, in 20 % HS / PBS, at 1 / 1000 dilution.

Day 3:

Washing

Reagents	Temperature	Time
PBS-TB	RT	3 X 15 min
PBS-TBN	RT	30 min
PBS-TB	RT	5 min
PBS-TB	4 °C	overnight

Day 4:

Alkaline phosphatase staining

Reagents	Temperature	Time
PBS	RT	2 X 5 min
APB	RT	2 X 5 min
*APB + NBT + BCIP	On ice	Open end

* NBT and BCIP were used at the same concentration as for WMISH.

VI.2.7. TUNEL Wholemount staining

This was performed according to Hensey and Gautier (1997) with modifications.

Fixation:

After -gal staining, embryos were refixed in 1 X MEMFA, for 1 hr at RT, and permeabilized by incubation in Dent´s fixative, overnight at – 20°C. permeabilized embryos were then transferred in 100 methanol and stored at – 20°C.

Day 1:

Rehydration

Reagents	Temperature	Time
Ethanol 100 %	RT	5 min
Ethanol 75 % in H_2O	RT	5 min
Ethanol 50 % in H_2O	RT	5 min
Ethanol 25 % in PBS	RT	5 min
PBS	RT	5min
PTw	RT	2 X 15 min
PBS	RT	2 X 15 min

End labelling

Reagents	Temperature	Time
1 X TdT buffer in PBS	RT	1 hr
1 X TdT buffer + 0.5 µM Dig-dUTP + 150 U / ml TdT enzyme in PBS	RT	overnight

Day 2:

Washing

Reagents	Temperature	Time
PBS / EDTA*	65 °C	2 X 1 hr
PBS	RT	4 X 1 hr

PBS / EDTA: 1 X PBS containing 1 mM EDTA

Antibody incubation

Reagents	Temperature	Time
PBT	RT	15 min
PBT + 20 % HS	RT	1 hr
PBT + 20 % HS + 1 / 2000 anti-DIG-AP	4 °C	overnight

Day 3:

Washing

Reagents	Temperature	Time
PBT	RT	6 X 1 hr
PBT	4 °C	overnight

Day 4:

Alkaline phosphatase staining

Reagents	Temperature	Time
APB	RT	2 X 5 min
APB + NBT + BCIP (same as above)	On ice	Watch for colour development

VI.2.8. Molecular biology methods

VI.2.8.1. Molecular cloning of the Xdhcr7 cDNAs

Total RNA was extracted from embryos, and Reverse Transcriptase reactions were performed according to the manufacturer's instructions.
PCR reactions were performed using the appropriate primers mentioned above.
The PCR products were analysed on agarose gel. Positive bands were excised from the gel and purified with the Qiagen kit, as described in the Handbook. Purified product were

ligated into pGEM-T vector, and transformed into *E. coli.* Amplified products were further sequence from both end, and the sequence information was submitted in the BLAST data bank for homology search.

VI.2.8.2. Molecular cloning of overexpression constructs

The open reading frame of each cDNA was amplified by PCR from the corresponding pGEMT recombinant plasmid, using the appropriate primers described above. Analysed by agarose gel electrophoresis, the amplified DNA fragments were purified from the gel with the Qiagen kit, as described in the Handbook. The DNAs, including our clones and the pCS2+ expression vector (Turner and Weintraub, 1994) were digested overnight with the corresponding restriction enzymes. The digested products were purified and ligated. The resulting recombinant plasmids were amplified in vivo, using XL1-Blue bacteria (Stratagene). Each clone was further sequenced and analysed by TnT *in vitro* transcription/translation system (Promega). ^{35}S-methionine was used for labelling and the translated products were analysed by SDS PAGE and phosphoimaging.

VI.2.8.4. Preparation and analysis of plasmid DNA

VI.2.8.4.1. Preparation of electrocompetent bacteria

Electrocompetent cells used in this study was prepared according to the BioRAD protocol as followed:

1. Inoculate a single colony of *E. coli* XL blue in 20 ml of LB broth with tetracycline and culture at 37 °C overnight. Simultaneously, incubate 2 liters of LB medium at the same condition without bacteria.
2. transfer the 20 ml bacteria culture into the 2 liters LB broth (1/100 dilution) and culture for additional 3-3.5 hours at 37 °C. After culturing for 2.5 hours check OD_{600} every 20-30 min until OD_{600} reaches to 0.8 and store the culture on ice.
3. Harvest the cells by centrifuging at 4000 rpm for 10 min at 4 °C. It is better to do all the following steps in the cold room. Decant the liquid from the cell pellets completely.
4. Wash the cells by resuspending the pellets in 1.2 liters of 10% glycerol or pure water and centrifuge at 4000 rpm for 10 min at 4 °C.
5. Wash again with 600 ml of 10% glycerol or pure water and centrifuge at 4000 rpm for 10 min at 4 °C.
6. Suspend the cells in 4 ml 10% glycerol, make 40 µl aliquots, freeze with liquid nitrogen and store at -80 °C.

VI.2.8.4.2. Transformation of bacteria and plating

1. Put on ice the electrocopetent bacteria (for thawing), an aliquot of LB medium, the probe (ligation mix or others, in a low ionic strength buffer), and the cuvettes.
2. Set Gene Pulser at 25 µF, 2.5 kV when using the 0.2 cm cuvettes.
3. Mix 40 µl bacteria and 1 µl probe then transfer into a pre-cooled cuvette. Cover with the lid and insert in the Gene Pulser.
4. Press the corresponding two butons on the Gene Pulser until the sound comes (time constant should be 4-5 msec).
5. Put 500 µl cooled LB-medium in the cuvette and resuspend the cells (steps 4 and 5 should be very face to improve the recovery of the transformants).

6. Plate 20 µl and 200 µl to LB-Amp (Kan or Tet) plates, incubate overnight at 37 °C.

VI.2.8.4.3. Plasmid DNA preparation from bacteria

Mini-preparation with TELT

1. Collect cells from 1.5 ml bacteria culture by centrifuging at 6000 rpm, RT, 5 min.
2. Remove supernatant completely with a vacuum system and resuspend the cells in 150 µl TELT solution.
3. add 15 µl of 10 mg/ml lysozyme to the cells, vortex and incubate at RT for 5 min.
4. Keep the cells in boiling water for 2 min and then transfer on ice for 5 min.
5. Centrifuge with full speed (14 000 rpm, microcentrifuge), RT, 10 min and remove the pellet of bacteria debris with a sterilized toothpick.
6. Add 100 µl of isopropanol to the sample and vortex.
7. Centrifuge with full speed at RT for 15 min. Remove the supernatant with pipette and wash the pellet with 200 µl of 70 % ethanol.
8. Centrifuge with full speed at RT for 5 min. Suck off the supernatant with pipette and dry the pellet under speed vacuum for 5 min or at 37 °C for about 15-30 min.
9. Dissolve the pellet in 30 µl TE with 10 ng/µl RNase A and incubate first at RT for 2-5 min and then 65 °C for 5 min. Store the preparation at -20 °C.

Large scale plasmid DNA preparation

For the preparation of the large amounts of highly pure plasmid to be use for in-vitro RNA synthesis, sequencing and TnT, Qiagen or Nucleobond Plasmid Midi kit was used according to manufacturer's instructions.

VI.2.8.4.4. Agarose gel electrophoresis of DNA

0.8 to 2.5 % agarose gels were used for analysis of DNA fragments 0.2-5 kb. The agarose gels were prepared using 1X TBE buffer with 0.5 µg/ml ethidium bromide; 1X TBE was used as running buffer. Low or high size molecular marker (Gibco BRL) was used. The DNA band were visualised at the UV-transillumination; the picture of the gels were made using the IMAGER computer. In case of cloning, the bands of interest were purified from the agarose gels according to Qiagen Handbook.

VI.2.8.5. Preparation and analysis of RNA

VI.2.8.5.1. Synthesis and purification of mRNA for injections

The constructs and the restriction enzymes used for the linearization are listed above. Approximately 10 µg of each clone were digested and purified using PCR Purification kit (Qiagen). Eluted in TE buffer, linearized constructs were diluted to 200 ng/µl. The mRNA synthesis was done according to the instruction manual of the mMESSAGE mMACHINE (Ambion). Capped-RNAs were purified using RNeasy kit (Qiagen). Eluted in RNAase-free water, mRNA were analysed on a 1% agarose gel store at -80 °C.

VI.2.8.5.2. Synthesis and purification of Dig- or Flu-labelled antisense RNA for *in situ* hybridization

The plasmid probes of interest were linearized using the appropriate restriction enzyme, as indicated above. Analysed on a 1 % agarose gel, the linearized DNAs were purified and

diluted to 200 ng/µl in TE buffer. For 25 ul of *in vitro* transcription reaction, the following components were mixed in a 1.5 ml eppendorf tube:

5X transcription buffer (Stratagene)	5 µl
ATP (10 mM)	1 µl
GTP (10 mM)	1 µl
CTP (10 mM)	1 µl
UTP (10 mM)	0.64 µl
Dig-or Flu-UTP (10 mM)	0.36 µl
DTT (0.75 M)	1 µl
RNAsin (40 U/µl)	1 µl
RNA polymerase	0.5 µl
DNA template (200 ng/µl)	5 µl
RNAase-free H2O	up to 25 µl

Mixed and centrifuged briefly, the reaction mix was incubated at 37 °C for 2.5 – 3 hours. The template DNA was next digested by treatment with 10 U of DNaseI RNAase-free for 20 – 30 min. The Digoxigenin (Fluorescein)-labelled RNA probes were purified using the RNeasy kit (Qiagen). Eluted in 35 µl of RNAase-free water, equivalent volume of formamid was immediately added to stabilize the antisense probes. The quality of the purified RNAs was analysed by electrophoresis on 1 % agarose gel. In hybridization mix, these probes are stable for years at -20 °C.

VI.2.8.6. Protein expression in yeast.

VI.2.8.6.1. Transformation of yeast cells.

Cell were grown overnight at 30 °C, and pellet by centrifugation. The cell pellet was washed twice in buffer and resuspended in TE buffer (50 µl of suspension per transformation). The suspension was supplemented with and equal volume of 2 X LiOAC solution, mixed and incubated 1 hr at 30 °C. The suspension was shared in 1.5 ml eppendorf tube as 100 µl aliquots. 5 µg of each plasmid construct was added to a cell aliquot and incubated 30 min at 30 °C. 1 ml of PEG solution was added to each sample, which was further incubated 1 hr at 30 °C. Cells were heat-shocked at 42 °C for 15 min, and pellet. The PEG solution was removed; cells were resuspended in 80 µl of culture, plated and incubated at 30 °C.

VI.2.8.6.2. Immunofluorescence.

For each construct, a single colony was picked from the transforming plate and grown overnight in selective medium. Cells were then diluted to 0.3 OD_{600}, with YEP medium and cultured to 0.8 – 1.0 OD_{600}. An equivalent of 3.5 OD_{600} was aliquoted in a 15 ml falcon tube and washed once with dH_2O. The pellet was transferred to 1.5 ml eppendorf tube and washed twice with 1 ml of dH_2O. The pellet was then resupended in 400 µl of fixative and incubated overnight at 4 °C. Meanwhile, eight-well chamber slides were coated by adding 20 µl of poly-L-lysine solution to each well. Fixed cells were washed 3 times with PBSS; the pellet was incubated with 100 µl of Zymolyase solution for 30 min at 25 °C, to induce spheroblast formation. Spheroblast were washed and resuspended in 50 µl of PBSS. 15 µl of spherobast were loaded per well and incubated 20 min at RT. The supernatant was

sucked, the well were covered with 20 µl of blocking solution for 10 min at RT. The primary antibody was added in 20 µl of blocking solution, and the slides were incubated 2 hrs in a humid chamber. Each well was then washed 5 times with 20 µl of PBSS. The secondary antibody was added in 20 µl of blocking solution, and the slides were incubated 30 min at RT, in a dark chamber. Each well was washed 10 times with 20 µl of PBSS, and covered with 20 µl of mounting / DAPI solution. The slides were the ready to be analysed using a fluorescence microscope.

VI.2.8.6.2. Preparation of microsomal fractions.

All solutions to be used in preparation of microsomes were prechilled on ice for 1 hr, prior to the start of the experiment.
A 300 ml overnight secondary culture was prepared from a 2 ml primary culture of a single transformant colony. Cells were pellet by centrifugation in 50 ml falcon tubes (2000 rpm / 3min / 4 °C), and washed with autoclaved water. 2 ml of lysis buffer was added per ml of pellet. The mixture was supplemented with 1/4 volume of glass beads. Cells were mechanically disrupted vortexing 4 X 30 sec (chill down after each 30 sec vortex). Debris and glass beads were sedimented by centrifugation (2000 rpm / 2 in / 4 °C). The supernatant was centrifuged 15 min at 20,000 g (15,000 rpm with a TLA 100.2 rotor) to precipitate nuclei and membranes. The supernatant was further ultracentrifuged at 100,000 g (52,000 rpm) to pellet the microsomes.

VII. REFERENCES

Bae SH, Lee JN, Fitzky BU et al. (1999) Cholesterol biosynthesis from lanosterol. Molecular cloning, tissue distribution, expression, chromosomal localization, and regulation of rat 7-dehydrocholesterol reductase, a Smith-Lemli-Opitz syndrome-related protein. *J Biol Chem*, **274**(21):14624-14631.

Bagnat M, Keranen S, Shevchenko A et al. (2000) Lipid rafts function in biosynthetic delivery of proteins to the cell surface in yeast. *Proc Natl Acad Sci U S A,* **97**(7):3254-3259.

Berger R, Smit, GPA, Schierbeek et al. (1985) Mevalonic aciduria: an inborn error of cholesterol biosynthesis? *Clin. Chim, Acta* **152**, 219-222.

Bjorkhem I and Meany, S (2004) Brain cholesterol: long secret life behind a barrier. *Arterioscler Thromb Vasc Biol*, 24(5):806-815.

Briscoe J and Ericson J (1999) The specification of neuronal identity by graded Sonic Hedgehog signalling. *Semin Cell Dev Biol*, **10**(3):353-362.

Brown MS and Goldstein JL (1999) A proteolytic pathway that controls the cholesterol content of membranes, cells, and blood. *Proc Natl Acad Sci U S A*, **96**(20): 11041–11048.

Burke R, Nellen D, Bellotto M et al. (1999) Dispatched, a novel sterol-sensing domain protein dedicated to the release of cholesterol-modified hedgehog from signalling cells. *Cell*, **99**(7):803-815.

Carl M, Loosli F, Wittbrodt J. (2002) Six3 inactivation reveals its essential role for the formation and patterning of the vertebrate eye. *Development*, **129**(17):4057-4063.

Chang CJ and Raymond PA (2002) Embryonic origin of the eyes in teleost fish. *BioEssays,* **24**, 519-529.

Chow RL, and Lang RA (2001) Early eye development in vertebrates. *Annu Rev cell Dev Biol,* **17**, 255 – 296.

Christenson LK, Strauss JF (2000) Steroidogenic acute regulatory protein (StAR) and the intramitochondrial translocation of cholesterol. *Biochim Biophys Acta*,, **1529**(1-3):175-187.

Cleaver O, Seufert DW and Krieg PA (2000) Endoderm patterning by the notochord: development of the hypochord in Xenopus. *Development,* **127**, 869-879.

Cooper MK, Wassif CA, Krakowiak PA et al. (2003) A defective response to Hedgehog signaling in disorders of cholesterol biosynthesis. *Nat Genet*, **33**(4):508-513.

Cornesse Y, Pieler T and Hollemann T (2004) Olfactory and lens placode formation is control by the hedgeho-interacting protein (*Xhip*) in *Xenopus. Dev. Biol,* (in press).

De Robertis EM, Larraín J, Oelgeschläger M and Wessely O (2000) The establishment of Spemann's organizer and patterning of the vertebrate embryo. *Nature Rev Genet* **1**, 171–181.

Dennis JW, Granovsky M and Warren CE (1999) Protein glycosylation in development and disease. *Bioessays,* **21**(5):412-421.

Dietschy JM and Turley SD (2001) Cholesterol metabolism in the brain. *Curr Opin Lipidol*, **12**(2):105-112.

Dietschy JM, Turley SD. (2004) Thematic review series: brain Lipids. Cholesterol metabolism in the central nervous system during early development and in the mature animal. *J Lipid Res,* **45**(8):1375-1397.

diIorio PJ, Moss JB, Sbrogna JL et al. (2002) Sonic hedgehog is required early in pancreatic islet development. *Dev Biol,* **244**(1):75-84.

Edwards PA and Ericsson J (1999) Sterols and Isoprenoids: Signaling Molecules derived from the Cholesterol Biosynthetic Pathway. *Ann. Rev. Biochem,* **68**, 157-185.

Farazi TA, Waksman G, Gordon JI (2001) The biology and enzymology of protein N-myristoylation. *J Biol Chem*, **276**(43):39501-39504.

Fisher KA (1976) Analysis of membrane halves: cholesterol. *Proc Natl Acad Sci U S A*, **73**(1):173-177.

Fitzky BU and Moebius FF (2001) 7-Dehydrocholesterol–dependent proteolysis of HMG-CoA reductase suppresses sterol biosynthesis in a mouse model of Smith-Lemli-Opitz/RSH syndrome. *J Clin Invest*, **108**(6):905-915.

Fitzky BU, Witsch-Baumgartner M, Erdel M *et al.* (1998) Mutations in the delta7-sterol reductase gene in patients with the Smith-Lemli-Opitz syndrome. *Proc Natl Acad Sci USA,* **95**, 8181-8186.

Fleming A, Keynes R and Tannahil D (2004) A central role for the notochord in vertebral patterning. *Development,* **131**, 873-880.

Gaoua W, Wolf C, Chevy F et al. (2000) Cholesterol deficit but not accumulation of aberrant sterols is the major cause of the teratogenic activity in the Smith-Lemli-Opitz syndrome animal model. *J Lipid Res,* **41**(4):637-646.

Garver WS and Heidenreich RA (2002) The Niemann-Pick C proteins and trafficking of cholesterol through the late endosomal/lysosomal system. *Curr Mol Med*, **2**(5):485-505.

Gerhart, J, Danilchik M, Doniach T et al. (1989). Cortical rotation of the *Xenopus* egg: Consequences for the anteroposterior pattern of embryonic dorsal development. *Development*, **107**, 3751.

Graw J (2003) The genetic and molecular basis of congenital eye defects. *Nat Rev Genet*, **4**(11): 876-888.

Hallonet M, Hollemann T, Pieler T, Gruss P (1999) Vax1, a novel homeobox-containing gene, directs development of the basal forebrain and visual system. *Genes Dev*, **13**(23):3106-3114.

Hanaka S, Abe T, Itakura H and Matsumoto A (2000) Gene expression related to cholesterol metabolism in mouse brain during development. *Brain Dev*, **22**(5):321-326.

Hanks SK, Hunter T (1995) Protein kinases 6. The eukaryotic protein kinase superfamily: kinase (catalytic) domain structure and classification. *FASEB J*, **9**(8):576-596.

Harland R, Gerhart J (1997) Formation and function of Spemann's organizer. *Annu Rev Cell Dev Biol*, **13**, 611-67

Harland RM. (1991) In situ hybridization: an improved whole-mount method for Xenopus embryos. *Methods Cell Biol*, **36**, 685-95

Hensey C, Gautier J (1997) A developmental timer that regulates apoptosis at the onset of gastrulation. *Mech Dev*, **69**(1-2):183-195.

Ho KS and Scott MP (2002) Sonic hedgehog in the nervous system: functions, modifications and mechanisms. *Curr Opin Neurobiol*, **12**(1):57-63.

Hoekstra D and van IJzendoorn SC (2000) Lipid trafficking and sorting: how cholesterol is filling gaps. *Curr Opin Cell Biol*, **12**(4):496-502.

Hoffmann G, Gibson KM, Brandt IK et al. (1986) Mevalonic aciduria - an inborn error of cholesterol and non-sterol isoprene biosynthesis. *New Eng. J. Med,* **314**, 1610-1614.

Hollemann T, Panitz F and Pieler T (1998) *In situ* hybridization techniques with *Xenopus* embryos. In Richter JD (ed.), *A Comparative Methods Approach to the Study of Oocytes and Embryos*. Oxford University Press.

Hollemann T, Schuh R Pieler T and Stick R (1996) *Xenopus Xsal-1*, a vertebrate homolog of the region specific homeotic gene *spalt* of *Drosophila. Mech Dev*, **55**, 19-32.

Honda M, Tint GS, Honda A et al. (1998) 7-dehydrocholesterol down-regulates cholesterol biosynthesis in cultured Smith-Lemli-Opitz syndrome skin fibroblasts. *J. Lipid Res* **39**, 647-657.

Incardona JP, Eaton S (2000) Cholesterol in signal transduction. *Curr Opin Cell Biol*, **12**(2):193-203

Ingham PW (2000) Hedgehog signalling: how cholesterol modulates the signal. *Curr. Biol,* **10**, R180-R183.

Ingham PW and McMahon AP (2001) Hedgehog signalling in animal development: paradigms and principles. *Genes Dev,* **15**(23):3059-3087.

Ishibashi M and McMahon AP (2002) A sonic hedgehog-dependent signalling relay

regulates growth of diencephalic and mesencephalic primordia in the early mouse embryo. *Development*, **129**, 4807-4819.

Jean D, Ewan K, Gruss P (1998) Molecular regulators involved in vertebrate eye development. *Mech Dev,* **76**(1-2):3-18.

Jira PE, Waterham HR, Wanders RJ et al. (2003) Smith-Lemli-Opitz syndrome and the DHCR7 gene. *Ann Hum Genet,* **67**(Pt 3):269-280.

Johnson GB. and Raven PH. (2002) Biology, Book 6th ed. 1215 – 1238.

Keller RK, Arnold TP, and Fliesler, SJ (2004) Formation of 7-dehydrocholesterol containing membrane rafts in vitro and in vivo, with relevance to the Smith-Lemli-Opitz syndrome. *J. Lipid Res*, **45**, 347-355

Kelley RI and Herman GE (2001) Inborn errors of sterol biosynthesis. *Annu. Rev. Genomics Hum. Genet,* **2**, 299-341.

Kennedy BN, Stearns GW, Smyth VA et al. (2004). Zebrafish rx3 and mab21l2 are required during eye morphogenesis. *Dev Biol*, **15**;270(2):336-349.

Khan N, Shen J, Chang TY et al. (2003) Plasma membrane cholesterol: A possible barrier to intracellular oxygen in normal and mutant CHO cell defective in cholesterol metabolism. *Biochemistry,* **42**, 23-29.

Kuwabara PE and Labouesse M. (2002) The sterol-sensing domain: multiple families, a unique role? *Trends Genet*, **18**(4):193-201.

Lachman MF, Wright Y, Whiteman DA et al. (1991): Brief clinical report. A 46,XY phenotypic female with Smith-Lemli-Opitz syndrome. *Clin Genet,* **39**:136–141.

Laubner D, Breitling R, Adamski J. (2003) Embryonic expression of cholesterogenic genes is restricted to distinct domains and colocalizes with apoptotic regions in mice. *Mol Brain Res*, **115**(1):87-92.

Lee JN, Bae SH, Paik YK. (2002) Structure and alternative splicing of the rat 7-dehydrocholesterol reductase gene. *Biochim Biophys Acta*, **1576**(1-2):148-156.

Lewis PM, Dunn MP, McMahon JA et al. (2001) Cholesterol modification of sonic hedgehog is required for long-range signaling activity and effective modulation of signaling by Ptc1. *Cell,* **105**(5):599-612.

Liem KFJ, Jessell TM and Briscoe J (2000). Regulation of the neural patterning activity of sonic hedgehog by secreted BMP inhibitors expressed by notochord and somites. *Development,* **127**,4855 –4866.

Lin AE, Ardinger HH, Robert H et al. (1997) Cardiovascular Malformations in Smith-Lemli-Opitz Syndrome. *Am J Med Genet*, **68**(3):270-278. Review.

Liscum L. (2002) Cholesterol biosynthesis. In: Vance DE and Vance JE (Eds), Biochemistry of lipids, lipoproteins and membrane, 4th ed., Elsevier Science B.V. pp 409-431.

Macdonald R, Barth KA, Xu Q et al. (1995) Midline signalling is required for Pax gene regulation and patterning of the eyes. *Development* , **121**,3267 –3278.

Mann RK and Beachy PA (2004) Novel lipid modifications of secreted protein signals. *Annu. Rev. Biochem*, **73**, 891–923.

Masaki R, Yamamoto A and Tashiro Y (1996) Membrane topology and retention of microsomal aldehyde dehydrogenase in the endoplasmic reticulum. *J Biol Chem*, **271**(28):16939-16944.

McCarthy RA and Argraves WS (2003) Megalin and the neurodevelopmental biology of sonic hedgehog and retinol. *J. Cell Sci,* **116**(6):955 – 960.

McCarthy RA, Barth JL, Chintalapudi MR et al. (2002) Megalin Functions as an Endocytic Sonic Hedgehog Receptor. *J. Biol. Chem,* **277**(28):25660-25667

Moebius FF, Fitzky BU, Lee JN et al. (1998) Molecular cloning and expression of the human delta7-sterol reductase. *Proc Natl Acad Sci U S A*, **95**(4):1899-1902.

Müller G, Hanekop N, Wied S, and Frick W (2002) Cholesterol Depletion Blocks Redistribution of Lipid Raft Components and Insulin-Mimetic Signaling by Glimepiride and Phosphoinositolglycans in Rat Adipocytes. *Mol. Med*, **8**(3):120-136

Nabi IR and Le PU (2003) Caveolae/raft-dependent endocytosis. *J. Cell Biol*, **161**(4):673-677.

Nieuwkoop PD and Faber J (1975) Normal Table of *Xenopus laevis* (Daudin). 2nd ed. North-Holland Publ., Amsterdam.

Nowaczyk MJM, Martin-Garcia D, Aquino-Perna A et al. (2004) Founder effect for the T93M DHCR7 mutation in Smith-Lemli-Opitz syndrome. *Am J Med Genet*, **125A**(2):173-176.

Nowaczyk MJM, Nakamura LM and Waye JS (2001). DHCR7 and Smith-Lemli-Opitz syndrome. *Clin Invest Med,* **24**(6):311-317.

Nowaczyk MJM, Waye JS (2001) The Smith–Lemli–Opitz syndrome: a novel metabolic way of understanding developmental biology, embryogenesis, and dysmorphology. *Clin Genet,* **59**:375–386.

Nwokoro NA, Wassif CA and Porter FD (2001) Genetic disorders of cholesterol biosynthesis in mice and humans. *Mol Genet Metab*, **74**(1-2):105-119.

Odent S, Atti-Bitach T, Blayau M et al. (1999) Expression of the *Sonic hedgehog* (*SHH*) gene during early human development and phenotypic expression of new mutations causing holoprosencephaly. *Hum Mol Genet,* **8**(9):1683-1689.

Pasca di Magliano M and Hebrok M (2003) Hedgehog signalling in cancer formation and maintenance. *Nat Rev Cancer*, **3**(12):903-911.

Petrescu AD, Gallegos AM, Okamura Y et al. (2001) Steroidogenic acute regulatory protein binds cholesterol and modulates mitochondrial membrane sterol domain dynamics. *J Biol Chem,* **276**(40):36970-36982.

Pfrieger FW (2003) Cholesterol homeostasis and function in neurons of the central nervous system. *Cell Mol Life Sci*, **60**:1158–1171.

Pfrieger FW (2003) Role of cholesterol in synapse formation and function. *Biochim Biophys Acta,* **1610**(2):271-280.

Pike LJ (2003 Lipid rafts: bringing order to chaos. *J. Lipid Res*, **44**:655-667.

Pinsky L, DiGeorge AM (1965) A familial syndrome of facial and skeletal anomalies associated with genital abnormality in the male and normal genitals in the female. *J Pediatr*, **66**:1049–1054.

Pommereit D, Pieler T, Hollemann T (2001) Xpitx3: a member of the Rieg/Pitx gene family expressed during pituitary and lens formation in Xenopus laevis. *Mech Dev*, **102**(1-2):255-257.

Porter FD, Drago J, Xu Y et al. (1997) Lhx2, a LIM homeobox gene, is required for eye, forebrain, and definitive erythrocyte development. *Development,* **124**(15):2935-2944.

Porter JA, Young KE and Beachy PA (1996) Cholesterol Modification of Hedgehog Signaling Proteins in Animal Development. *Science*, **274**(5285):255-259.

Rader DJ, Cohen J, Hobbs HH. (2003) Monogenic hypercholesterolemia: new insights in pathogenesis and treatment. *J Clin Invest*, **1**(12):1795-1803.

Ruiz i Altaba A, Jessell TM, Roelink H (1995) Restrictions to floor plate induction by hedgehog and winged-helix genes in the neural tube of frog embryos. *Mol Cell Neurosci,* **6**(2):106-121.

Russell C (2003) The role of hedgehogs and fibroblast growth factors in eye development and retinal rescue. *Vision Research*, **43**:899 – 912.

Santos AC and Lehmann R (2004) Isoprenoids control germ cell migration downstream of HMGCoA reductases. *Dev cell*, **6**(2):283-293.

Schell-Apacik C, Rivero M, Knepper JL et al. (2003) Sonic hedgehog mutations causing human holoprosencephaly impair neural patterning activity. *Hum. Genet,* **113**: 170-177.

Schmitz G, Orsó E (2001) Intracellular cholesterol and phospholipid trafficking: comparable mechanisms in macrophages and neuronal cells. *Neurochem Res*, **26**(8-9):1045-1068.

Schrick K, Mayer U, Martin G et al (2002) Interactions between sterol biosynthesis genes in embryonic development of *Arabidopsis*. *Plant J*, **31**(1):61-73.

Scott G (2003) Developmental Biology, 7th ed. Text book, ISBN 0-87893-258-5.

Shim YH, Bae SH, Kim JH et al. (2004) A novel mutation of the human 7-dehydrocholesterol reductase gene reduces enzyme activity in patients with holoprosencephaly. *Biochem Biophys Res Commun*, **315**(1):219-23.

Simons K and Ehehalt R (2002) Cholesterol, lipid rafts, and disease. *J Clin Invest,* **110**:597-603.

Steinberg D (2004) Thematic review series: the pathogenesis of atherosclerosis. An interpretive history of the cholesterol controversy: part I. *J Lipid Res*, **45**(9):1583-1593.

Strutt H, Thomas C, Nakano Y et al. (2001) Mutations in the sterol-sensing domain of Patched suggest a role for vesicular trafficking in Smoothened regulation. *Curr Biol* **11**(8):608-613.

Tabas I (2002a). Cholesterol in health and disease. *J Clin Invest,* **110**:583-590.

Tabas I (2002b). Consequence of cellular cholesterol accumulation: basic concepts and physiological implication. *J Clin Invest*, **110**, 905-911.

Taipale J, Cooper MK, MAITI T and Beachy PA. (2002) Patched acts catalytically to suppress the activity of Smoothened. *Nature,* 418, 892 – 896.

Tint GS Salen G Batta A et al (1994) : Correlation of severity and outcome with plasma sterol levels in variants of the Smith-Lemli-Opitz syndrome. *J Pediat,* **127**, 82-87.

Tsujishita Y, Hurley JH (2000) Structure and lipid transport mechanism of a StAR-related domain. *Nat Struct Biol*, **7**(5):408-414.

van Meer G (2001) Caveolin, cholesterol, and lipid droplets ? *J Cell Biol*, **152**, F29-F34.

Wallis D, Muenke M. (2000) Mutations in holoprosencephaly. *Hum Mutat.* **16**(2):99-108.

Wassif CA, Maslen C, Kachilele-Linjewile S et al. (1998) Mutations in the Human Sterol D7-Reductase Gene at 11q12-13 Cause Smith-Lemli-Opitz Syndrome. *Am J Hum Genet,* **63**:55–62.

Weiss H, Schiffmann E, and Titus E (1961) Effect of mevalonate analogues upon cholesterol biosynthesis. *J Lipid Res* **2**(3): 258-262.

Wijgerde M, McMahon JA, Rule M, McMahon AP (2002) A direct requirement for Hedgehog signaling for normal specification of all ventral progenitor domains in the presumptive mammalian spinal cord. *Genes Dev* **16**(22):2849-2864.

Witsch-Baumgartner M, Gruber M, Kraft HG et al. (2004). Maternal apo E genotype is a modifier of the Smith-Lemli-Opitz syndrome. *J Med Genet,* **41**, 577-584.

Witsch-Baumgartner M, Loffler J, Utermann G. (2001) Mutations in the human DHCR7 gene. *Hum Mutat*, **17**(3):172-182.

Wittbrodt J, Shima A, Schartl M. (2002) Medaka a model organism from the far East. *Nat Rev Genet*, **3**(1):53-64.

Wolpert L (1998) Principle of development. Text book, ISBN 0-19-850263-X
Yu H, Wessels A, Chen J et al. (2004) Late gestational lung hypoplasia in a mouse model of the Smith-Lemli-Opitz syndrome. *BMC Dev Biol,* **4**(1).

Zhang XM and Yang XJ (2001) Temporal and spatial effects of sonic hedgehog signalling in chick eye morphogenesis. *Dev Biol*, **233**, 271-290.

Zuber ME, Gestri G, Viczian AS et al. (2003): specification of the vertebrate eye by a network of eye field transcription factors. *Development*, **130**(21):5155-5167.

VIII. ACKNOWLEDGEMENTS

Carrying this work to the end was made possible thanks to the contribution of several kind-hearted people, of whom I cannot present an exhaustive list here. May each and everyone feel acknowledged.

I would like to thank Prof. Dr. Tomas Pieler and the "*Graduiertenkolleg für Molekulare Genetik der Entwicklung*" (GRK 242), for giving me the opportunity to join the graduate program and fulfil my will of pursuing my doctorate studies.

My profound gratitude goes to Prof. Dr. Thomas Hollemann who, despite his numerous duties, followed up this work with kind attention.

I would like to acknowledge Dr. Yvonne Cornesse, Marin Kriebel, and Marco Winkler for the friendly collaboration that we shared in the lab.

Part of this work was carried out in the labs of Dr. Hans Dieter Schmidt (MPI-BC, Goettingen) and Dr. Peter Lindermann (ML University of Halle), whom I would like to acknowledge.

The writing of this work received constructive critics from Solomon Afelik, Fong Cheng Pan, Dr. Yonglong Chen, Dr. Jacob Souopgui and Dr. Edgar Pera. May all of them feel deeply acknowledged.

All members of the department of Developmental Biochemistry of the GZMB (Abt. Pieler) are acknowledged for the friendly atmosphere that we shared within the group.

I would also like to acknowledge my college mates of the GRK 242 for the friendly moments that we shared together.

I would finally like to acknowledge my family and friends, for their moral support during difficult moments.